Laboratori Nazionali di Frascati

LNF-92/033 (P)
24 Aprile 1992

DAΦNE MACHINE PROJECT

Contributions to the
3rd European Particle Accelerator Conference (*EPAC 92*)
Technical University of Berlin - Germany, 24-28 March, 1992

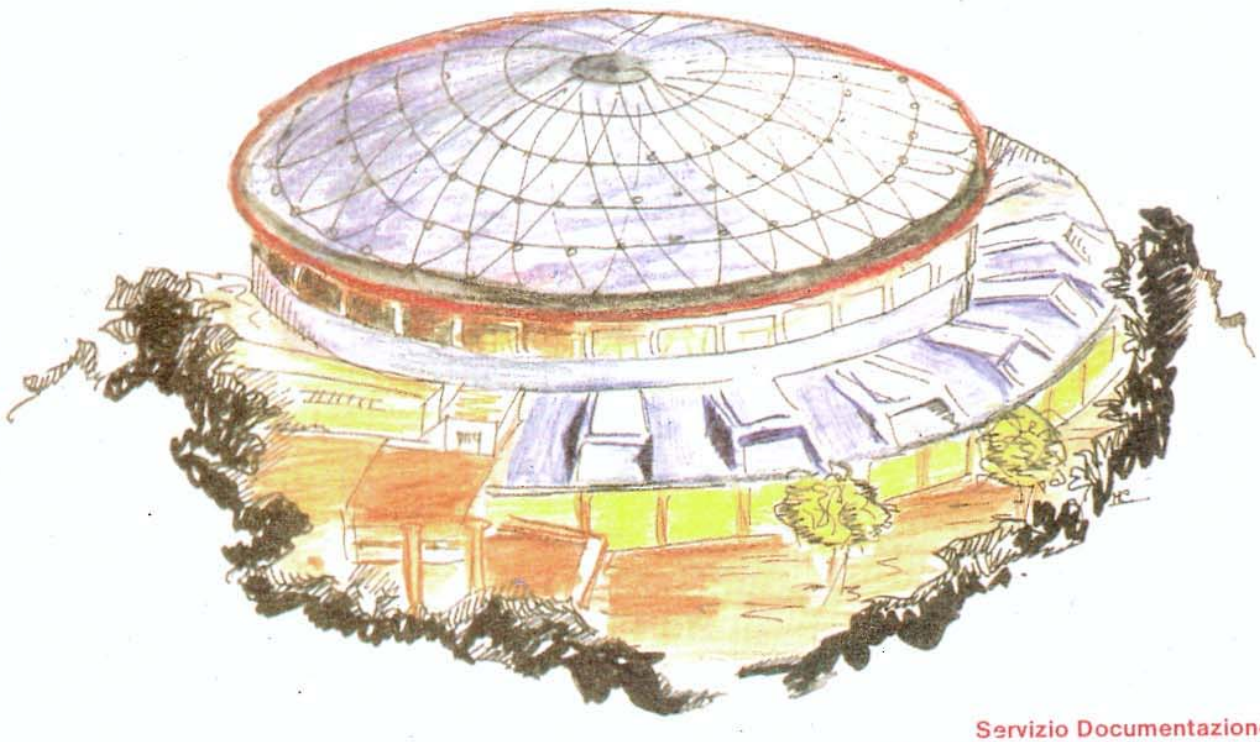

Servizio Documentazione
dei Laboratori Nazionali di Frascati
P.O. Box, 13 - 00044 Frascati (Italy)

INFN - Laboratori Nazionali di Frascati
Servizio Documentazione

LNF-92/033 (P)
24 Aprile 1992

DAΦNE MACHINE PROJECT

Contributions to the
3rd European Particle Accelerator Conference (EPAC 92)
Technical University of Berlin - Germany, 24-28 March 1992

CONTENTS

DAΦNE* Status Report

The DAΦNE Project Team**
presented by M.E. Biagini
INFN Laboratori Nazionali di Frascati - C.P. 13 - 00044 Frascati (Roma) - Italy

Abstract

The Frascati National Laboratories Φ-factory project consists of a two rings e^+e^- collider, an accumulator ring and a full energy linac injector. The lattice for the main ring and the accumulator is frozen, the vacuum system has been dimensioned, and the engineering design of the various components is in progress. An R&D program on the suppression of high order modes, leading to multibunch instabilities, is also in progress. In the following a general overview of the project is given.

1. INTRODUCTION

The DAΦNE project [1] has been approved and fully funded in June1990, commissioning is foreseen to start at the end of 1995. The accelerator complex will be housed in the existing LNF buildings, after the decommissioning of Adone (shutdown December 1992).

The major physics aim of a Φ-factory is to perform CP violation experiments with high accuracy. This sets very tough requirements on the peak and average luminosity and on the design of the interaction regions. Up to now, three experiments are foreseen: one, operating at the maximum luminosity, with the aim to improve the measurement of the decay ratios of K_L and K_S in two pions, the other two, with less demanding requests on the luminosity, will study multihadronic production and hypernuclei. The luminosity is optimized at 510 MeV, the short term luminosity goal is 10^{32} $cm^{-2}s^{-1}$, while the ultimate target is 10^{33} $cm^{-2}s^{-1}$.

2. DESIGN PARAMETERS

The main features of the design are:
- many bunches
- very flat beams
- relatively high emittance.

Four 1.8 T normal conducting wigglers are installed in each ring, to have full emittance tunability and increase the radiation damping.

At the space charge limit the luminosity, in the hypothesis of equal tune shift in both planes, can be written as:

$$L = hL_o = \pi \left(\frac{\gamma}{r_e}\right)^2 hf_o \frac{\xi^2 \varepsilon (1+\kappa)}{\beta_y^*}$$

where: L_o = single bunch luminosity, h = number of bunches, f_o = revolution frequency, γ = beam energy in units of the rest mass, r_e = classical electron radius, ξ = linear tune shift, ε = beam emittance, β_y^* = vertical beta function at the interaction point (IP), κ = coupling factor.

To get a high luminosity, we have chosen a reasonable value of the single bunch luminosity L_o, comparable to the one achieved in the VEPP-2M machine [2], and a very high number of bunches. To gain the factor h in the luminosity, without a reduction of the maximum tune shift, the bunches have to be kept separated out of the interaction point. Therefore the two beams circulate in two separate rings crossing at an horizontal angle 2θ in two interaction points.

For flat beams, the horizontal crossing should not excite synchro-betatron resonances, which limit the maximum achievable tune shift, due to the reasonably small value of the geometrical factor:

$$a = \theta \frac{\sigma_z}{\sigma_x^*} = .14$$

where σ_x^* is the r.m.s. horizontal size at the IP and σ_z is the bunch length.

In Table I the parameters relevant to the luminosity are given.

Table I - DAΦNE design parameters

E (MeV)	510.	θ (mrad)	10÷15
L_o ($cm^{-2}s^{-1}$)	$4.5\ 10^{30}$	σ_x^* (mm)	2.
κ	.01	σ_y^* (mm)	.02
ξ	.04	σ_z (m)	.03
ε^{max} (m-rad)	10^{-6}	h^{max}	120
β_x^* (m)	4.5	f_o (MHz)	3.17
β_y^* (m)	.045	N^{max} /bunch	$8.9\ 10^{10}$

A complete lattice overview is presented in [3]. The machine is based, as much as possible, on conventional technology. The challenge is the very high design current: RF and feedback systems have to be carefully studied in order to get rid of multibunch instabilities and the vacuum system has to cope with a very high synchrotron radiation power.

The commissioning strategy is, first of all, to maximize the single bunch luminosity: the design has enough flexibility to fine tune most of the parameters appearing in Table I. Then the total luminosity will be raised by gradually increasing the number of bunches.

The short term luminosity goal can be reached with 30 bunches. As explained in the following, the achievement of 10^{33} $cm^{-2}s^{-1}$ requires the improvement of the crossing region geometry to overcome the problems connected to parasitic crossings and the upgrade of the longitudinal multibunch feedback system.

---

* Double Annular Φ-factory for Nice Experiments.

** A. Aragona, S. Bartalucci, M. Bassetti, M.E. Biagini, C. Biscari, R. Boni, A. Cattoni, V. Chimenti, A. Clozza, S. De Simone, D. Di Gioacchino, G. Di Pirro, A. Esposito, S. Faini, R. Fedele, G. Felici, A. Gallo, A. Ghigo, S. Guiducci, H. Hsieh, S. Kulinski, M.R. Masullo, C. Milardi, M. Modena, L. Palumbo, M. Pelliccioni, M. Preger, G. Qiao, G. Raffone, C. Sanelli, F. Sannibale, M. Serio, F. Sgamma, B. Spataro, A. Stecchi, T. Tanabe, L. Trasatti, C. Vaccarezza, V. G. Vaccaro, L. Verolino, M. Vescovi, S. Vescovi, G. Vignola, J. Wang, M. Zobov.

3. INTERACTION REGION

The machine has two 10 m long interaction regions. The low-β quadrupoles are .45m far from the IP and are confined in a cone of 8.5° half aperture, leaving a free solid angle for the apparatus of 99%. The only solution to fit them in such a narrow space is to use permanent magnet quadrupoles.

On one interaction region there is an experimental detector with a .6T, 5m long solenoidal field. A correction scheme to compensate the coupling due to the solenoid is presented below.

3.1 Parasitic crossing points

One of the main problems in going to very high collision frequency is that of the unwanted parasitic crossing points. We have adopted a scheme whereby the separation at the interaction regions is given only by the horizontal crossing angle at the IP.

The crossing angle has to be kept small in order to avoid synchro-betatron resonances. Anyway, an interaction region design suitable to work with all the 120 bunches, i.e. a maximum collision frequency of 368 MHz, is necessary. Two different configurations are presented here, both with β_y^* = .045 m:

- β_x^* = 4.5 m and θ = 10 mrad
- β_x^* = 3.0 m and θ = 15 mrad.

From beam-beam simulations [4], it seems that the minimum required separation between the two beams at the parasitic crossings should be at least 7 σ_x, since particles in the tails must not see the non-linear field in the core of the other beam. Table II shows the ratio $2\Delta x/\sigma_x$ for the two crossing angles: the above criterion is satisfied with 60 bunches for 10 mrad and with 120 bunches for 15 mrad.

An estimate of the influence of the parasitic crossings on the luminosity is the corresponding value of the tune shift parameter ξ^p in both planes. This is also shown in Table II, for the two cases, as a function of the number of bunches N_b and the bunch spacing s. In the worst case (N_b = 120 and 60) the parasitic tune shifts are less than 10% of that at the IP, for N_b = 30 this is much smaller, so that a 10 mrad crossing angle is still acceptable.

Table II
First parasitic crossing

θ(mrad)	N_b	s(m)	Δx(mm)	ξ_x^p	ξ_y^p	$2\Delta x/\sigma_x$
10.	120	.4	4.0	.0028	.0022	3.8
10.	60	.87	4.0	.0006	.0037	8.1
10.	40	1.2	14.5	.0002	.0008	13.
10.	30	1.6	20.7	.0002	.0003	15.
15.	120	.4	6.0	.0008	.0010	6.9
15.	60	.81	0.5	.0002	.0016	14.
15.	40	1.2	21.8	.0001	.0003	22.
15.	30	1.6	31.0	.0001	.0001	26.

3.2 Solenoid compensation scheme

Due to the relatively high magnetic field (.6 T), the dimensions (5 m) and the position (the low-β triplet is not shielded) of the detector solenoid, a new approach has been studied to compensate the field integral on the beam trajectory. This method [5], giving to each quadrupole of the triplet a rotation angle around its axis proportional to the field integral at its location, and adding at both ends two shorter (1 m) compensating solenoids (1.5 T), allows to decouple the machine at the IP and at the end of the interaction region, with a small perturbation of the optical functions, easily matched with the following quadrupoles. Since the quadrupoles are fully immersed in the solenoidal field, an ideal compensation scheme would require to continuously rotate the quadrupoles in order to track the rotation generated by the solenoid. This is technically too complicate, therefore four skew quadrupoles, located in the arcs, will be used to compensate the residual coupling.

4. STATUS OF THE PROJECT

The lattice design is completed and exhibits a good dynamic aperture. The sensitivity to alignment and field errors and the vacuum chamber aperture required to get a good beam lifetime have been estimated [3]. A complete single ring parameter list is given in Table III.

Table III
DAΦNE single ring parameter list

Energy (MeV)		510.
Circumference (m)		97.69
Dipole bending radius (m)		1.4
Wiggler bending radius (m)		0.94
Wiggler length (m)		2.0
Wiggler period (m)		.64
Horizontal β-tune		4.87
Vertical β-tune		4.85
Natural chromaticities	Horizontal	-6.9
	Vertical	-16.9
Momentum compaction		.017
Energy loss/turn (KeV):	Bend.magnets	4.27
	Wigglers	4.96
	Total	9.3
Damping times (msec):	τ_z	17.8
	τ_x	36.0
	τ_y	35.7
Natural emittance (m-rad)		10^{-6}
Natural relative rms energy spread		$3.97\ 10^{-4}$
Natural bunch length σ_z (cm)		.81
Anom. bunch length σ_z (cm) @ Z/n = 2 Ω		3.0
RF frequency (MHz)		368.25
Number of bunches		1 ÷ 120
Max. bunch peak current (A)		57.
Max. total average current (A)		5.3
Max. synchrotron power/beam (KW)		49.
V_{RF} (KV) @ Z/n = 2 Ω		254.
Parasitic losses (KeV/Ω) @ σ_z = 3 cm		7.

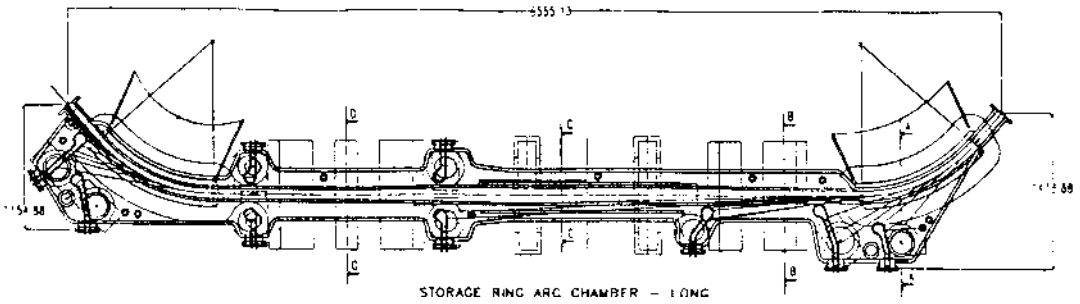

Figure 1. Storage Ring Arc Vacuum Chamber.

4.1 Vacuum system

The vacuum system for the Linac, accumulator and transfer lines will make use of standard technologies, like stainless steel for the vacuum chamber and sputter ion pumps for the pumping system; no *in situ* bake-out is foreseen. The working pressure will be in the range of low 10^{-8} Torr. The storage rings vacuum system [6] must reach a pressure of 10^{-9} Torr with 5 A of stored beam current. Such a requirement will be satisfied only by using advanced technologies, like aluminum vacuum chambers, synchrotron light absorbers and a combination of titanium sublimators and sputter ion pumps for the main pumping system. The project of the chamber for the whole complex has been completed. In Fig.1 the storage ring arc chamber design is shown.

4.2 RF cavity

The multibunch instability is one of the most serious concerns for the high luminosity, high current operation of DAϕNE. Much effort is presently put in the development of a 'single-mode' cavity [7], with the lowest contents of HOMs. Various damping techniques are investigated, in order to optimize the cavity final design. A prototype of a Single Trapped Mode Resonator [8] consisting of a pill-box with 3 waveguides and dissipative loads is presently being measured. The effect of various absorbing materials is also thoroughly investigated. A prototype of the 'day-one' accelerating cavity has been designed and its construction will be committed to industry soon. Its main feature is the presence of very long tapers, to reduce both the total loss factor and the effect of transverse deflecting modes.

4.3 Feedback system

A preliminary study of the growth rate of the longitudinal multibunch instabilities has evidenced the need for a powerful active feedback system. The proposed system [9] is a bunch by bunch, time-domain feedback. The preliminary design is a mixed analog/digital feedback system employing Digital Signal Processor techniques, which can be used with 30 and is upgradable to 120 bunches, capable of a damping time of 0.1-0.2 ms.

4.4 Injector complex

The Linac, operating at full energy with a repetition rate of 50 Hz, has been committed turn-key to industry. The delivery time, with a 10 mA e^+ beam as acceptance test, is two years from now. In Table IV the main parameters for electrons and positrons are shown.

Table IV
Linac parameter list

	e^-	e^+
Max energy (MeV)	800	590
Emittance (m-rad)	10^{-6}	10^{-5}
Rel. energy spread	±.005	±.01
Pulse width (ns)	10.	10.
Peak current (mA)	150.	40.

A compact positron/electron accumulator, at 510 MeV, is used to damp the longitudinal acceptance and the transverse emittance of the linac beam, thus relaxing the injection requirements in the design of the main rings. All the details can be found in [10]. The magnetic structure is made of four quasi-achromatic bending sections and four long straights to accommodate RF, injection and extraction pulsed elements. Two channels will transport the beams from the Linac to the accumulator. Positrons will be injected from one channel and extracted from the other one, while electrons will follow the opposite path. The extraction of the single damped bunch will take place at 1 Hz, filling one main ring bucket at a time. The design of the transfer lines to the DAΦNE ring has been completed too.

4.5 Magnetic components

The magnetic components design is well advanced. Details can be found in [11]. Their procurement will begin within few months.

5. REFERENCES

[1] The DAΦNE Project Team: "DAΦNE: the Frascati Φ-Factory",Proc. IEEE 1991 PAC, S.Francisco, May 1991.
[2] P.M.Ivanov et al, Proc. of the Third Advanced ICFA Beam Dynamics Workshop, Novosibirsk, 1989, p.26,(1989).
[3] M.E. Biagini et al, This conference, TUP092A.
[4] A.Hutton, M.S.Zisman: "An Asymmetric B Factory Based on PEP", Proc. IEEE 1991 PAC, S.Francisco, May 1991.
[5] M. Bassetti, M.E. Biagini, DAΦNE Technical Note L-5, to be published.
[6] V.Chimenti et al, This conference, TYP142B.
[7] S.Bartalucci et al, This conference, FRP102D.
[8] G.Conciauro, P.Arcioni, Proc. of EPAC 90, Nice, France, 1990,p.149, (1990).
[9] M.Bassetti et al, This conference, TUP042D.
[10] R.Boni et al: "The Frascati Φ-Factory Injection System", Proc. IEEE 1991 PAC, S.Francisco, May 1991.
[11] H.Hsieh et al, This conference, FRP023B.

DAΦNE Lattice Update

M.E. Biagini, S. Guiducci, M.R. Masullo, G. Vignola
INFN Laboratori Nazionali di Frascati
C.P. 13 - 00044 Frascati (Roma) - Italy

Abstract

The final version of the lattice for the DAΦNE main rings is presented. This solution satisfies all the design requirements and has a larger dynamic aperture respect to the previous one. A systematic analysis of the effect of magnetic errors on the dynamic aperture has been performed on it. The criteria for the choice of the vacuum pipe aperture are discussed and the beam lifetime is calculated.

1. INTRODUCTION

An improved version of the DAΦNE high emittance lattice[1] is presented. The basic criteria of the design are the same as in [2], but the structure of the arcs has been slightly modified in order to achieve a better β separation at the location of the chromaticity correcting sextupoles, and a higher momentum compaction. Moreover, a new working point has been chosen in order to improve the dynamic aperture and a more realistic model for the wiggler magnet has been adopted. Let us remind that each ring is divided in a long and a short part, for simplicity called hereafter *Long* and *Short*, each simmetrically reflected.

2. BEAM OPTICS

The optical functions of half of the ring (*Short* and *Long*) are shown in Fig 1. In Table I the single ring lattice parameters are shown.

The working point is below the integer in both planes: this results in a larger dynamic aperture.

The **low-β insertion** is essentially the same as in the previous design (quadrupole lengths and strengths have been slightly modified).

Table I
Single ring lattice parameters

Circumference (m)	97.69
Horizontal betatron tune Q_x	4.87
Vertical betatron tune Q_y	4.85
Horizontal natural chromaticity Q'_x	- 6.9
Vertical natural chromaticity Q'_y	- 16.9
Emittance ε (m-rad)	1.0×10^{-6}
Energy loss/turn with wigglers (keV)	9.3
Momentum compaction α_c	0.017
Betatron damping time τ_x (msec)	36.02
Relative energy spread (rms)	3.97×10^{-4}

In the **achromat**, the D quadrupole near to the second bending magnet has been eliminated and the vertical focusing is provided by the parallel faces of the dipole. This gives a very good separation of the β-functions at the sextupole locations. Moreover the lattice has been modified in order to have a similar structure between *Short* and *Long* and to place the F and D sextupoles in the same locations.

The main modification for the ***Long* straight section** is the decision to allow a non-vanishing negative dispersion in the injection region, in order to obtain a higher value of the momentum compaction. In fact the value of the momentum compaction has an influence on the instability thresholds and on the RF parameters.

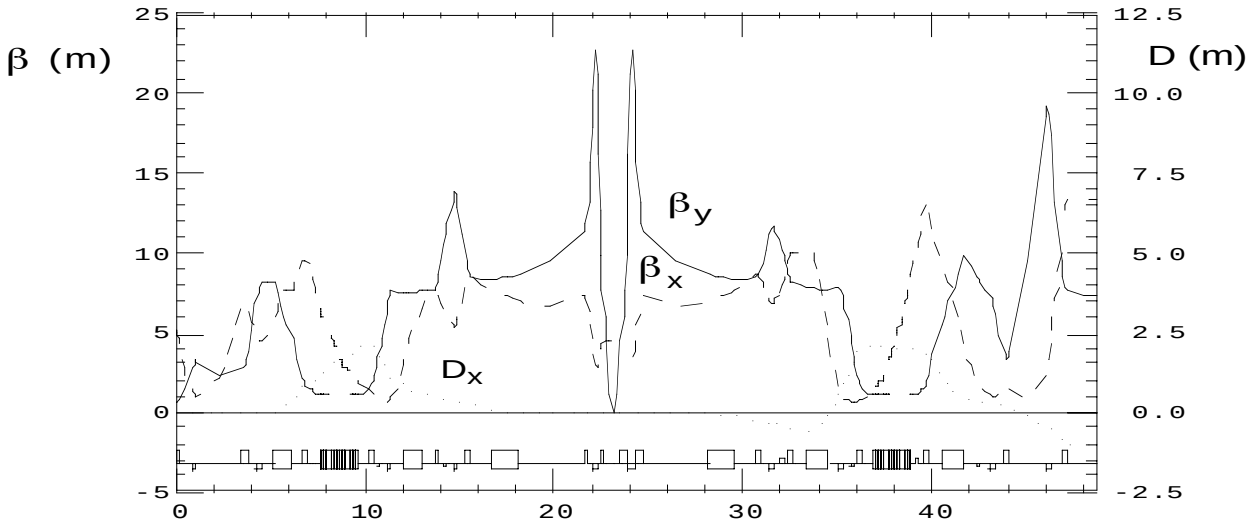

Fig. 1 - Optical functions for half ring

Due to the low value of the energy spread of the beam coming from the accumulator (~10^{-3}) the injection efficiency should not be affected by a dispersion of about one meter at the injection point.

The horizontal betatron phase in the *Long* is related to the value of the dispersion in the injection section, therefore, to easily tune the betatron wavenumber of the ring in both planes, a quadrupole has been added in the *Short* (which still has zero dispersion in the RF straight section).

3. THE DYNAMIC APERTURE

The good separation of the optical functions in the arcs allows a more efficient chromaticity correction, with lower sextupole strengths and therefore less sensitivity to the resonances and a larger dynamic aperture.

The total tunes, 4.87 for the horizontal and 4.85 for the vertical one, are quite far from the integer. The resulting tune and beta functions dependence from the energy is very good.

The dynamic aperture is quite good: as large as the vacuum chamber in the horizontal plane and much larger in the vertical one (± 14 σ_x out coupling in the horizontal plane and ±26 σ_y full coupling in the vertical).

Fig. 2 shows the the on-energy dynamic aperture at the IP, compared to the off-energy ones. There is a small reduction for positive energy deviations and an increase for the negative ones. For comparison the physical aperture is shown on the same scale.

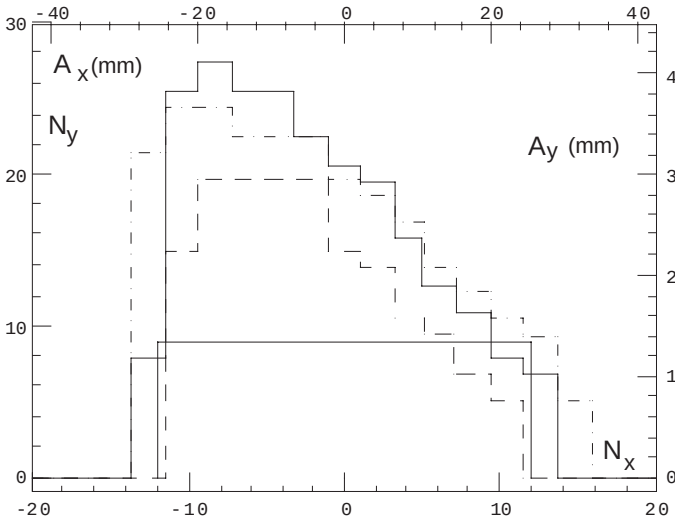

Fig. 2 - Dynamic aperture for Δp/p=0 (solid line), .5% (dashed), -.5% (dot-dashed) compared with the vacuum chamber aperture (solid)

3.1 Multipole errors sensitivity

The effect of sistematic multipole errors in the magnetic elements on the dynamic aperture has been simulated with the code Patricia. We have considered separately the effect of each type of multipole term. The strength for the multipolar coefficients has been calculated assuming for each one a value of $\Delta B/B = 5\ 10^{-4}$ at 3 cm from the center. We have considered: dodecapoles in the quadrupoles, sextupoles and decapoles in the dipoles and sextupoles in the wigglers.

The results of these simulations have been used to give upper limits for the design of the magnetic components.

Finally we have made a simulation inserting all together the multipolar terms calculated from the magnet design[4] for both bendings and quadrupoles. The resulting dynamic aperture for three different values of the relative energy deviation (Δp/p = +.5%,0 and -.5%) is shown in Fig. 3.

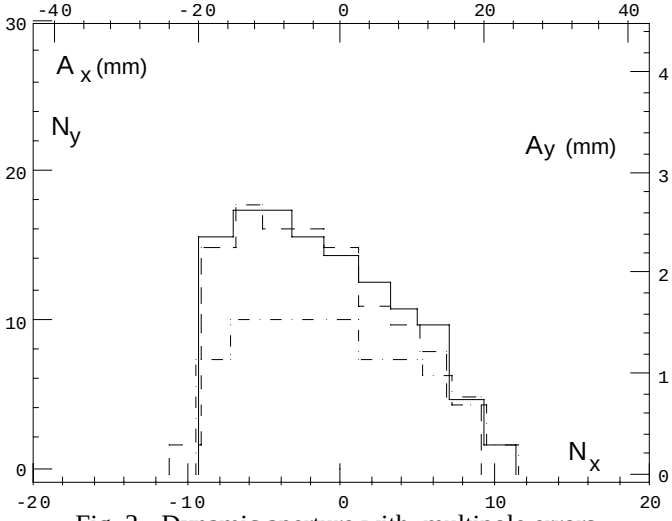

Fig. 3 - Dynamic aperture with multipole errors Δp/p=0, .5%, -.5%

4. ALIGNMENT TOLERANCES AND ORBIT CORRECTION

At the start-up, our idea [5] is to run the machine without sextupoles, operating at low current. At this stage the possibility of a quadrupole mechanical displacement, to correct the orbit distortion, is foreseen to perform a first alignment correction. Later on all the sextupoles are switched on and an appropriate corrector scheme can be used to minimize the residual closed orbit distortion.

The computer code MAD[6] has been used to study the machine sensitivity to errors and to look for an optimal corrector configuration in three different cases: without and with sextupoles and finally adding monitor errors.

The study on the lattice sensitivity, assuming error values from experience in operating machines, has shown that the particle orbit remains inside the physical aperture of the machine, ± 4 cm in horizontal and ± 3 cm in vertical.

No errors have been included in the wigglers and in the low-β quads, that are to be treated as a separate problem. In particular due to the lack of space for correctors and monitors in the low-β, the possibility of correcting the orbit by just moving the magnetic elements has been considered .

The following errors have been assumed in all bends and quads:

$$\Delta x = \Delta y = 0.2 \text{ mm};$$

$$\Delta\theta = \Delta\Phi = 0.25 \text{ mrad}; \quad \Delta B/B = 5 \times 10^{-4}$$

The proposed layout includes 30 beam position monitors and 18 correctors. In **Table II** the averaged data before and after correction are reported, compared with the ideal ones, for the case with sextupoles on and monitor misalignment errors $\Delta x=\Delta y$ = 0.2 mm.

Table II

Closed orbit parameters before and after correction

	no errors	before corr.	after corr.
X_{rms} (mm)	0	7.7±5.7	0.44±0.16
X_{max} (mm)	0	16.8±10.9	1.35±0.48
Y_{rms} (mm)	0	3.2±1.3	0.36±0.09
Y_{max} (mm)	0	8.48±3.38	1.01±0.25
α_{Xrms} (mrad)	0		0.46±0.09
α_{Xmax} (mrad)	0		0.96±0.23
α_{Yrms} (mrad)	0		0.31±0.09
α_{Ymax} (mrad)	0		0.72±0.29
β_x (m) @ IP	4.5	4.49±0.58	4.52.±.006
β_y (m) @ IP	0.045	0.0456±0.012	0.0451±.0008
η_x (m) @ IP	0	-.18±0.30	-.014±0.046
η_y (m) @ IP	0	-0.009±0.038	-.0006±0.003

The results are satisfactory showing a maximum residual orbit less than 1.5 mm in the horizontal plane and around 1 mm in the vertical one with a corrector strength always lower than 1 mrad.

5. BEAM LIFETIME AND VACUUM CHAMBER APERTURE

Due to the low energy of the machine, the main effect limiting the beam lifetime is the single Touschek scattering, which gives a lifetime proportional to the third power of the energy. The Touschek lifetime has been calculated using the formulae given by H. Bruck[7], assuming that the machine acceptance is limited by the RF bucket height and by the transverse aperture (physical or dynamic aperture).

The parameters used for beam lifetimes calculations, listed in **Table III**, correspond to the design values for the maximum luminosity. The bunch length has been calculated in the anomalous lengthening regime, assuming a vacuum chamber broad band impedance of 2 Ω.

The Touschek lifetime is very sensitive to the horizontal aperture R_x (increases nearly linearly with the aperture up to 10 cm). The choice of the aperture is crucial for this machine because we want a high emittance (for high peak luminosity) and a good beam lifetime (for high average luminosity). Therefore we want the largest vacuum chamber aperture compatible with the technical constraints; moreover also the dynamic aperture has to be as large as the physical aperture. We have chosen a value of R_x = 4 cm, which gives a Touschek beam lifetime of nearly three hours.

The vertical vacuum chamber aperture has been chosen in order to get a good value of the gas scattering beam lifetime. With a value of 3 cm the scattering lifetime, calculated assuming a gas pressure of 1nTorr with a nitrogen equivalent gas composition (Z = 8), is ~17 hours, much larger than the Touschek lifetime, and therefore has a small influence on the total lifetime.

In **Table III** the contributions of the various phenomena to the beam lifetime for the single beam mode are listed, together with the beam-beam bremsstrahlung lifetime.

We want to point out that, due to the choice of many bunches and high crossing frequency, the beam-beam bremsstrahlung gives a negligible contribution to the beam lifetime also at the maximum luminosity.

Table III

Beam lifetime

N particles/bunch	$8.9\ 10^{10}$
RF energy acceptance	1.23%
Bunch length (cm)	3
Relative energy spread	$1.46\ 10^{-3}$
Coupling factor	.01
Single beam lifetime (min):	
Quantum lifetime	$8.18\ 10^{9}$
Gas bremsstrahlung	1832
Gas scattering	967
Touschek	207
Total	156
Two beams lifetime @ L=6.0 10^{32} cm^{-2} s^{-1}:	
Beam-beam bremsstrahlung	1426
Total	141

REFERENCES

[1] M.E. Biagini, S. Guiducci, M.R. Masullo, G. Vignola: "DAΦNE lattice update", DAΦNE Technical Note L-4, 2/12/1991.

[2] M. Bassetti, M.E. Biagini, C. Biscari, S. Guiducci, M.R. Masullo, G. Vignola: "High Emittance Lattice for DAΦNE", DAΦNE Technical Note L-1, 30/10/1990.

[3] H. Wiedemann: "Users guide for PATRICIA Version 85.5", SSRL ACD Note 29.

[4] C. Sanelli, private communication.

[5] M.R. Masullo: "Orbit Correction Analysis for DAΦNE Lattice", DAΦNE Technical Note L-3, 12/4/1991.

[6] H. Grote, F.C. Iselin: "The MAD Program", CERN/SL/90-13 (AP).

[7] H. Bruck: "Accélérateurs circulaires de particules", Presses Univérsitaires de France, 1966.

DAΦNE Vacuum System

V. Chimenti, A. Clozza, H. Hsieh, C. Vaccarezza
INFN Laboratori Nazionali di Frascati
C.P. 13 - 00044 Frascati (Roma) - Italy

Abstract

The preliminary design for an all metal ultra high vacuum (UHV) system for DAΦNE machine is described. The machine is composed by 4 main items: linac, accumulator, transfer lines, and storage ring; each item has its own vacuum system designed accordingly with the operating requirements. The linac will be bought turn on key from an external firm, with its vacuum system, the accumulator and transfer lines vacuum systems will be made using standard technologies capable to reach a working pressure in the range of 10^{-8} torr, the storage ring vacuum system will be made using special technologies in order to obtain a pressure of $1 \cdot 10^{-9}$ torr with 5 A of stored beam current.

1. INTRODUCTION

The vacuum system designed for DAΦNE machine will provide the required working condition needed to reach the luminosity goal, at $\gamma = 1000$, of $L = 2.6 \cdot 10^{32}$ cm^{-2} s^{-1} with 60 stored bunches.

The required vacuum pressure is $1 \cdot 10^{-9}$ torr with two stored beams of 5 A each, this pressure value is mainly needed to obtain a low background noise in the interaction region and to give a contribution as small as possible to the beam life time, already limited by Touschek scattering.

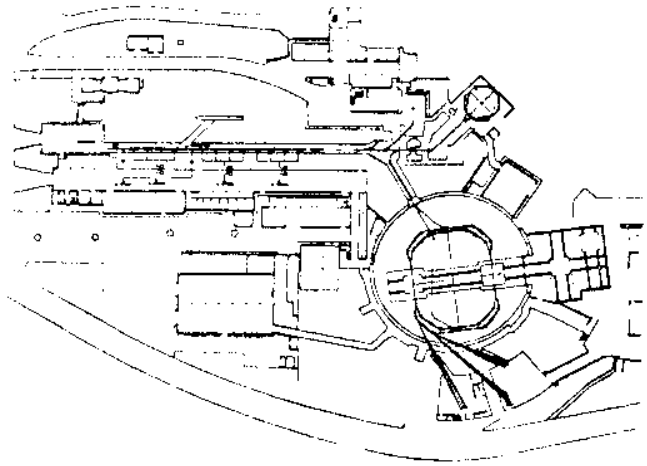

Figure 1. The DAΦNE project layout

2. LINAC VACUUM SYSTEM

The vacuum system of the linear accelerator will be supplied from the firm according to our specifications, and it must be able to reach a pressure in the range of 10^{-8} torr. All the pumps (fore vacuum and high vacuum) must be oil free.

3. ACCUMULATOR VACUUM SYSTEM

3.1. Machine vacuum related parameters

The vacuum system for an electron storage ring is closely related to certain machine parameters, in table 1 the vacuum related parameters are listed.

Table 1
Vacuum related parameters for the accumulator

Beam energy (MeV)	510
Beam current (mA)	130
Dipole bending radius (m)	1.1
Maximum working pressure (torr)	$\sim 10^{-8}$
Photon flux (phot/s)	$5.4 \cdot 10^{19}$
Synchrotron light critical energy (eV)	270

3.2. Vacuum chamber

The vacuum chamber of DAΦNE accumulator will be made of 304 L stainless steel, its shape is: in the straight sections a cylindrical pipe 291 cm long and 85 mm inside diameter, in the kicker section a 200 mm inside diameter pipe, and in the curved sections an almost rectangular pipe 86.5 cm long and 30 by 100 mm inside aperture. No in situ bake out is foreseen for the accumulator, so a very well cleaned (even with glow discharge) [1,2] and prebaked sections of the vacuum chamber must be employed. The ring, shown in fig 2, is divided into four arcs by five sector valves: two valves will isolate the RF cavity, and the other three will be placed one in each remaining long straight section.

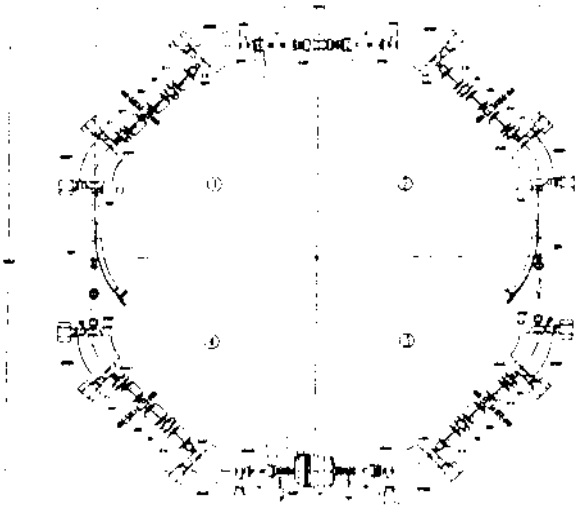

Figure 2. The accumulator ring.

3.3. Pumping system

The high vacuum pumping system for the accumulator must provide a sufficient pumping speed to reach a pressure P in the range of low 10^{-8} torr with a maximum of 130 mA of stored beam, such a current produce a photodesorbed gas load Q of about $2 \cdot 10^{-5}$ torr l/s, so the required pumping speed S is:

$$S = \frac{Q}{P} = 2000 \text{ l/s} \qquad (1)$$

a value easily obtained with traditional lumped sputter ion pumps. A total of 16 pumps are placed along the accumulator vacuum chamber, one of 200 l/s on the RF cavity, one of 400 l/s in the middle of the kicker straight section and the remaining 14 pumps, 200 l/s each, are placed at each end of bending magnets, connected as close as possible to the vacuum chamber via a short pipe, in this way is possible to obtain an effective total pumping speed, taking into account the conductances of the connecting pipes with the vacuum chamber, of about 2000 l/s.

The fore vacuum system consists of a portable magnetic bearing turbo molecular pump backed by an oil free mechanical pump, this system is able to reach a pressure of 10^{-5} torr.

4. TRANSFER LINES VACUUM SYSTEM

A system of vacuum transfer lines, about 130 m long, is used to connect the linac, the accumulator and the main ring, the working pressure of this system is about 10^{-8} torr. 304 L stainless steel has been selected for the beam pipe, no in situ bake out is foreseen except for about 10 m at the entrance to the main ring. The vacuum pipe will be prebaked and cleaned with glow discharge before installation.

The pumping system for the transfer lines is based on sputter ion pumps. Because the conductance of the pipe is about 20 l/s for meter, and the gas load is $2 \cdot 10^{-8}$ torr l/s per meter of vacuum pipe, a 100 l/s pump every 10 meters is sufficient to reach a pressure of about 10^{-8} torr.

The fore vacuum system is the same as for the accumulator.

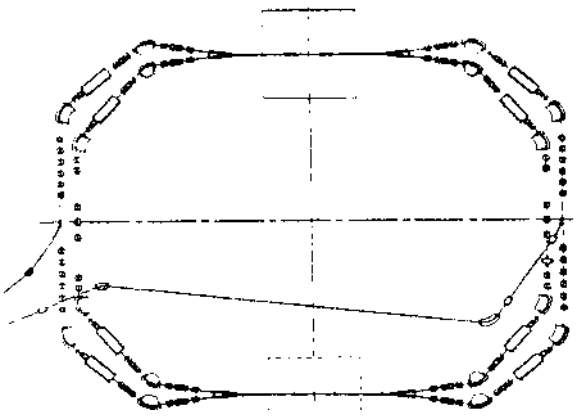

Figure 3. DAΦNE storage rings layout.

5. STORAGE RING VACUUM SYSTEM

5.1. General

The DAΦNE machine is made by two intersecting storage rings, see figure 3, one for electrons and the other one for positrons.

The vacuum system goal is to reach a mean pressure P = $1 \cdot 10^{-9}$ torr with a stored beam of 510 MeV and 5.5 A of full current.

Table 2
Vacuum related parameters for the storage rings

Beam energy (MeV)	510
Beam current (A)	5.5
Dipole bending radius (m)	1.4
Maximum working pressure (torr)	$1 \cdot 10^{-9}$
Dipole photon flux (phot/s)	$2.9 \cdot 10^{20}$
Wiggler photon flux (phot/s)	$3.3 \cdot 10^{20}$
Dipole synchrotron light critical energy (eV)	220
Wiggler synchrotron light critical energy (eV)	330
Total synchrotron radiation power/beam (kW)	50

5.2. Synchrotron radiation photon flux and thermal load

The very high value of the stored current generates high gas desorption so special and unusual solution are needed in order to obtain the desired mean pressure in the vacuum chamber. In our case the total number of photons emitted per second from the bending magnets is:

$$\frac{dN}{dt} = 8.08 \cdot 10^{20} \cdot E \cdot I = 2.3 \cdot 10^{21} \frac{\text{phot.}}{\text{s}} \qquad (2)$$

with E in GeV and I in A. For the wigglers a detailed calculations give a value of $3.3 \cdot 10^{20}$ phot./s. The emitted power form the bending magnets is:

$$P = \frac{88.5 \cdot E^4 \cdot I}{\rho} = 24 \text{ kW} \qquad (3)$$

with E in GeV, I in A and ρ in m. The emitted power from a wigglers is about 6.5 kW.

In this machine the synchrotron light is generated locally in that sectors, called arcs, including a wiggler magnet and the two neighboring bending magnets. In each arc we have a total photon flux of $9 \cdot 10^{20}$ phot./s and an emitted power of about 13 kW. Assuming for the desorption efficiency η the value $1 \cdot 10^{-6}$ mol/phot, after conditioning [3], the gas load Q for each arc is $3 \cdot 10^{-5}$ torrl/s, that in order to obtain a pressure P = $1 \cdot 10^{-9}$ torr a total pumping speed S, given by equation (1), of 30000 l/s is needed. To cope with such high gas loads some special criteria must be followed for the design of the vacuum system: no photons must hit the vacuum chamber walls, all the synchrotron radiation must be intercepted, possibly at normal incidence [4], by water cooled photon absorbers, the vacuum pumps must be located as close as possible to the photon absorbers, the thermal load of the synchrotron radiation must be dissipated.

5.3. Vacuum chamber

Three materials are mainly used in vacuum technology: stainless steel, aluminum and copper. The arc vacuum chamber, see figure 3, will be made using 6061-T4 aluminum alloy, because of its low outgassing rate, even after a 150° C

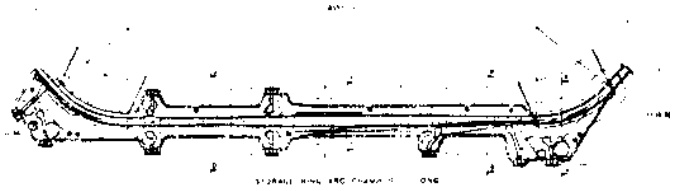

Figure 3. Arc vacuum chamber

bake out, its high thermal conductivity, and it is easily machinable and also the chemical cleaning treatments are easy. In figure 4 it is shown the cross section of the arc vacuum chamber in correspondence of a quadrupole.

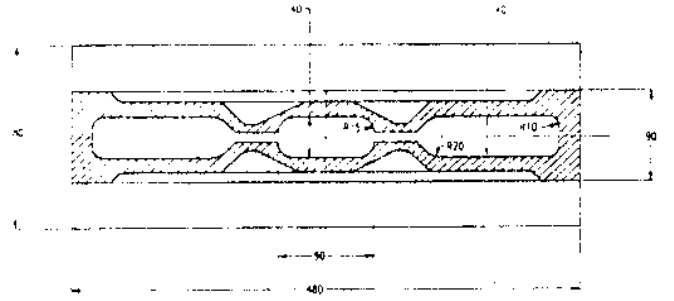

Figure 4. Arc vacuum chamber cross section (quadrupole)

The synchrotron radiation absorbers will be made using a rod of OFHC copper with a water cooling channel in order to take away the synchrotron radiation thermal load.

The straight sections vacuum chamber does not present any particular requirement, its cross section is almost rectangular and a not so high photon flux hits the vacuum chamber, in this case it is possible to use 316-L stainless steel for the vacuum pipe.

5.4. Pumping system

The very high and concentrated gas load and the relatively little room to put pumps bring us to discard the following pumping system solutions: non evaporable getters, distributed sputter ion pumps, lumped sputter ion pumps and other similar devices.

The only solution that seems to give some positive results is to use very big pumps concentrated placed over the gas sources, the absorbers, in order to increase as much as possible the conductance from the pump to the source. The devices that can give the needed pumping speed are: titanium sublimators, cryopumps and turbo molecular pumps. Excluding the solutions with cryopumps and turbomolecular pumps because they are very expensive and they need maintenance, our choice falls on the titanium sublimation pumps. This kind of pumps are cheap, they need very low maintenance and they can give a very high pumping speed, about 8 l/s for each square centimeter of active surface, so a pump with a inner surface of 4000 cm^2 will have about 3200 l/s of pumping speed for CO, in this case we need a total of 10 titanium sublimation pumps for each arc. Using sublimators we must take into account that they do not pump noble gases and methane, that is produced by the interaction of the synchrotron radiation with the residual gas and with the inner walls of the vacuum chamber; a possible solution to this problem is to add a few sputter ion pumps capable to pump well noble gases and methane, triode ion pumps are an example. As the desorption efficiency for methane is more than 10 times lower than that for CO, it possible to estimate the required pumping speed in the range of about 1000 l/s at $1 \cdot 10^{-9}$ torr.

The fore vacuum pumping system consists of a portable station composed by a magnetic bearing turbomolecular pump baked by an oil free mechanical pump, this system must be able to reach a pressure in the range of 10^{-7} torr, a pressure at which the ion pumps can easily start.

6. CONCLUSIONS

A fully oil free vacuum system for DAΦNE machine has been designed using both standard and special solutions. The linear accelerator, the transfer lines and the accumulator use a relatively simple vacuum system based on standard technologies, while the storage ring vacuum system requires special solution for the vacuum chamber, made of aluminum machined in a particular shape, and for the pumping system, mainly based on titanium sublimators. The total pumping speed installed on the storage ring is about 250000 l/s over 200 meters of vacuum chamber. With this pumping system is possible to reach the pressure of $1 \cdot 10^{-9}$ torr with stored beam of a maximum current of 5.5 A.

7. REFERENCES

[1] C.L. Foerster, H. Halama, and C. Lanni, J. Vac. Sci. Technol. A8,1990, (2856).

[2] H. Halama, and C. Foerster, Vacuum, 42, 1991, (185).

[3] A. G. Mathewson, O. Gröbner, P. Strubin, P. Marin, R. Souchet, CERN report, CERN/AT-VA/90-21.

[4] O. Gröbner, A. G. Mathewson, P.Strubin, E. Alge, and R. Souchet, J. Vac. Sci. Technol. A7, 1989, (223)

Design of the 1.8 Tesla Wiggler for the DAΦNE Main Rings

C. Sanelli and H. Hsieh
INFN Laboratori Nazionali di Frascati
C.P. 13 - 00044 Frascati (Roma) - Italy

Abstract

This paper describes the electromagnetic and mechanical design of the eight wiggler magnets for DAΦNE Main Rings. The wigglers have a large 1.8 Tesla flat top magnetic field, 64 cm period and 4 cm gap. The magnetic 3-D calculations, the electromagnetic design and the adopted mechanical solutions, with particular attention to the vacuum chamber problems are described. A full scale prototype (5 full poles and two half pole) will be constructed in order to verify the accuracy of magnetic calculations, the end pole design and the multipole content.

1. INTRODUCTION

A 510 MeV electron positron colliding beam facility, known as DAΦNE, is currently under design and construction at INFN's Frascati National Laboratory, Frascati, Italy. The project consists of two storage rings, Accumulator, electron/positron linac and transfer lines. There are four wigglers needed in each storage ring for radiation damping purpose. The magnet is iron core electromagnetic type, the median plane field is 1.8 Tesla at a magnetic gap of 40 mm. It has a period length of 640 mm, a total number of three periods are needed to satisfy the storage ring lattice requirements. We have carried out very careful magnetic calculation, both in two and three dimensional, to assure that both the dipole field uniformity and the higher harmonic content of this magnet are within the limits set by the machine physics group. In view of the critical nature of this wiggler to the performance of the storage rings, we deem necessary to have a full size prototype to verify, by careful magnetic measurements, the validity of our magnetic computations. In addition, the shaping of the end poles and field clamps will also be determined iteratively by the magnetic measurements.

2. ELECTROMAGNETIC DESIGN

2.1. Magnetic computations

The initial profile of the center pole was investigated by utilizing POISSON. The combination of high on-axis field (1.8 Tesla) and long field flat top (16cm) results in very high induction in the steel. therefore a three dimensional study was deemed necessary to obtain more accurate field characteristic of this magnet. The half "full" pole, the end pole and the ending field clamp were simulated by means of Magnus (magnetostatic 3-D code). It was not possible to investigate the entire magnet structure due to the limitation of the mesh point number that even in this simplified case was increased to about 32000. The condition that $\int B_Z * ds = 0$ (where B_Z is the vertical component of the field and s is the longitudinal coordinate) was achieved by few iteration of varying the mechanical length of the end pole. It was decided that the end poles of the prototype will be made 10 mm longer than that of computational result, the final length will be iteratively determined by the magnetic measurements. The following results are referred to this configuration. The transverse dimension of the magnet was optimized to reduce the harmonic content of the magnetic field. Fig. 2.1.1 shows the geometry of the wiggler iron core analyzed by Magnus.

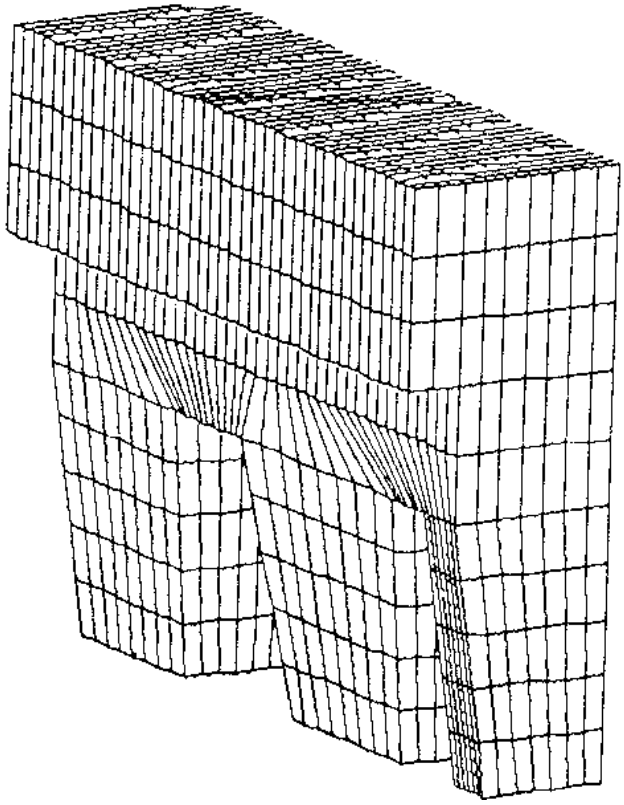

Fig. 2.1.1 - The wiggler iron core simulated in 3-D

The field profile along the longitudinal axis of the magnet, is shown in Fig. 2.1.2.

The maximum positive field is 1.81 Tesla and the negative peak field is -1.65 Tesla. A slight positive overshoot is predicted by the code due to the field clamp, approximately 215 Gauss.

With the above geometry, the $\int B_Z * ds$ is strongly negative (-9553.4 Gauss) mainly due to the end pole length increase. The same integral at 10 mm parallel offset is about -1 Gauss lower. These data give an idea of the transverse field flat top, whose profile, at the wiggler midplane, is shown in Fig. 2.1.3.

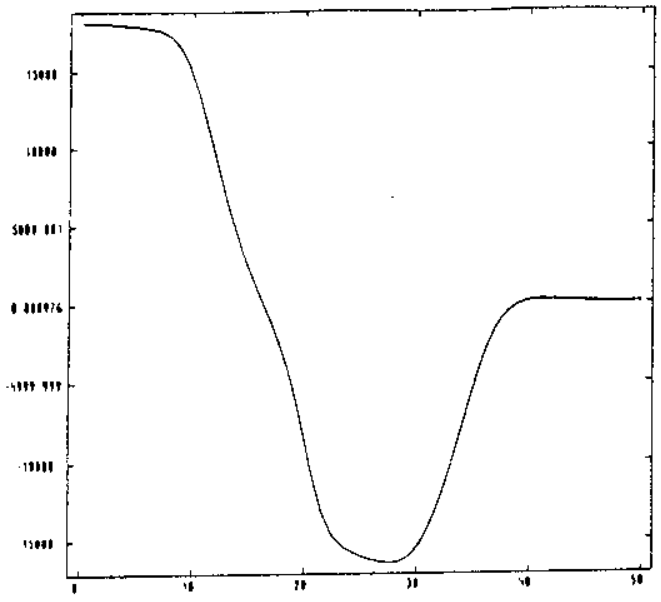

Fig. 2.1.2 - Longitudinal magnetic field profile

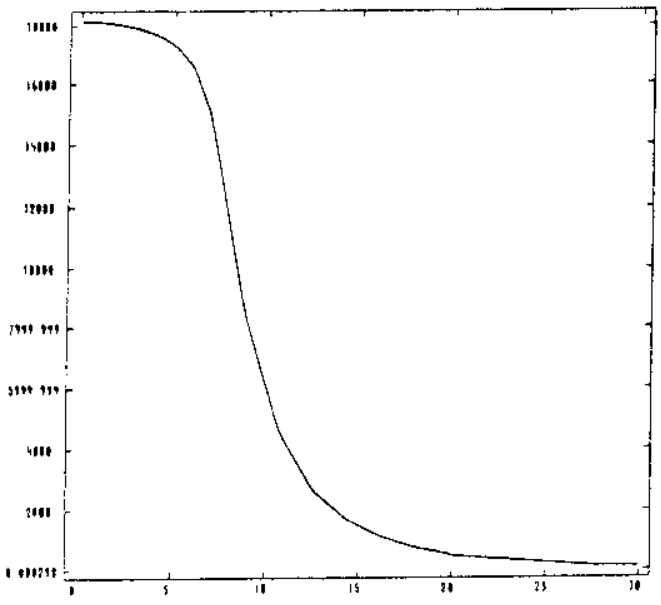

Fig. 2.1.3 - Transversal magnetic field profile

2.2. Electrical and hydraulic design

Following up the magnetic computations, the mechanical dimensions of the wiggler poles have been fixed. The special vacuum chamber for this wiggler imposes strong constraints to the coil dimensions. The coil cross section is rectangular with slight tilt to conform to the shape of the magnet pole. The equivalent electric center of the coil was conscientiously placed as close as possible to the magnet median plane, this results in reducing , pole to pole, magnetic flux with the benefit of increasing the lateral reluctance and then the flat top field at the gap. Table 1 lists the magnet parameters.

Table 1. Wiggler magnet parameters

Nominal beam energy (Mev)	510
Magnetic field at the gap center (Tesla)	1.8
Wiggler period (mm)	640
Number of periods	3
Amper - turns per pole (A)	54000
Turns per pole	80
Cu cond. cross section (mm * mm)	7 * 7
Cooling hole diameter (mm)	4.0
Nominal Current (A)	675
Maximum Current (A)	750
Current density (A/mm^2)	18.5
Max. Current density (A/mm^2)	20.6
Nominal Voltage (V)	376
Max. Voltage (V)	418
Nominal Power (kW)	254
Max. Power (kW)	313
Water circuits per coil in parallel	5
Total cooling water flow rate (l/min)	160
Water velocity (m/sec)	3
Pressure drop (Atm)	4.5
Water temperature increase (°C)	30

3. MECHANICAL DESIGN

3.1 Magnet structure

Figure 3.1.1 shows the complete mechanical design of the wiggler system. The magnet yoke is made of low carbon steel equivalent to AISI 1006 or lower carbon content. The pole pieces are bolted to the return leg with appropriate locating dowels so that they can be detached and modifications can be made during the cause of magnetic measurement. The return leg is made with mechanical stiffness as criteria, it is anticipated that the deflection along the longitudinal direction will be less than 30 micrometers.

Wiggler vacuum chamber is made of aluminum alloy and it is an integral part of the storage ring arc chamber, no mechanical flanging is contemplated. The width of the chamber is in the order of 50 cm wide, the synchrotron radiation will only strike the down stream copper photon absorbers where thermal and gas desorption problems can be effectively dealt with. Due to the width of this chamber, the transverse ribbings are mandatory from both stress and strain points of view. These ribbings prevent the total utilization of the available space between the poles by the coil package. This constraint results in high power consumption to some extent. The axis of the wiggler is 12.5 mm offset from that of vacuum chamber due to the beam orbit offset through the wiggler. The coils are partially nested inside the chamber cavity, the cooling water supply and return will utilize the void space between coils and chamber wall due to the axis offset.

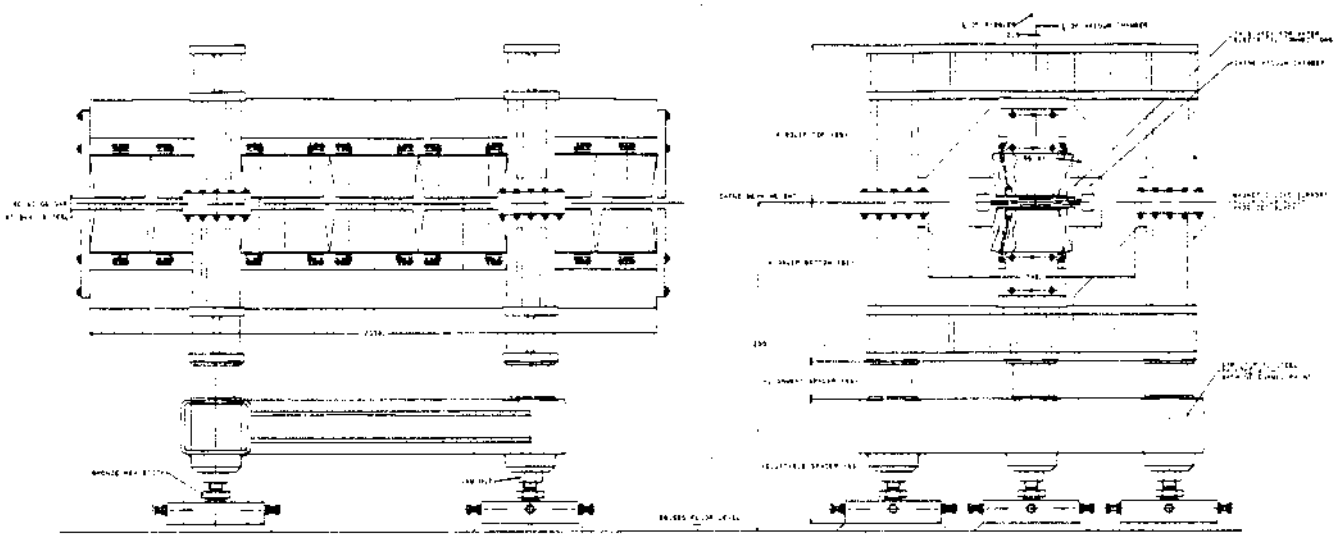

Fig. 3.1.1 - Wiggler system

3.2 Wiggler support structure

The magnetic pressure between the poles is in the order of 40 metric tons. The support structure near the wiggler will be made of non-ferromagnetic material to avoid the possible electromagnetic coupling with the stray field resulting in perturbation to the field quality. The geometry of the vacuum chamber dictates that the wiggler assembly has to be parted along the magnet median plane during the installation process, top half of the assembly to be lifted by building crane, the bottom half assembly to be lowered by removing the alignment spacers. It is further required that re-installation of the wiggler and ring chamber shall need no re-alignment to recover the original placement accuracy, therefore, the locating dowels have to be implemented at all interface planes. The adjustable frame assembly will provide the necessary adjustments during the initial alignment process.

3.3 Wiggler Prototype

There are four wigglers required for each storage ring, total of eight for the total project. The first wiggler delivered by the industry will be utilized as a prototype. Extensive magnetic measurements will be carried out prior to the release of serial production.

Beam Loading in DAΦNE Cavities

M. Bassetti, R. Boni, A. Gallo, *M. Migliorati, *L. Palumbo, M. Serio, L. Verolino
I.N.F.N., Laboratori Nazionali di Frascati
C. P. 13, 00044 Frascati, Rome (Italy)
*University of Rome "La Sapienza", Dipartimento Energetica
via A. Scarpa 14, 00161 Rome (Italy)

Abstract

The beam-cavity interaction is a fundamental topic in high current storage rings and it strongly affects the RF system design in order to avoid coherent instabilities.

In this paper we present some considerations on the DAΦNE beam stability at the RF accelerating mode, according to analytical and numerical evaluations.

Transient and stationary regime results are shown, including the effect of RF amplitude and tuning servo loops.

1. INTRODUCTION

Due to the very high current value foreseen for DAΦNE operation [1] - 1.3 Amps/ring into 30 bunches as short term goal, up to 5.5 Amps/ring into 120 bunches for the highest luminosity - the longitudinal beam stability is among the most challenging task of the project.

The interaction between the beam and cavity spectra can drive any kind of multibunch instability; the rigid mode is a particular multibunch oscillation that arises from the interaction to the cavity accelerating mode. In fact, over some current thresholds, the beam center of mass may be longitudinally unstable as effect of either anti-damping (Robinson limit) [2] or repulsive force (Sands limit) [3].

The aim of this paper is to present some considerations on this topic using two different approaches: a frequency domain analytical method and a time domain code simulation.

The first is a stationary regime analysis based on a simple circuital model representing the beam as a current source at RF frequency [4]. This method allows to predict how much current one can adiabatically store with a given configuration of the RF parameters, but it does not give information on the transient behaviour of the system.

The second is a numerical approach based on a tracking code especially developed to study the beam to cavity fundamental mode interactions in the time domain. The code follows the bunches in the phase space for a selected number of turns starting from the injection, and it describes the transient regime behaviour of the system including the non-linearity of the accelerating field.

2. STATIONARY REGIME ANALYSIS

The main parameters of the DAΦNE RF system are listed in Table I , where Z/n is the machine broadband impedance.

We made our estimations by solving the circuit of Fig. 1 that represents a model of the RF system, including the RF source, the transmission line, the cavity and the beam [4].

Table I
DAΦNE RF System main parameters

RF Frequency	368.25 MHz
Harmonic number	120
RF Peak Voltage	130 kV (@ Z/n=1Ω)
	260 kV (@ Z/n=2Ω)
Bunch Current	43.75 mA
Max Beam Current	5.5 A/120 bunches (@ Z/n=1Ω)
	2.75 A/60 bunches (@ Z/n=2Ω)
Total Losses	16.3 keV/turn (@ Z/n=1Ω)
	23.3 keV/turn (@ Z/n=2Ω)
Cavity Shunt Impedance	2.25 MΩ
Unloaded Cavity Q	30,000
Max Available RF Power	150 kW

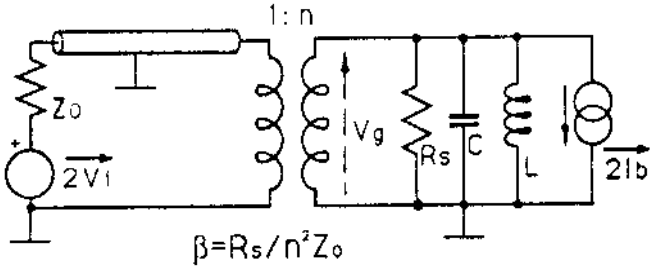

Figure 1. Circuital Model of DAΦNE RF System

This model explicitly takes into account the generator to cavity coupling coefficient β and it gives direct information on the incident power required in the various configurations of the system.

The beam center of mass is stable as long as the cavity tuning angle (the phase of the cavity impedance) is negative [2], and the phase between the bunch and the gap voltage due to the RF generator alone (Sands phase) is positive [3].

These parameters have been calculated at any beam current value using the equivalent circuit of Fig. 1. The gap voltage and the overall tuning angle (including the beam) have been taken as independent variables in the calculations because they are parameters directly controlled by the RF servo loops. Typical results are reported in Figs. 2 and 3. They represents the working point loci of the RF system plotted in a plane having the normalized beam current $Y = 2I_bR_{sL}/Vg$ on the vertical axis [5], where R_{sL} is the loaded cavity shunt impedance, and the overall tuning angle ϕ_L on the horizontal one.

Shaded areas are the forbidden regions due to Sands and Robinson limits, together with RF main power limitation.

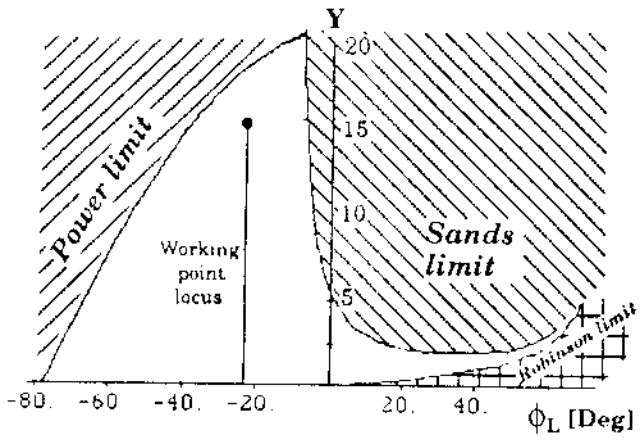

Figure 2. Working Point Locus (@ 130 kV)

The curves have been calculated for a beam current from 0 to 2.7 Amps, equivalent to 60 bunches stored in the Z/n=2Ω case. The coupling coefficient β has been set to 5 to well match the full beam current.

The gap peak voltage has been set to the minimum value (130 kV) in Fig. 2 , which is the worst operating situation for the center of mass stability, and to the nominal value (260 kV) in Fig. 3. The working point paths are vertical segments because the overall tuning angle is kept constant at any current by the dedicated servo loop.

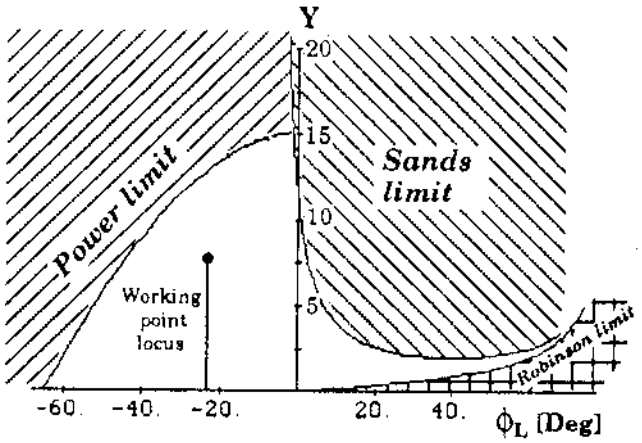

Figure 3. Working Point Locus (@ 260 kV)

The plots of Figs. 2 and 3 show that positive values of ϕ_L lead the system to Robinson instability at low current and to Sands instability at high current. The "compensate case" ϕ_L = 0 becomes unstable crossing the Sands limit at high current for any gap voltage lower than the nominal value (260 kV).

A fully stable configuration is achieved setting a negative ϕ_L value (ex. : ϕ_L = - 23 Deg). In this case the working point lays roughly in the middle of stability region between Sands and power limits.

However these fully stable configurations of the RF system have a rather small stability margin. The possibility to install a fast RF feedback chain to lower as much as possible the apparent beam loading should be considered [5].

3. THE TIME DOMAIN TRACKING CODE

Transient effects are not included in the previous results. Nevertheless they are not negligible and they have to be studied carefully both because the stability margin is always small and the injection of a whole bunch in a single shot can not be considered adiabatic. A Time Domain Tracking Code has been developed to take them into account.

A schematic flow chart of the code is shown in Fig. 4.

The code simulates the injection of the N^{th} bunch with a certain phase and energy errors while the other N-1 are in the equilibrium position on the synchronous phase. Each bunch interacts to the cavity and evolves in the machine turn by turn accordingly to its own instantaneous phase and energy errors, while the wakefields left in the cavity are responsible for the coherent motion. So the code follows each bunch in the longitudinal phase space.

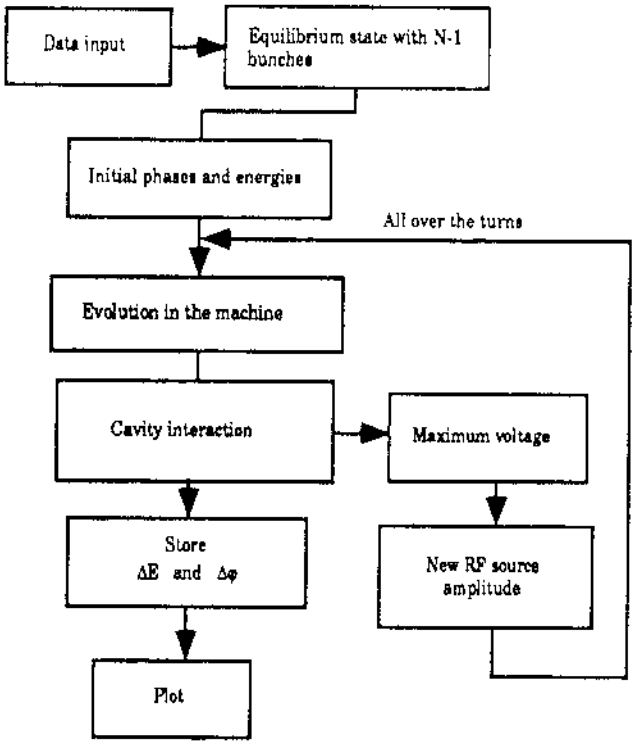

Figure 4. Tracking Code Flow Chart

The schematic model for the bunch to cavity interaction together with the RF supply and the RF amplitude feedback circuit are shown in Fig. 5.

The bunches are treated as macroparticles and any internal charge distribution is neglected. They are represented by impulsive current sources (Dirac-δ like) in the schematic circuit. The cavity is treated again as an RLC resonator supplied by an RF generator, suddenly discharged by the impulsive current and left to evolve freely between bunch passages [7].

Besides transient effects, the code accounts for the nonlinearity of the accelerating fields and for any dynamic interactions between the beam synchrotron motion and the RF amplitude feedback. Furthermore, by simply adding a multimodal cavity circuit, the code can be upgraded to check the system stability at any multibunch mode [6].

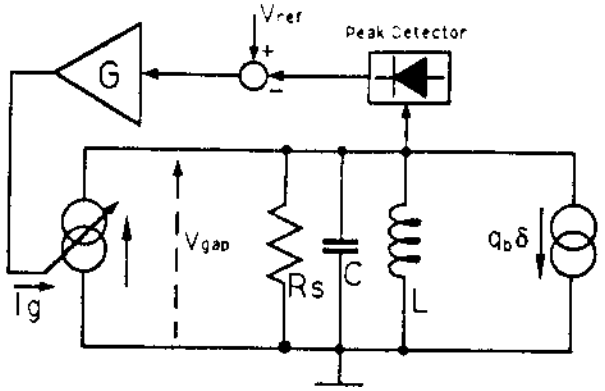

Figure 5. Equivalent Circuit for the Tracking Code

A typical simulation result is reported in Figs. 6 and 7. It represents the injection of the 30th bunch in the machine filled with other equal and stable 29 bunches previously stored. A 260 kV accelerating voltage has been set together with a - 75 Deg cavity tuning angle to match the current of the 29 bunches. A moderate bandwidth of the RF amplitude feedback has been chosen (less than 1 KHz) because other simulations showed that a too large bandwidth can couple the feedback to the synchrotron motion and get the beam to be unstable.

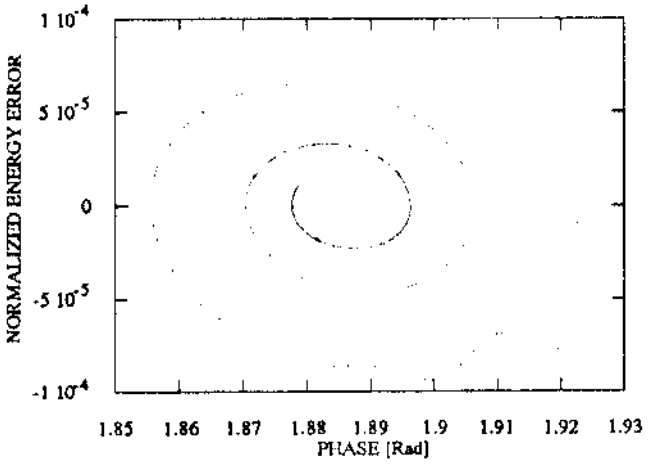

Figure 6. Bunch Phase Space Trajectory

The path of the 30th bunch in its own longitudinal phase space for the first 500 machine turns is reported in Fig. 6. The phase and energy errors at injection decrease turn by turn and the bunch tends to reach its stable equilibrium position with a characteristic damping time that is given by the machine natural damping plus the extra Robinson damping due to the cavity detuning [2].

The amplitude of the RF accelerating voltage for the first 500 turns is reported in Fig. 7.

The perturbation caused by the injection of the 30th bunch is damped with the feedback characteristic time. As the feedback bandwidth is much smaller than synchrotron frequency, the transient synchrotron oscillations can modulate the RF amplitude, as clearly shown in Fig. 7.

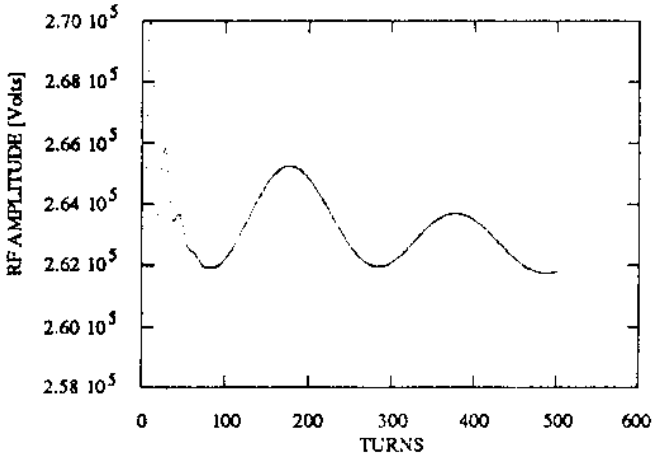

Figure 7. Envelope of the RF Accelerating Voltage

4. CONCLUSIONS

The previous results show that in principle any beam current in the DAΦNE operating range can be stored avoiding both transient and stationary beam center of mass instability conditions, providing that RF system parameters were properly set. The cavity tuning angle is the most crucial variable to be controlled to prevent beam instability, but also the gain and the bandwidth of dc feedback loops has to be chosen carefully.

Nevertheless, at high current values, the stability region around the working point is rather small and the system behaviour could be negatively affected by any cavity phase perturbations, such as large tuning system oscillations.

A fast RF feedback seems to be a possible solution to lower the apparent beam loading and then to broaden the stability region around the working point. The simulation code can be easily upgraded to implement such a feedback and a cross check between analytical and numerical consideration can be performed again for this new arrangement of the RF system.

5. REFERENCES

[1] The DAΦNE Project Team, "DAΦNE Status Report", this conference.

[2] K.W. Robinson, "Stability of Beam in Radiofrequency System", CEAL, Cambridge 38 Massachusetts, 1964.

[3] M. Sands, "Beam-Cavity Interaction - Basic Considerations", Tech. Rep. 2-76, Lab. de l' Acc. Lin. Orsay, 1976.

[4] R. Boni et al., "Stationary Beam Loading on DAΦNE Cavity Accelerating Mode", DAΦNE note RF5, LNF 1992.

[5] D. Boussard, "Design of a Ring RF System", CERN SL/91-2 (RFS), 1991.

[6] S. Bartalucci et al., " Impedance and Beam Dynamics in DAΦNE", this conference.

[7] M. Bassetti, "Finite Difference Equations Calculations of Beam-Cavity Coupling Stability" LNF note 67/45, 1967

Impedance and Beam Dynamics in DAΦNE

S. Bartalucci, L. Palumbo, M. Serio, B. Spataro, G. Vignola, M. Zobov
INFN Laboratori Nazionali di Frascati
C.P. 13 - 00044 Frascati (Roma) - Italy

R. Fedele, G. Di Massa, M.R. Masullo, V.G. Vaccaro
INFN - Sezione di Napoli
C.P. 13 - Pad 20, Mostra D'Oltremare 80125 - Napoli - Italy

Abstract

In DAΦNE single bunches of $9*10^{10}$ electrons or positrons are stored in an accumulator where they reach the suitable intensity necessary for a smooth injection into the multibunch e^+e^- rings. DAΦNE is envisaged to operate with 30 bunches, with about 1.3 Amps, in order to achieve the goal luminosity of a few 10^{32} (cm^{-2} s^{-1}). Then operation with a higher number of bunches, up to 120, might be necessary to explore the limits of the machine.

Single bunch and multibunch instabilities are among the main concerns for this high current machine. In this paper we report the main results of the analysis of dynamics for the e+ e- beams in the accumulator and in the main rings of DAΦNE machine. The impedances of both machines have been estimated by fitting the loss factor calculated by the TBCI and MAFIA codes [1] for all the ring components. Some results of the loss factor bench measurements performed on the accumulator kicker are shown as comparison with the computer estimates.

The single bunch longitudinal and transverse microwave thresholds appear to be safely far from the nominal current. An investigation of the multibunch instabilities excited by the RF cavity HOMs is presented. Absorption of e.m. energy stored in the parasitic modes is necessary in order to keep the instability rise time long enough to be acted upon by a feedback system.

1. ACCUMULATOR RING

1.1. Impedance estimate

Bunches with $9*10^{10}$ electrons and positrons are stored and ejected from the accumulator with a repetition frequency of 1 Hz. The single bunch instabilities can limit the performance of the accumulator ring. The instabilities are driven by the short term wake-fields resulting from the bunch interaction with the vacuum chamber broad-band impedance.

We estimate the longitudinal Z_l and transverse Z_T broad-band impedances using numerical calculation of the longitudinal k_l and transverse k_T loss factors by 2D TBCI and 3D MAFIA codes [1] for different bunch lengths σ. To obtain Z_l and Z_T from the above numerical results for k_l and k_T, we use the relation between the loss parameters of a Gaussian bunch with rms length σ and the broad-band model impedance:

$$k_l(\sigma) = \frac{1}{\pi}\int_0^{+\infty} d\omega\, \mathrm{Re}\{ Z_l(\omega) \} \exp\{ -(\omega\sigma/c)^2 \}$$

$$Z_l(\omega) = R_l / \{ 1 - jQ_l(\frac{\omega_l}{\omega} - \frac{\omega}{\omega_l}) \}$$

$$k_T(\sigma) = \frac{1}{\pi}\int_0^{+\infty} d\omega\, \mathrm{Im}\{ Z_T(\omega) \} \exp\{ -(\omega\sigma/c)^2 \}$$

$$Z_T(\omega) = R_T\, \omega_T/\omega\, \{ 1 - jQ_T(\frac{\omega_T}{\omega} - \frac{\omega}{\omega_T}) \}$$

and find the shunt impedances R_l, R_T, the angular resonant frequencies ω_l, ω_T and the quality factors Q_l, Q_T of the model broad-band resonator by fitting the numerical results to the analytical dependences $k_l(\sigma)$ and $k_T(\sigma)$. The analytical dependences $k_l(\sigma)$ with R_l = 1.527 kOhm, $\omega_l/2\pi$ = 4.14 GHz, Q_l = 0.82, and $k_T(\sigma)$, with R_T = 69 kOhm/m, $\omega_T/2\pi$ = 4.3 GHz, Q_T = 1, fit well the numerical estimates.

1.2 Kicker loss parameter measurements

As the numerical simulation shows, the main contribution to the loss factor (and impedances) in the accumulator comes from the injection-extraction kickers (almost 90%). So it is very important to measure the RF energy loss and compare it with numerical results. The longitudinal loss factor has been measured for an accumulator kicker prototype by an indirect method [2]. The experimental and numerical results are shown in Fig.1. The agreement between the two is satisfactory, showing the goodness of both approaches (simulation and measurement method).

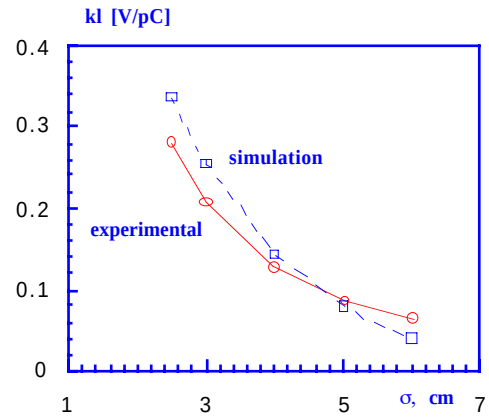

Figure 1. Loss factor k_l as function of bunch length σ: experimental (solid line) and simulation (dashed line) data.

1.3 Single bunch instabilities

Above the threshold of longitudinal microwave instability a bunch lengthens turbulently. The threshold average current is given by [3]:

$$I_l^{th} = \sqrt{2\pi}\,\alpha_c^2 (E/e)\,\sigma_{p0}^2 / (|Z_l/n|\,\nu_s)$$

where α_c is the momentum compaction, E is the total energy of a particle, ν_s is the synchrotron tune, σ_{p0} is the rms energy spread at zero current.

At low frequencies the normalized longitudinal impedance $Z_l/n = R_l\omega_0 Q_l/\omega_l$, where $n = \omega/\omega_0$ is the mode number and ω_0 is the angular revolution frequency. For the accumulator ring $\omega_0/2\pi$ = 0.0092 GHz and hence Z_l/n = 4.14 Ohm. Taking into account the contributions of diagnostics, which is 0.16 Ohm for the accumulator, the total normalized longitudinal impedance is Z_l/n = 4.3 Ohm.

For Z_l/n = 4.3 Ohm a bunch is in the turbulent regime and its equilibrium length is equal to 5 cm and the rms energy spread $\sigma_p = 9.15*10^{-4}$ at the average current of 130 mA and RF voltage of 200 kV. The loss factor that corresponds to this bunch length is k_l = 0.115 V/pC. It means that the bunch loses 1.66 keV per turn because of RF radiation.

The transverse single bunch instabilities are destructive for a stored bunch. The most dangerous are the transverse fast blowup instability, transverse mode-coupling instability and resistive wall instability. For $\sigma > (4\sqrt{\pi}/3)b$, where b is the beam pipe radius, the transverse mode-coupling instability dominates over the transverse fast blow up. That is the case of the accumulator ring. The mode coupling instability is driven by the imaginary part of the transverse impedance and its threshold is given by [4]:

$$I_T^{th} = \frac{4\,(E/e)\,\nu_s}{[\mathrm{Im}(Z_T)]\,\langle\beta_T\rangle\,R}\,\frac{4\sqrt{\pi}}{3}\,\sigma$$

where $\langle\beta_T\rangle$ is ring-averaged transverse beta function and R is the ring average radius.

At low frequencies for long bunches $\mathrm{Im}(Z_T) = Z_T = R_T/Q_T$. This approximation is valid for the accumulator because the bunch in the turbulent regime is rather long (5 cm). Taking the numbers from the broad-band impedance model the threshold current is by a factor ~5 higher than the nominal current.

2. MAIN RING

2.1 Single bunch dynamics

For the main ring we also use the broad-band impedance fit of the numerical dependences k_l (σ) and k_T (σ). The same procedure as described in 1.1. is used for this purpose. The normalized longitudinal impedance Z_l/n comes out to be about 1.2 Ohm and the transverse one Z_T about 64 kOhm/m.

Table 1 shows the relative contributions of different vacuum chamber elements to the total loss factors at the nominal bunch length σ = 3 cm. The main contribution comes from the 2 injection kickers. Now other possible kicker designs are under consideration to reduce the impedance [5].

In our calculation we did not take into account the contributions of bellows and flanges. Since DAΦNE is a rather small machine, the number of bellows and flanges is not large and in any case they will be RF shielded. So the goal of Z_l/n = 2 Ohm is quite achievable for the main ring. To keep the bunch length σ = 3 cm we need to supply V_{RF} = 270 kV at full current.

The transverse current threshold with a transverse impedance of 64 kOhm/m is by a factor 1.5 higher than the nominal current I = 45 mA.

Table 1

	k_l [V/pC]	k_T [V/pCm]
RF cavity	0.129	4.71
Longitudinal feedback kicker	0.0485	2.37
Injection kicker	0.255	40.9
Slot in the vacuum chamber (100cm* 2cm)	$2*10^{-7}$	0.002
Taper in the interaction region.	0.0013	1.5
Transition between the beam chamber and the wiggler section	0.0004	20.1
Vacuum chamber in the split magnet (intersection of two rings)	$4*10^{-6}$	0.716

2.2. Multibunch Instabilities

Coupled-bunch instabilities, driven by the parasitic HOMs of the RF cavity, are one of the main concerns in the design of the machine. A longitudinal feedback system for DAΦNE may provide at best a damping time of about 100 μsec , much faster than the natural radiation damping, not sufficient, however, to damp those relative modes significantly coupled to strong resonances. The spectrum of the unperturbed motion of k_b bunches shows frequencies at

$$\omega_{p,s,a} = (p\,k_b + s + a\,\nu_s)\,\omega_o$$
$$p = 0, \pm1, \pm2,...$$
$$a = 1, 2, 3,.....$$
$$s = 0,1,.... 29.$$

where $\omega_o = 19.295*10^6$ rad/sec is the revolution angular frequency, "a" describes the longitudinal motion in the phase space (dipole mode a=1, quadrupole mode a=2 etc), and "s" specifies the longitudinal mode number. When a relative mode of oscillation "s" is excited by the e.m. resonating fields, the motion is intrinsically stable or unstable depending on the sign of the rise time:

$$\tau_{s,1} = \frac{4\pi\,(E/e)\,\nu_s}{k_b\,I_b\,\omega_o\,\alpha_c}\;\frac{1}{(Z_{s,1})^{eff}}$$

where the effective impedance $(Z_{s,l})^{eff}$ is computed for each relative mode s, interacting with N parasitic HOM of the RF cavity:

$$(Z_{s,l})^{eff} = \sum_{-\infty}^{\infty}{}_p \sum_{1}^{N}{}_n \; F(\omega_p) \frac{R_{s,n}}{1 + Q_r^2 \left(\frac{\omega_p}{\omega_{r,n}} - \frac{\omega_{r,n}}{\omega_p} \right)^2}$$

R_S, ω_p and Q_r being the relevant parameters of the parasitic resonators. The form factor for a gaussian beam is:

$$F(\omega_p) = \pm \frac{\omega_o}{\omega_p} (k_b p + s)^2 \, e^{-\left(\frac{(k_b p + s)\,\sigma_l}{R} \right)^2}$$

We have analyzed for the dipole-mode (a=1) the instability rise time due to a sample HOM with a resonant frequency spanning the region where the maximum of the form factor occurs, i.e. at around 1.125 GHz. We assumed $k_b I_b$ = 1.3 A, R_S/Q_r = 20 Ω, and consirered four significative cases Q_r = 50000, 5000, 500 and 100. For Q_r = 50000 the rise time becomes dramatically low, of the order of fraction of microseconds, when the resonant frequency is fully coupled to a relative mode sideband. However, as soon as the resonant frequency shifts from the full coupling condition, the rise time goes to much higher values, increasing by a factor 10^4. These results are explained by the fact that for such a short machine two consecutive stable or unstable sidebands are spaced of about the revolution frequency, i.e. 3 MHz. A single high Q HOM may excite only one relative mode at time. The instability rise time is due to the resistive impedance of the parasitic resonator at the sideband frequency. Its effect is maximum when the resonant frequency overlaps an "unstable" relative mode sideband. For $Q_r \leq 500$, corresponding to a shunt impedance of 10 kΩ of the sample HOM, the rise time remains above 100 μs for all relative modes that, therefore, can be stabilized by a powerful feedback system. In this case the resonator bandwidth is large enough to cover two consecutive unstable sidebands, so that a frequency shift of the HOM is ineffective. A compensation effect, occurring around s = 0 (an identical compensation happens for s = 15) because of the Robinson damping, is also recognized.

In Fig. 2 we plot versus the frequency what is the shunt impedance exciting the instability with a rise time τ=100 μs, for a stored current of 0.1, 0.5, 1.0 and 1.5 Ampere. On the same plot are reported for comparison the parasitic shunt impedances of the "day one" cavity [6] proposed for the beginning of the machine operation.

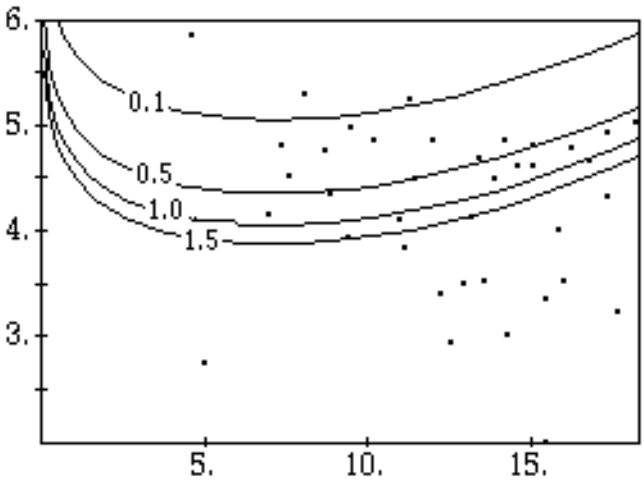

Figure 2. $\mathrm{Log}_{10}[R_S(\Omega)]$ vs. ω_r (*10^9 rad/sec) for τ = 100 μs; I_o = 0.1, 0.5, 1.0 , 1.5 A.

The results show that, despite the small contribution of the cavity to the overall parasitic loss, many individual modes are characterized by a shunt impedance too high for storing 1.3 Amps. A recent further optimization of the cavity shape has improved the shunt impedance of the TM_{011} by a factor 6, and within the present constrains, we hardly expect that a further optimization of the cavity shape can reduce the HOM shunt impedances below the desired values. This goal can in principle be pursued by developing either the damping technique (by coupling the cavity to energy absorbers such as loops, loaded waveguides etc.), or the shifting technique, changing the resonant HOM frequency such that the resistive coupling impedance is strongly reduced. R&D activities on this field are reported in Ref.[6]. It seems hard today, however, to control the frequency of many potentially dangerous modes, whereas damping techniques based on the absorption of the e.m. energy stored in the HOMs, by means of antennas or waveguide couplers look more promising.

3. REFERENCES

[1] T. Weiland, IEEE Trans. Nucl. Sci., NS-32, 2738 (1985).

[2] G. Di. Massa, M. R. Masullo and V. G. Vaccaro, DAΦNE Technical Note, G-12, Jan. 28 1992.

[3] A. Hofmann, Proc. of First Course of Int. School of Particle Accelerators, Erice 1976, CERN 77-13, p.139.

[4] B.Zotter and F. Sacherer, ibid., p.175.

[5] R.Fedele and V. G. Vaccaro, DAΦNE Technical Note,G-4, Feb.4, 1991.

[6] S. Bartalucci et al., "DAΦNE Accelerating Cavity: R&D", this conference.

DAΦNE Longitudinal Feedback

M. Bassetti, O. Coiro, A. Ghigo, M. Migliorati*, L. Palumbo*, M. Serio.
INFN Laboratori Nazionali di Frascati, C.P. 13, 00044 Frascati (Roma) - Italy
*Dipartimento Energetica Università di Roma "La Sapienza", Via A. Scarpa 14, Roma - Italy

Abstract

A preliminary assessment of the growth rate of the longitudinal multibunch instabilities in DAΦNE has evidenced the need for a powerful active feedback system. In this report we present a preliminary design of a mixed analog/digital feedback system employing DSP techniques, which can be used with 30 bunches and is upgradable to 120 bunches, capable of a damping time of 0.1 - 0.2 ms.

1. INTRODUCTION

DAΦNE is a high-luminosity Φ-factory based on two intersecting storage rings. Details of the project are given elsewhere in these proceedings [1].

Calculations [2] and simulations show that the resistive impedance of undamped HOM's in the accelerating cavities can drive coupled-bunch (CB) modes of oscillation with unmanageably fast rise-time. Although a small frequency shift can in principle reduce by a large amount the growth rate, damping of at least two orders of magnitude of the HOM may prove more viable [3]. Even so, the rise-time of CB modes can be much faster than the natural (radiation and Landau) damping time; moreover the probability for a damped HOM to cross a CB mode frequency is larger, due to the wider bandwidth. An all-mode feedback system capable to damp all the CB modes and the injection transients is thus necessary. The system proposed for DAΦNE is a bunch by bunch, time-domain feedback. This approach is common to other factories with intense beams and a large number of bunches. In fact, a collaboration has been set up with the B-Factory group at SLAC, where considerable R&D on feedback systems for the next generation of electron colliders [4,5] is being carried out.

2. FEEDBACK BASICS

In Table I we list the machine parameters relevant to the feedback.

Table I

Energy E_0 (MeV)	510
Revolution frequency f_{rev} (MHz)	3.07
Harmonic number h	120
Average current/bunch (mA)	44
Number of bunches B	30 -> 120
Bunch spacing (ns)	10.9 -> 2.7
RMS Bunch duration σ_z (ps)	100
Synchrotron tune Q_S	~ 1/80
Momentum compaction factor α_C	0.017
Synchrotron damping time τ_S (ms)	17.8

The damping rate α_{FB} [sec^{-1}] provided by a longitudinal feedback system is

$$\alpha_{FB} = \frac{1}{\tau_{FB}} = \frac{1}{2} f_{rev} * \frac{\Delta U_{FB}}{\Delta E}$$

where ΔU_{FB} is the energy correction/turn by the feedback kicker and ΔE is the energy error.

The following scheme can be applied: detect the individual synchrotron phase error with a longitudinal pick-up, rotate the signal in the synchrotron plane by means of an appropriate filter, amplify and give an energy kick with a longitudinal kicker. The differential equation governing the synchrotron phase ϕ of a bunch is then, in the smooth approximation:

$$\frac{d^2}{dt^2}\phi + \alpha \frac{d}{dt}\phi + \Omega_s^2 \phi = \text{feedback forcing term} =$$

$$= -2\pi f_{RF} \frac{\alpha_c}{E_0} f_{rev} (\mathbf{g}\,\phi) \text{ , with } \mathbf{g} = \frac{\Delta U_{FB}}{\Delta \phi} ,$$

where α is the combined damping (or antidamping) rate from radiation and HOM excitation, f_{RF} is the RF frequency, Ω_S the synchrotron angular frequency and $\mathbf{g}(\Omega)$ [eV/rad] is the (complex) feedback gain

$$\mathbf{g}(\Omega_s)\phi = |g| \underbrace{(\phi \cos\theta}_{\text{in-phase}} + \underbrace{j\,\phi \sin\theta}_{\text{quadrature}}) \approx$$

$$\approx |g| (\phi \cos\theta + \frac{\dot{\phi}}{\Omega_s} \sin\theta) .$$

The overall damping time is determined by the quadrature component of the feedback forcing term:

$$\frac{1}{\tau} \approx \frac{1}{2}\left(\alpha + 2\pi f_{RF} \frac{\alpha_c}{E_0} \frac{f_{rev}}{\Omega_s} |g| \sin\theta \right) .$$

On the other hand, the in-phase component contributes to a small shift of the synchrotron frequency, but not to the damping. Therefore the optimum damping effectiveness is achieved when $\theta = \pi / 2$.

It is worth noting that, in order to maintain the optimum phase-shift, the filter should be tuneable in the range of the allowable synchrotron tunes and that it is necessary to replicate the filter B times in order to damp independently B bunches. The phase detector and the kicker do not need to be replicated, provided that their bandwidth is such to detect the phase and kick individual bunches with no "memory" of the adjacent ones.

With a maximum B of 120, however, the above basic approach can become very complex, if not prohibitive at all. A different solution, still based on individual detection and correction of the different bunch phases will be discussed in the following section.

3. ANALOG - DIGITAL FEEDBACK

Available electronic technology allows the realization of a mixed analog/digital system employing Digital Signal Processors (DSP) as filters. With reference to Fig. 1, the front-end is a phase detector followed by a fast (bandwidth 1.2 GHz) digitizer capable of sampling the phase signal of individual bunches at full rate with 8-bit resolution [6]. The DSP's run at some lower frequency than the digitizer, thus a digital demultiplexer is needed to convey to different units the

digitized phase. The DSP's perform the filtering algorithm, after which the feedback correction information from different parallel processors is multiplexed into a fast digital to analog converter [7], then amplified with a power amplifier and fed to a longitudinal kicker.

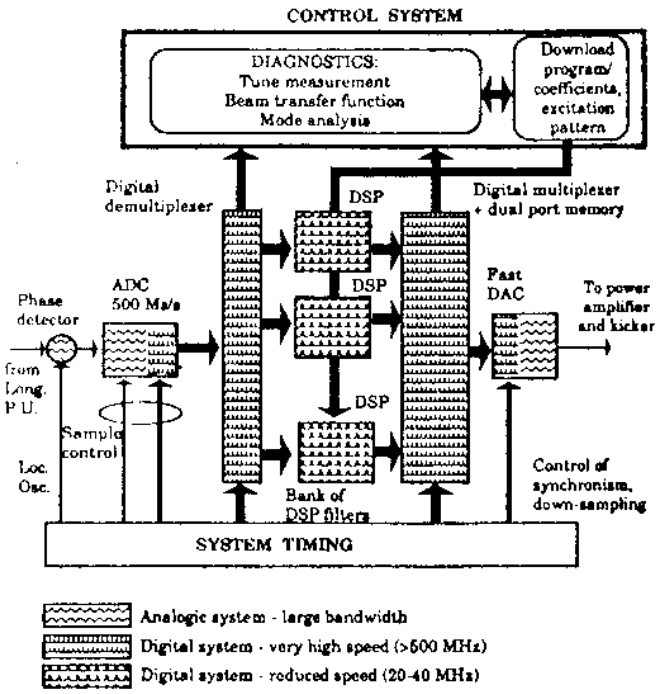

Figure 1. Analog-digital feedback.

The main advantage of such a system is that the same DSP can serve as a filter for several different channels, thus reducing the overall complexity. Indeed, the use of programmable devices allows also the flexibility to program the gain and to *tune* the frequency response of the filters on-line, according to the beam current intensity and to machine parameters which affect the synchrotron motion. Moreover, the digital system can be programmed in such a way as to maintain the correction signal just below the saturation limit of the power amplifier, so that, even in the presence of large phase excursions (i.e. at injection), the final power amplifier never goes into saturation, an undesirable condition during which the effective feedback gain is considerably reduced and whose recovery could take a time longer than the bunch to bunch spacing.

3.1. Phase Detector

We need to measure the single bunch phase with no signal feed-through by the preceding bunches. The use of a narrow-band tuned detector is thus precluded.

A coherent burst of bipolar pulses can be produced by time-shifting and summing the output of a longitudinal stripline pickup. The phase of this pseudo-sinusoidal burst is compared, by means of a double balanced mixer (DBM), to that of a local oscillator (LO) locked to a harmonic of the ring RF. The output of the DBM phase detector is fed to a fast digitizer and processed by the DSP system.

A laboratory test, based on that described in [4], has been set-up at SLAC, with which it has been possible to characterize the performance of the front-end detector.

In this test (see Fig. 2) we send two narrow pulses of ~100 ps FWHM, produced by step-recovery diodes, into the inner conductor of a 3" coaxial line, to simulate two bunches spaced at 2.7 ns in the accelerator pipe.

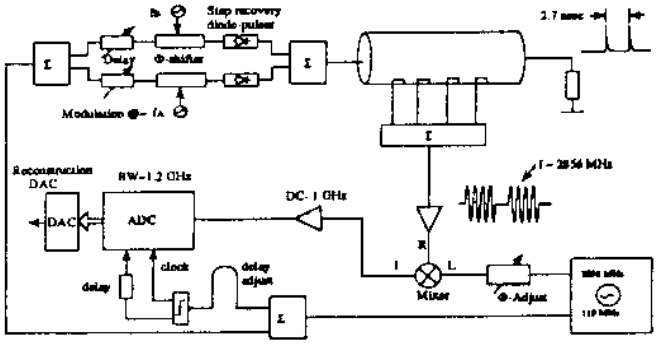

Figure 2. Schematic layout of the front-end test.

The output of four -36 dB stripline couplers in the coaxial line are combined to form a coherent burst in correspondence to the passage of each pulse (Fig. 3).

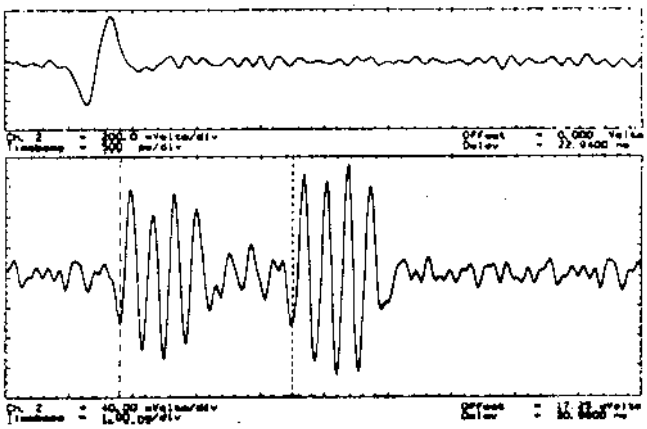

Figure 3. Pickup signal and coherent burst in the bunch simulator.

We modulate the time position of the pulses with two sinusoids at slightly different frequencies. The detected phase of each burst is digitized by gating the ADC on either one or the other bunch. The ADC output is converted back into analog by a reconstruction DAC and the output measured with a spectrum analyzer. The feed-through of one modulating frequency on the detected phase of the other bunch is a measure of the bunch to bunch isolation. The measured isolation is ~ -30 dB; an improvement can be expected by choosing a DBM with a better isolation of the LO port at the carrier frequency. The full scale range in the phase measurement is ± 15˚ and the measured rms noise is comparable to the least significant bit (1/128 of FSR) of the ADC.

3.2 Digital Filter

The correction signal is calculated by a discrete-type non-recursive digital filter with *N*-taps. In such a filter the output signal y_n at the instant t_n is computed as the convolution sum of *N* prior values of the input signal ϕ_{n-i}:

$$y(t_n) = G * \sum_{i=1}^{N} \phi(t_{n-i}) \bullet h_i \;;$$

$G*\{h\}$ is the *N*-samples reconstruction of the desired pulse

response of the filter, a sinusoid in our case.

The period of the synchrotron oscillation is ~80 revolution times, but to reconstruct it in the digital filter we can use a smaller number of points by sampling at a rate D (down-sampling factor) times slower than the revolution frequency [8]. The number of taps in the filter is then $N \sim 1/DQ_S$ and the number of multiply-accumulate (MAC) cycles in each DSP filter is reduced accordingly. The total number of operations/second is reduced by $1/D^2$ because the number of MAC's is reduced by $1/D$ and the rate at which the correction kicks are computed is reduced by the same amount.

The main advantage of down-sampling is that the number of digital processors can be limited to a number much smaller than in a system sampling at full rate. On the other hand, a fast dual-port memory register is necessary to hold the last computed correction kick for each individual bunch and to provide a correction signal to the kicker, synchronously with each bunch passage.

According to simulations, the feedback system performs satisfactorily with a number of taps as small as 5. A preliminary estimate of the number of DSP's needed for 30 bunches is ~5, assuming a DSP with an instruction time of 50 ns [8].

3.3 Longitudinal Kicker

The energy correction, in terms of the output power P_0 of the final amplifier is

$$\Delta U_{FB} = \sqrt{2P_0 (R T^2)} ,$$

where (RT^2) is the kicker shunt impedance, corrected by the transit time factor. The bandwidth required to damp all bunches separately is roughly $\geq 1/2$ the bunch frequency Bf_{rev}. The kicker resonant frequency f_r and the bandwidth must be such to encompass with a substantial value of the shunt impedance all possible CB mode frequencies. The optimum resonant frequency is at

$$f_R = (p + 1/4)\, B\, f_{rev}$$

with p an integer.

The present choice for the kicker is a structure of three $\lambda/4$ striplines with full coverage, broadly resonating at ~1.2 GHz, series-connected with $\lambda/2$ delay lines [9]. With such arrangement, a peak shunt impedance of up to 900 Ω and a half-power bandwidth in excess of 1/2 the bunch frequency are achievable. Proper design of the kicker electrode is crucial in reducing the power demand on the final stage of the feedback system and mismatches at the power port must be minimized to reduce reflections.

4. SIMULATION STUDIES

We have used the simulation code developed at SLAC [5] to assess the system performances in a realistic context. All simulations are performed in the time domain taking into account the interaction between the beam, the offending HOM's and the correcting action of the feedback, including noise and bunch to bunch coupling in the detector circuit, the implementation of the digital filter and independent adjustment of the filter gain and saturation and the kicker power.

The conditions under which we have tested most feedback configurations are :

- nominal intensity of the bunch current;
- number of bunches B = 30, 25 ("gap" of five RF buckets);
- initial time offset of 100 ps of one injected bunch;
- *dummy* HOM (see [2])
  R/Q = 20 Ω, Q = 250, 500
  $f_{HOM} = (12*30 + 1 + Q_S)\, f_{rev} \sim 1.1$ GHz;
- number of taps in the digital filter = 5, 20
- feedback gain ~ 20 KeV/rad;
- kicker voltage = 400, 500 V.

Under all the above conditions we have consistently measured a damping time of ~ 100 μs with no HOM's, and an overall damping of all the bunches even in the presence of a dummy mode with 10 KΩ shunt impedance at the frequency where the fastest growth rate occurs. The maximum time offsets of 30 bunches tracked over 3000 revolutions in the presence of such HOM are reduced from ~ 700 ps without feedback, down to ~ 12 ps with feedback (5 taps).

5. CONCLUSIONS

From the results of this preliminary study we are convinced that a longitudinal feedback system largely based on digital techniques is feasible and works well according to the initial performance specifications that we aim to (damping time of 0.1 - 0.2 ms, 30 bunches).

Down-sampling to a level of a 5-taps digital filter is acceptable. The number of DSP's needed is *modest.*

Although many components in the system are the state of art of electronics, all the required hardware, from the front-end to the power amplifiers, is market-available. Expected improvements of the performances of future DSP's can furtherly reduce the complexity of the digital system.

A power amplifier of ~500 W is enough to damp transients of 100 ps with 30 bunches at the full design current. The number of power amplifiers-kickers will be increased four-fold when we run DAΦNE with 120 bunches.

The performances are not affected in the case of an asymmetric fill.

6. ACKNOWLEDGEMENTS

We are pleased to acknowledge the technical support and warm hospitality provided to us by all the members of the SLAC B-factory group, in particular J. Dorfan, A. Hutton, J. Fox and A. Pacheco. We also like to thank D. Briggs, W. Hosseini, H. Hindi, G. Lambertson, F. Pedersen and J. L. Pellegrin for the very enlightening discussions on the subject of this paper and for the friendly atmosphere in the feedback group. Finally, we thank cheerful Pina Possanza for converting a chaotic draft into this final form.

7. REFERENCES

[1] The DAΦNE Project Team: "DAΦNE status report " - This Conference.
[2] S. Bartalucci et al.: "Impedance and Beam Dynamics in DAΦNE" - This Conference.
[3] S. Bartalucci et al.: "DAΦNE Accelerating Cavity R&D" - This Conference.
[4] D. Briggs et al.: "Prompt bunch by bunch synchrotron oscillation detection via a fast phase measurement" - SLAC-PUB 5525, LBL-30604 (1991).
[5] D. Briggs et al.: "Computer modelling of bunch-by-bunh feedback for the SLAC B-factory design" - SLAC-PUB 5466, LBL-30772 (1991).
[6] Tektronix: TKAD10C.
[7] Triquint Semiconductor: TQ 6113 .
[8] J. Fox et al.: "Undersampling and the B-factory CDR", SLAC unpublished note (1991).
[9] G. Lambertson : "Electromagnetic detectors", in Lecture Notes in Physics, 343, Springer - Verlag (1989).

High Current Density Septa for DAΦNE Accumulator and Storage Rings

M. Modena, H. Hsieh and C. Sanelli
INFN Laboratori Nazionali di Frascati
C.P. 13 - 00044 Frascati (Roma) - Italy

Abstract

An injection/extraction magnetic system composed of two septa is being designed for both the accumulator and the storage rings of the DAΦNE project. A multi-turn DC high current density septum provides the principal bend of 0.593 radians it is followed by a 0.038 radians capability thin septum which is located nearer the machine. This septum is of high current density and edge cooled type. This paper describes the magnetic and thermal results by FEM. Mechanical design of the septa is also presented.

1. INTRODUCTION

A 510 MEV electron positron colliding facility [1], known as DAΦNE, is currently under design and construction at INFN's Frascati National Laboratory. The project consists of two storage rings and one energy injector system. Electrons and positrons will be injected into the DC accumulator alternatively from Linac at a frequency of 50 Hz. The storage rings will only have injection frequency of once per second. Figure 1 depicts the physical layout of the system. Keeping long term operational reliability in mind, we have elected to build DC septa instead of rapid pulsing ones in spite of all the problems associated with high current density devices. Both septa are placed outside of machine vacuum chamber, so that the possibility of water leak inside a ultra high vacuum environment can be avoided. The penalty of this approach is thinner septum therefore higher current density.

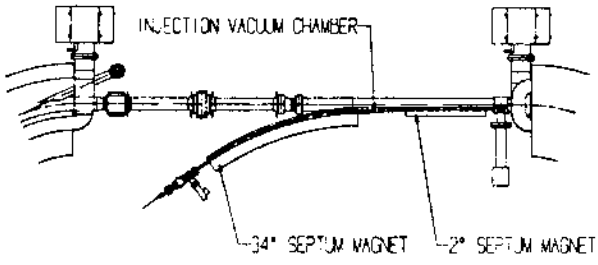

Figure 1. Injection/extraction Septum System

2. EDGE COOLED DC SEPTUM

2.1. Configuration

Figure 2 shows the cross section of the thin septum. The allowable maximum septum thickness set by machine physics group is in the order of 4 mm, it of course includes the thickness of two vacuum chambers, this reduces the current carrying conductor to 1.5 mm thick. The resulting current density is in the order of 60 ampere per square mm. There are two thin wall, rectangular tubings either brazed or electroformed to form an intimate contact with conductor for proper heat transfer, these tubings will be Inconel alloy or stainless steel 304 L to avoid excessive current sharing with the conductor. The back coil is of conventional copper hollow conductor.

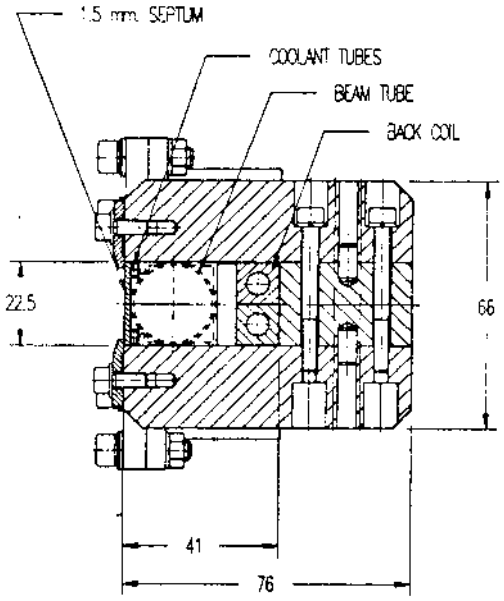

Figure 2. Thin Septum Section

All the electrical insulation will be provided with 130 μm thick pressure sensitive Kapton tape. The additional function of the Kapton tape, due to its extreme low thermal conductivity, is to insulate thermally the beam chamber from high temperature septum, this will prevent the thermal outgassing of the stainless steel septum beam tube so near to the machine that it is considered as part of machine vacuum. The iron yoke is of low carbon steel solid type, it is detachable so that the septum can be installed or removed from its location with ease. Table I shows some of the more relevant parameters of this septum

Table I
Thin Septum Parameter List

Field	0.104	T
Bend angle	38	mrad
Gap height	22.5	mm
Magnetic length	623	mm
Septum conducting area	33.75	mm^2
Current	2125	A
Current density	63	A/mm^2
Resistance	0.33	mΩ
Power	1.49	kW
Voltage	0.7	V
Number of water circuit	1	
Water flow rate	0.1	L/s
Water pressure drop	3	Atm
Water temperature rise	5	°C

2.2 Analysis Results

The thermal loading of the thin septum is rather severe due to high current density and edge cooled feature. Heat transfer has been performed by using ANSYS code, with initial water temperature of 30 °C, the maximum temperature along the median plane is in the order 51 °C, there are negligible thermal gradient across the tube wall. Assuming tubings remain rigid, the maximum thermal compressive stress in the copper will be in the order of 440 kg/cm^2, which is below endurance limit of the copper. Magnetic calculation has been carried out with POISSON code, taking into account the real current distribution within the septum and coolant tubes.

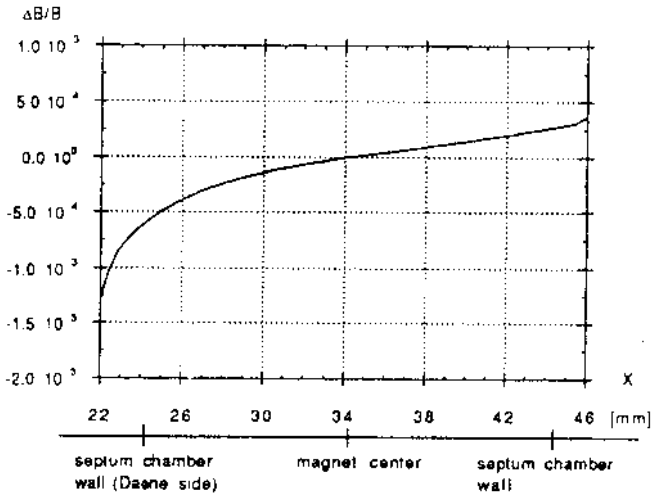

Figure 3. Thin Septum Field Quality

Figure 3 shows the field quality along the x-direction, the uniformity is in the order of ± 5 10^{-4} within the beam tube region. The fringe field outside the gap is shown in Figure 4, they are 1.2 Gausses at 2 mm from machine vacuum chamber wall and 0.75 Gausses at the injection straight section, the gradient is in the order of 0.25 G/cm.

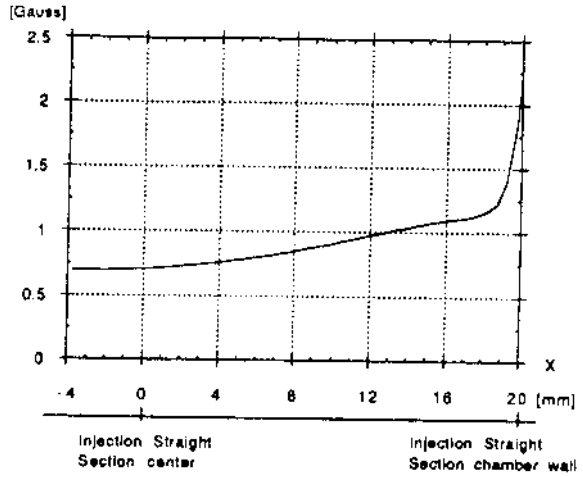

Figure 4. Thin Septum Fringe Field

3. THE MULTITURN CURVED SEPTUM

3.1 Configuration

Figure 5 shows the cross section of multiturn curved septum. It is of conventional hollow conductor coils and solid low carbon steel yoke. The coil package consists of eight turns of hollow conductor, 6 mm x 6 mm with 3.8 mm coolant hole diameter. The coil insulation will be either with kapton tape or conventional fiber glass tape and impregnated with epoxy resin system. The magnet yoke assembly is also of detachable type for the ease installation and removable of this magnet in situ.

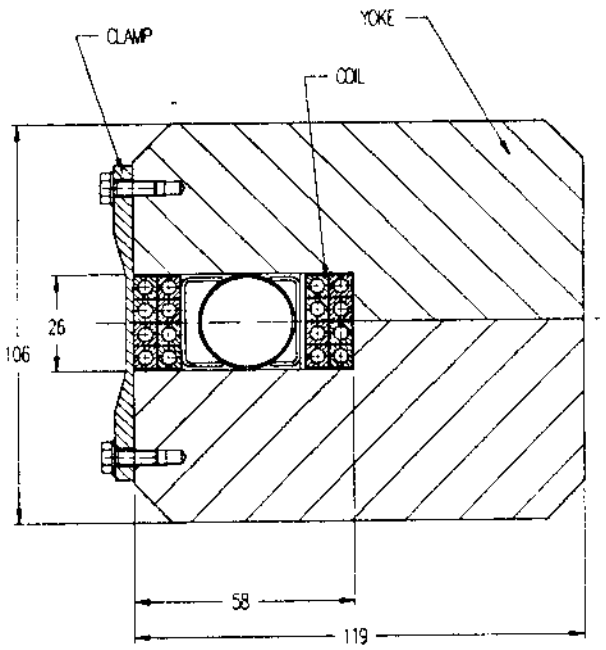

Figure 5. Curved Septum Section

3.2 Analysis Results

The current density of this magnet is in the order of 90 amperes per sq. mm. The power consumption is 68 kW, therefore each turn has to be cooled individually in order to have reasonable water pressure drop. The operating mean temperature of the coil package will be in the order of 50 °C, this may necessitate the cooling of magnet yoke in order to keep the beam chamber at lower temperature. Thermal analysis had been done by classical method and later on checked with ANSYS code. Table II is the parameter list of this magnet.

Table II
Curved Septum Parameter List

Field	0.818	T
Bend angle	593	mrad
Gap height	26	mm
Magnetic length	1233	mm
Ampere turns	17000	
Conductor dimentions	6 x 6	mm^2
Cooling hole dia.	3.8	mm
Conductor area	23.8	mm^2
Current	2125	A
Current density	89.3	A/mm^2
Resistance	15.1	mΩ
Power	68	kW
Voltage	32	V
Number of water circuit	8	
H_2O Rate per magnet	0.653	L/s
H_2O Δpressure/circuit	5.3	Ate
Water temperature rise	33	°C

The magnetic calculation has been carried out by using POISSON code. Figures 6 and 7 depict the field quality inside the magnet gap and fringe field outside the septum. The field quality is well within ± 5 10^{-4} range. The fringe field outside the septum is very low. The perturbation due to the end nearer the machine will be studied and shielded if neces sary.

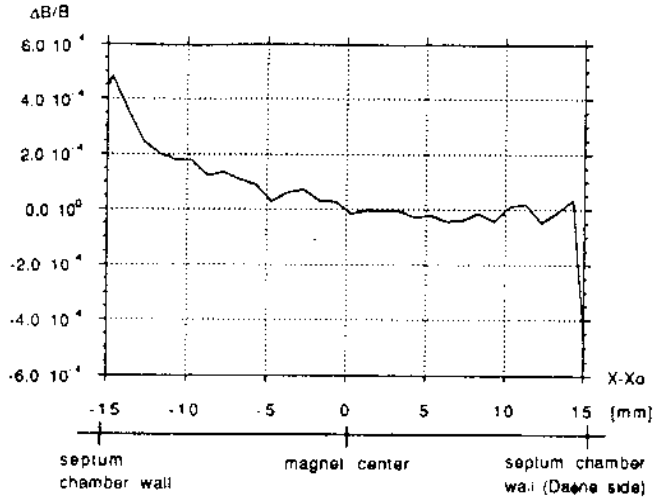

Figure 6. Curved Septum Field Quality

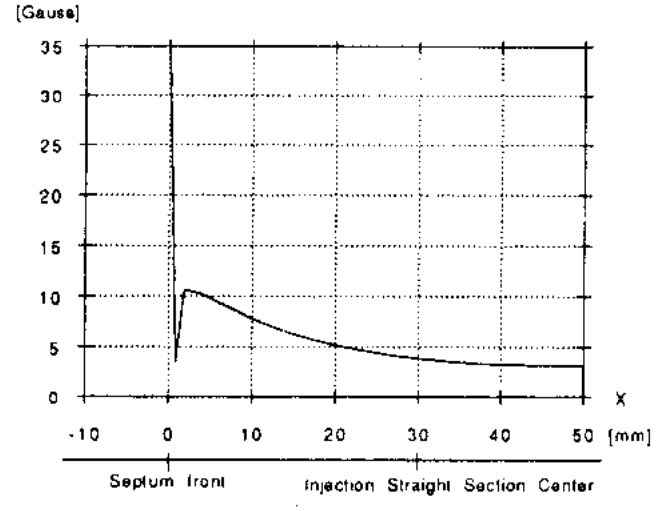

Figure 7. Curved Septum Fringe Field

4. CONCLUSION

We have determined the approach of septa design is feasible and the magnetic performances will satisfy the requirement set by the machine physics group. The mechanical design of the septa is under way. The prototypes will be built to verify the validity of computation. The fringe field will be carefully studied, magnetic shield will be implemented if necessary.

5. REFERENCES

[1] The DAΦNE project team, "DAΦNE status report", this Conference.

DAΦNE Accumulator Kickers

S. De Simone and A. Ghigo
INFN Laboratori Nazionali di Frascati
C.P. 13 - 00044 Frascati (Roma) - Italy

Abstract

The injection and extraction system for the DAΦNE accumulator and main rings is under study. Single-turn single-bunch injection has been adopted.

In the accumulator four symmetric kickers are used to inject and extract both electrons and positrons without changing field polarity.

A kicker prototype has been tested: design and realization of the magnet, HV pulser, control circuit, and measurements are presented.

1. INTRODUCTION

The injection scheme for the DAΦNE Frascati Φ-factory is fully described in [1,2].

In this report we present the injection and extraction kicker magnet prototypes and the pulsed power supply realized and tested for the DAΦNE accumulator.

The single-turn single-bunch injection scheme has been chosen for the accumulator and the idea to extract positrons from the electron injection channel and vice-versa has been adopted.

The maximum repetition rate from the LINAC to the booster is the inverse of the accumulator damping time (50 Hz); in the e^+ operation 45 shots are injected and accumulated in a single bunch; after 5 damping times the beam is extracted and sent to the main ring.

In the accumulator injection scheme four fast kickers are used with the same polarity for both electrons and positrons; three of them are fired for extraction: the required field values are shown in Table I.

Table I
Kicker magnetic fields

Integrated magnetic field (Gauss*m)	K1	K2	K3	K4
Positron injection	12	92	12	92
Electron injection	92	12	92	12
Positron extraction	110	107	68	0
Electron extraction	107	110	0	68

As shown in Fig. 1 the kickers are symmetrically inserted in two straight sections at ~3π/2 phase distance from the injection and extraction septa.

The accumulator injection and extraction timing system, synchronized with the Linac gun trigger and with the the DAΦNE accelerating RF, allows injection into any of the 120 RF buckets of each main ring.

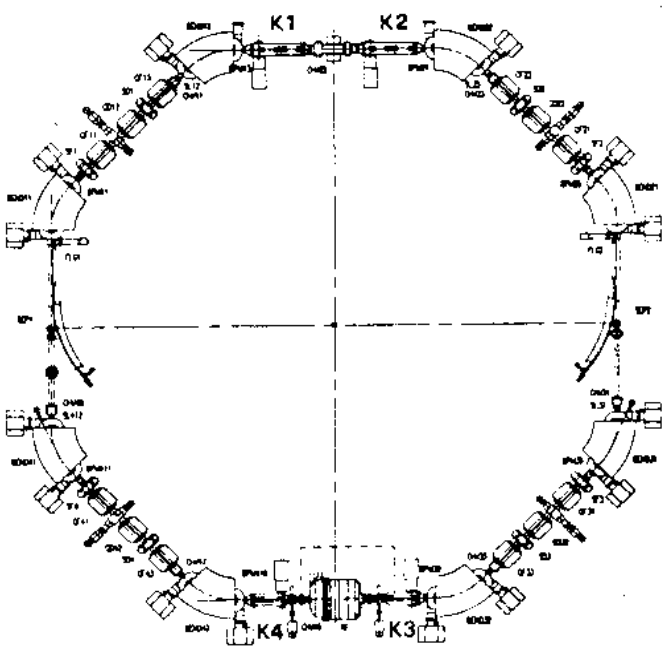

Figure 1. Accumulator Layout.

2. DESIGN CRITERIA

The nominal field in the kicker magnets at the injection energy of 510 MeV is shown in Table I.

The pulse length must be shorter than two revolution periods (218 nsec) to avoid particle losses from the injected beam on the septum wall.

The kicker design, described in the following, is derived from the experience gained in ADONE, where a similar device is running successfully since 1988 [3].

The kicker is realized with four rods inside the vacuum chamber, as shown in Fig. 2. The distance between the rods is dictated by aperture requirements. The vertical distance is determined by the injected beam emittance, while the horizontal one comes from field requirements.

The vacuum chamber inner diameter around the kicker coils must be the largest possible in order to minimize the reduction of the effective field due to the image currents in the surrounding wall. The proposed inner diameter, compatible with the current-voltage characteristic of our pulsed power supply, is ~200 mm: in this case the field reduction is less than 20%.

The kicker coils are paralleled to halve the self-inductance presented to the power pulser and hence the maximum voltage.

The transition from atmosphere to the accelerator vacuum is accomplished by means of two diametrically opposite ceramic feed-throughs: these are modified low profile insulators in order to minimize the parasitic inductance; a thoroidal current monitor is used to measure the current in the kicker coils.

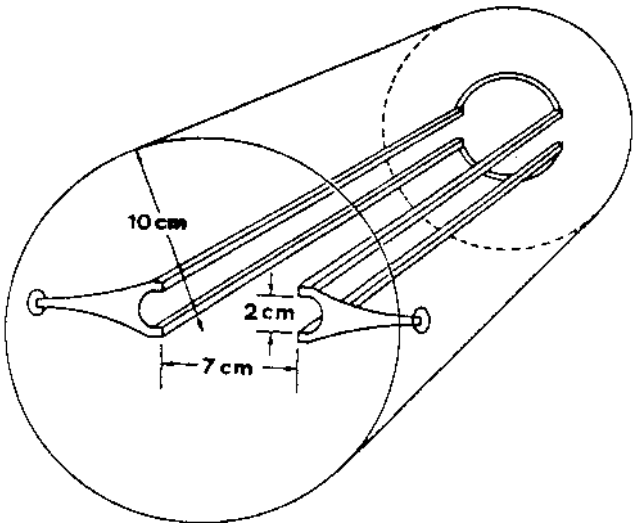

Figure 2. Kicker Magnet Artistic View.

In order to reduce the high voltage of the pulsers two different lengths are designed for the kicker: K1 and K2, which must deliver a higher magnetic field at extraction, are 75 cm long while K3 and K4 are 50 cm long. The measured inductance of the two kicker types is: 740 nH for K1 and K2, 610 nH for K3 and K4.

The connections from the large circular kicker vacuum chamber to the bending magnet one are tapered in order to reduce the longitudinal impedance to the beam.

3. POWER PULSER

The pulser scheme is shown in Fig. 3. Each kicker is powered by a thyratron switch pulser resonantly discharging a capacitor into the coils inductance.

The resulting waveform is almost half-sinusoidal as shown in Fig. 4.

As mentioned before, the pulse length must not exceed ~220 nsec. Then we use an EEV CX1154D thyratron with a 120 KA/μsec current rise rate and a 6 nF capacitor (Murata).

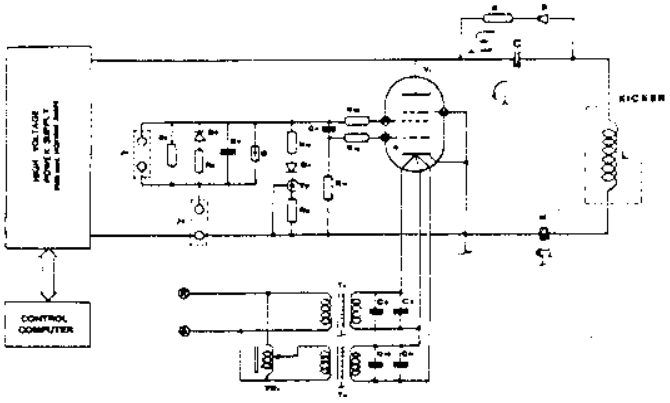

Figure 3. Kicker Power Pulser Circuit.

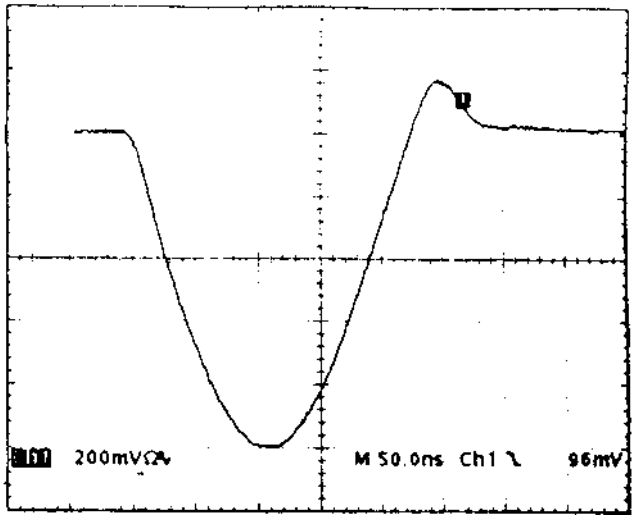

Figure 4. Current Pulse Shape.

A series of fast solid-state diodes and resistances is paralleled connected to the capacitor to prevent high inverse voltage at the thyratron when this is switched off and to avoid the inverse current in the kicker coils.

It is necessary to continuously control the trigger delay to correct temperature-induced effects in the thyratron pulsers.

The pulser is located very close to each kicker section in order to reduce the wiring parasitic impedance. The current pulses are monitored and the power supplies are computer controlled from the control room.

The kicker prototype measurements show that the maximum power supply voltage needed should not exceed 35 KV.

4. MAGNETIC MEASUREMENTS

The magnetic field in the kicker prototypes is detected by a copper coil (100*1.6 $mm^{2)}$ aligned on the mechanical axis of the coils and the induced voltage is measured at an oscilloscope after time integration by means of a passive circuit.

The measured field/current characteristic is 80.7 G/KA: we need therefore a maximum current of ~2700 A from the pulser (the coils are paralleled).

Fig. 5 shows the dependence of the vertical field normalized to its central values as a function of the distance from the axis: the measurement is performed by moving the probe coil in the transverse plane.

Figure 6 shows a tridimensional plot of the magnetic field as a function of both horizontal and vertical coordinates.

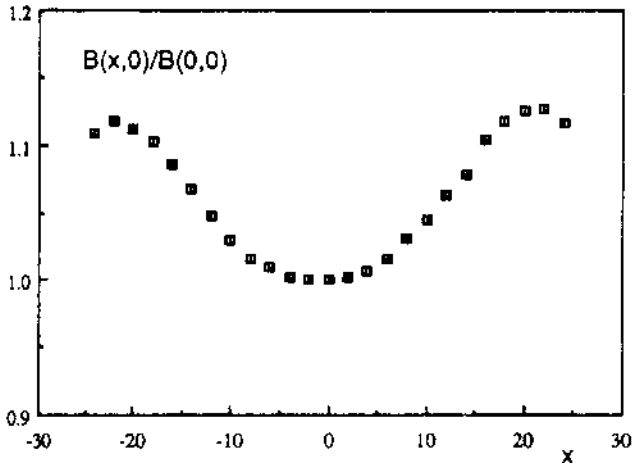

Figure 5. Measured Ratio of the Centre Value Versus the Distance x from the Axis.

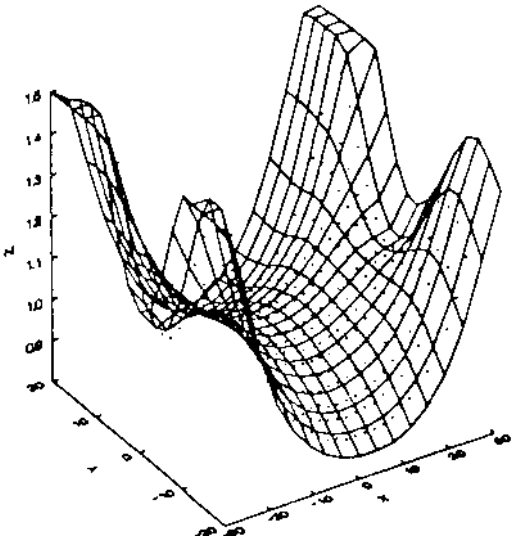

Figure 6. Tridimensional Plot of the Measured Magnetic Field.

5. ACKNOWLEDGMENTS

We would like to thank all members of the Mechanical and Electronic groups of the Accelerator Division for the work of construction of the kicker and power pulser prototypes, C. Milardi, M.A. Preger and M. Serio for the useful discussions, and P. Possanza for editing and fine-typing the manuscript.

6. REFERENCES

[1] R. Boni et al.: “The Frascati Φ-Factory Injection System” , IEEE 1991 Particle Accelerator Conference, S. Francisco, USA, May 1991.

[2] M. Masullo, C. Milardi and M.A. Preger: "DAΦNE Accumulator Update-3", DAFNE Technical Note I-8, Frascati, Rome, Italy, March 1992.

[3] A.Aragona et al., "New Injection System for ADONE", EPAC1990 Proceedings, Nice, France, June 1990.

DAΦNE Accelerating Cavity: R&D

S.Bartalucci, R. Boni, A. Gallo, L. Palumbo*, R. Parodi+, M.Serio, B.Spataro and G. Vignola
INFN Laboratori Nazionali di Frascati
C.P. 13 - 00044 Frascati (Roma) - Italy

* Dipartimento di Energetica, Università di Roma 'La Sapienza'
Via A. Scarpa 14, 00161 Roma, Italy

+ INFN Sezione di Genova, Via Dodecaneso 33 - 16146 Genova - Italy

Abstract

Multibunch instability is one of the most serious concerns for the high luminosity, high current DAΦNE Storage Rings which will be built at Frascati. Much effort is presently put in on the development of a true 'single-mode' cavity, with the lowest contents of Higher Order Modes (HOMs). Various damping techniques are currently investigated, in order to optimize the final design of the cavity. The first theoretical and simulation results, and experimental tests on prototypes are described, together with the HOM Tuning technique to get rid of multibunch instabilities.

1. INTRODUCTION

One of the basic requirements of DAΦNE is an accelerating RF cavity with the lowest possible interaction of the HOMs with the beam . This is to minimize both single bunch and multibunch instabilities, which are a serious concern for the machine performance. Extensive and thorough calculations and simulations of such instabilities are still in progress [1], showing the need for very low HOM shunt impedance, even in the presence of a fast digital feedback system. A careful design of the cavity geometry is required, together with the use of various techniques (HOM global damping with waveguides, Insertion of lossy materials, Shifting, i.e. Tuning of some very dangerous HOMs), which are described in this paper.

2. RF CAVITY DESIGN

The main feature of the DAΦNE accelerating cavity is the presence of very long tapers, which provide a smooth transition from the cell iris to the ring vacuum pipe (Fig. 1). This design is rather unconventional as compared with the usual geometry of both normal conducting and superconducting structures, which include, besides the tapers, two straight, large-radius beam tubes where RF and HOM couplers are installed [2]. Nevertheless, the longitudinal loss factor to the HOMs, k_{pm}, is very low as compared to the total loss factor k_l, hence this cavity offers a very small contribution to the whole impedance budget. Furthermore also the transverse loss factor k_t' is definitely lower than in the usual design, and in general the contribution of dipolar modes is less significant.

Much work was done on the optimization of the cell profile. The original requirement was to have a cavity with a shunt impedance $R_s = V^2 / 2P = 3\ M\Omega$ on the fundamental mode, low impedance on the transverse modes, and no special care was taken on the lowest monopolar mode, the TM_{011} mode, which must be strongly damped anyway. These requirements are well satisfied with a geometry like that of superconducting cavities, often called 'bell-shaped' cavities. An example is shown in Fig. 2, which displays a smooth, rounded profile (i.e. high Q) with a straight insertion to allow the connection of one or more waveguides to the lateral surface of the resonator. Later on, the requirements on the R_s were made less stringent, while it seemed more useful to have a very low design value also for the R/Q of the TM_{011} mode. Following an idea of SLAC-LBL people, we introduced nose cones (Fig. 3), which decrease the Q's noticeably, but increase the R/Q and the loss factor k_0 of the TM_{010} and the R'/Q of the TM_{110}, while strongly reducing the TM_{011} mode. A full comparison of the two cell parameters is shown in Table I.

An elliptical contour was adopted for the upper part of the nosecone cell, since extensive studies of multipactoring effects have clearly shown the risk of other designs. For instance, in the case of a square shaped profile, a simulation with the multipactoring code NEWTRAJ [3] has revealed the existence of three thresholds at the cavity voltages of 180, 250 and 370 kV in the upper part of the cavity, where the resonant RF discharges are located. To avoid such troubles, a multipactoring-free elliptical contour was chosen.

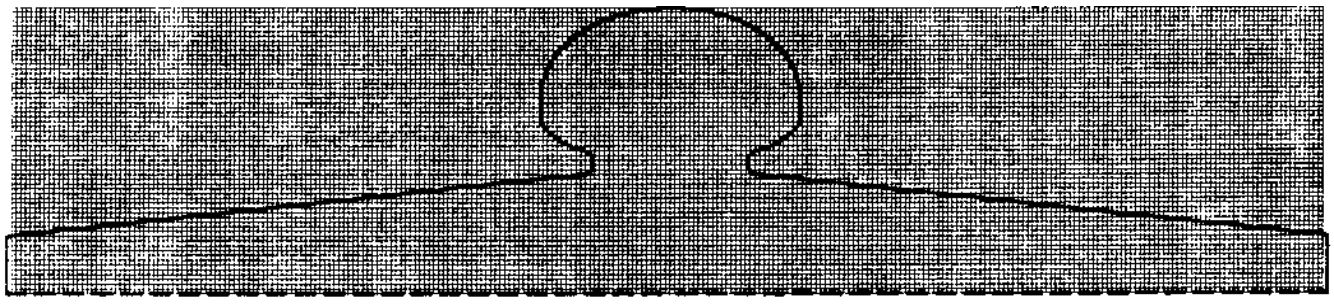

Figure 1. The Long Tapered Cavity.

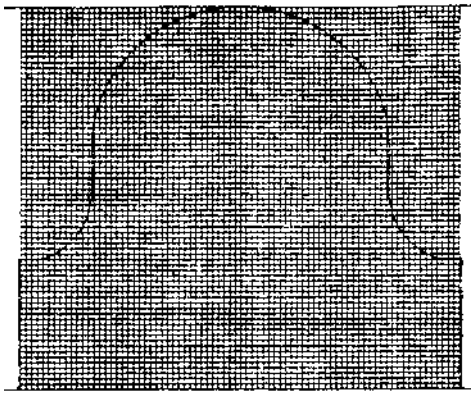

Figure 2. The 'Bell Shaped' Cell.

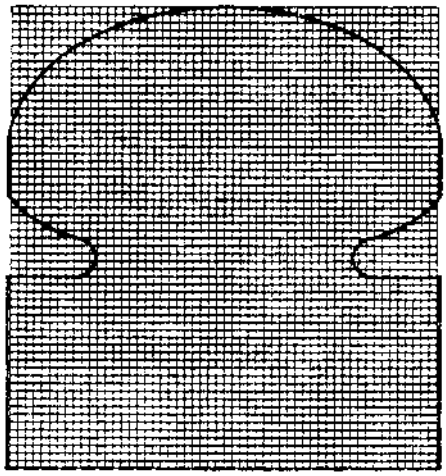

Figure 3. The 'Nosecone' Cell.

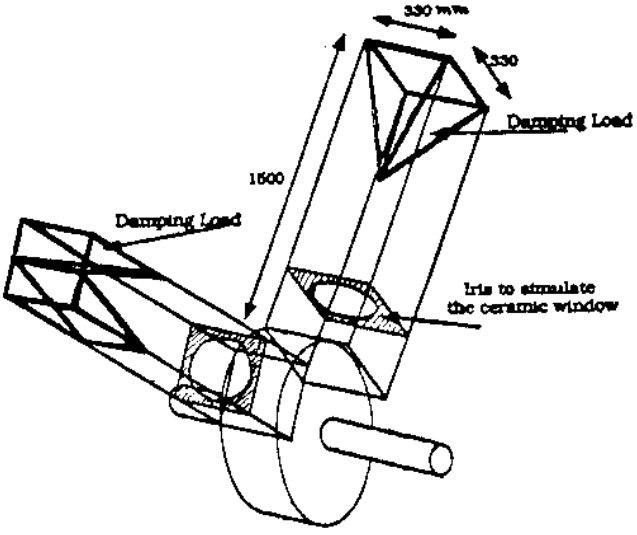

Figure 4. The Large Waveguide Test Cavity.

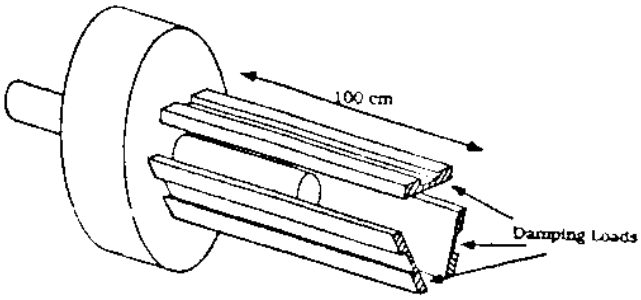

Figure 5. The Small Ridged Waveguide Test Cavity.

Table I
Design parameters for the DAΦNE nosecone cavity and comparison with a typical bell-shaped structure

	Nosecone	Bell-shaped
Frequency (MHz)	367.0	368.5
R/Q (Ω)	70.0	62.2
Q	34000	46800
R_S (MΩ)	2.37	2.91
k_l (V/pC)	0.101	0.121
k_0 (V/pC)	0.077	0.068
k_{pm} (V/pC)	0.024	0.053
k_t' (V/pC/m)	1.16	1.26
k_{pm} / k_l	0.24	0.44
k_t' / k_0 *1 mm	0.015	0.019
TM_{011} mode:		
Frequency (MHz)	703.7	733.7
R/Q (Ω)	4.0	13.9
Q	30400	49000
R_S (kΩ)	120	680
TM_{110} mode:		
Frequency (MHz)	564.0	531.5
R'/Q (Ω)	30.6	15.7
Q	41200	52500
R'_S (MΩ)	1.26	0.82

3. HOM DAMPING STUDIES

Several laboratory measurements on a copper pill-box cavity resonating at 370 MHz were done and are still in progress. Two main approaches have been followed to couple off the parasitic HOMs:

a) by means of large waveguides, which directly look at the beam axis (Fig. 4) according to the proposal of Conciauro and Arcioni [4];

b) by means of small, ridged waveguides, parallel to the beam axis (Fig. 5), according to the SLAC-LBL Design [5].

In both cases the cut-off frequencies are adjusted to be little below the frequency of the lowest HOM and the waveguides are filled with highly dissipative materials, like graphite loaded polyurethan foams, which are properly shaped for RF broadband matching.

The amount of global damping is excellent in the a) case, as shown in Fig. 6, but some problems have to be faced:
- high degradation of the Q of the accelerating mode (≈30% less than the unperturbed Q_0);
- large size ceramic windows must be used in the waveguides to separate the cavity main body, which is under deep vacuum, from the damping loads;
- multipactoring will very likely occur on the waveguide inner surface, where the e.m. fields are evanescent; TiN coating will therefore be necessary;
- efficient cooling of the damping loads has to be provided.

In the b) the HOM damping is less effective than in a) case (Fig. 6), but it displays some advantages:
- the accelerating mode Q_0 is almost unaffected;
- the waveguide ceramic windows may be smaller;
- the reduced size and compact structure make manufacturing and operation easier.

TiN coating will be necessary, anyway, and also great care is needed for the cooling of the absorbers.

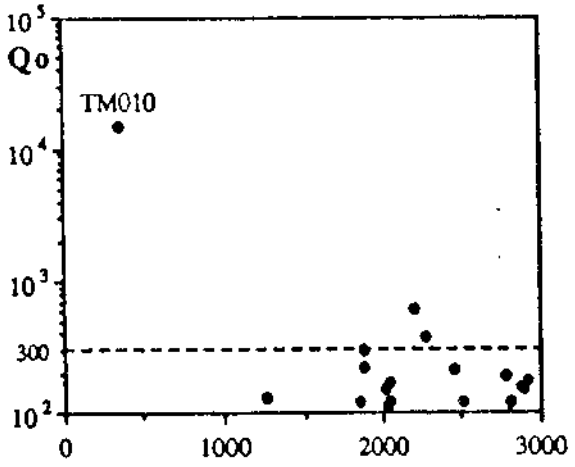

Figure 6a. Damped HOM Spectrum of the Cavity in Fig. 4.

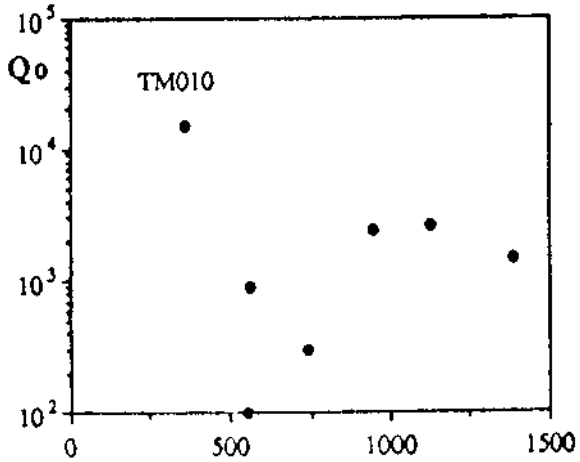

Figure 6b. Damped HOM Spectrum of the Cavity in Fig. 5.

3. HOM TUNING

An alternative way to fight collective coupled-bunch instabilities consists in shifting the HOM frequency, without affecting the fundamental mode, by means of perturbing metallic objects, which are located in some appropriate positions on the inner surface of the cavity. Preliminary measurements on a test pill-box cavity at Frascati gave encouraging results [6] and showed the validity of the principle. Further studies on a more realistic cavity model are presently in progress at the INFN Laboratories in Genoa. As an example, the shift of the TM_{011} mode by the presence of a movable small metallic cylinder is shown in Fig. 7. The Q degradation is very small, while the fundamental mode TM_{010} remains absolutely unaffected. The amount of frequency shift is 1.4 MHz, what corresponds to about half distance between two adjacent lines in the coupled-bunch mode spectrum. This result seems very promising, and suggests that this technique can be applied to decouple a particularly offending HOM from an unstable relative mode in a real cavity. Since the perturbing object must be used in connection with the cavity tuning system, a careful control of the operation of both tuners is required to fully assess the feasibility of the method.

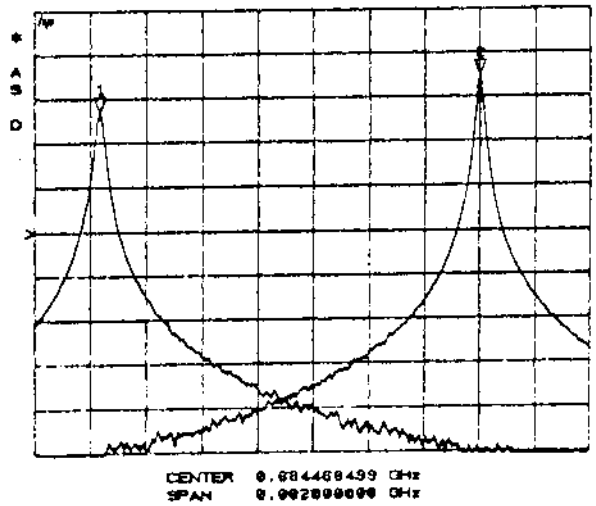

Figure 7. Frequency Shift of the TM_{011} Mode.

4. REFERENCES

[1] S.Bartalucci, et al., "Impedance and Beam Dynamics in DAΦNE", paper submitted to this Conference.

[2] S. Bartalucci, L. Palumbo and B. Spataro, "A low loss cavity for the DAΦNE Main Ring", DAΦNE Technical Note G-6, 1991.

[3] P. Fernandes and R. Parodi, "NEWTRAJ,a computer code for the simulation of the electron discharge in accelerating structures", Proc. of the 1987 Particle Accelerator Conference, Washington, USA, p. 1857, May 1985.

[4] G. Conciauro and P. Arcioni, "A new HOM-free accelerating resonator", Proc. of the 2nd European Particle Accelerator Conf., Nice, France, June 12-16, 1990, p.149.

[5] R. Rimmer, F. Voelker, G. Lambertson, M. Allen, J. Hodgeson, K. Ko, R. Pendleton, H. Schwartz and N. Kroll, "An RF Cavity for the B-factory", Proc.of the 1991 Particle Accelerator Conference, S. Francisco, USA, May 1991.

[6] S. Bartalucci, R. Boni,A. Gallo, L. Palumbo, M. Serio, R. Scalia, B. Spataro and G. Vignola, "A perturbation method for HOM tuning in, a rf cavity", Nucl. Instr. and Meth. in Phys. Res., A309, p.355, 1991.

Design Criteria and Measurements of the Prototype of the DAΦNE Accumulator Cavity

S. Bartalucci, R. Boni, A. Gallo, H. Hsieh, G. Raffone and B. Spataro
I.N.F.N., Laboratori Nazionali di Frascati
C. P. 13, 00044 Frascati, Rome (Italy)

Abstract

This paper deals with the design criteria of the accumulator RF cavity of the Frascati 510 MeV Φ-Factory DAΦNE. Particular care was given in defining the cavity geometry in order not to have resonant electron loading. Other important engineering aspects, such as cooling and thermal effects, are outlined. The possibility of damping the parasitic cavity modes is investigated and the preliminary RF tests on a copper prototype are presented.

1. INTRODUCTION

The Φ-Factory project at LNF [1] includes an accumulator ring to store electrons or positrons injected from the 510 MeV Linac before filling the main rings. A single 130 mA bunch will be stored in the accumulator and extracted at a 1 Hz rate for the injection in the DAΦNE rings.

The main parameters of the Accumulator Radiofrequency (RF) System are listed in Table 1. The RF frequency is exactly one fifth of the main ring to synchronize the injection into any desired bucket of DAΦNE [2]. An accelerating cavity peak voltage of 200 kV is also required to have large energy acceptance. The beam synchrotron and parasitic losses are estimated to be about 3.6 kW.

Table 1
Accumulator RF System main parameters

RF Frequency	73.651 MHz
Harmonic number	8
RF Peak Voltage	200 kV
RF Energy Acceptance	2.38 %

2. CAVITY DESIGN CRITERIA

Due to the low operating frequency and the short straight section available in the accumulator (1.2 m), the cavity is necessarily a reentrant single ended coaxial resonator which is compact in size and simple to manufacture. The cavity drawing is shown in Fig.1. The profile of the surface has been studied in order not to have multipacting (mp) that often makes the cavity operation unreliable. The computer code Newtraj [3] has been run to predict the areas of the inner cavity surface where the resonant electron loading is most probable. The cavity profile was then optimized according to the results given by the code.

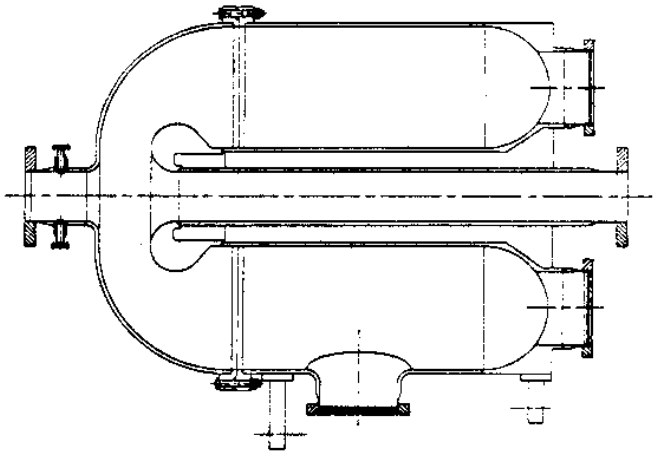

Figure 1. Profile of the Accumulator Cavity

In Fig. 2 is shown the only mp trajectory evidenced by Newtraj. In some cases, RF conditioning is helpful to cure mp but a moderate coating of TiN on those areas should however be necessary.

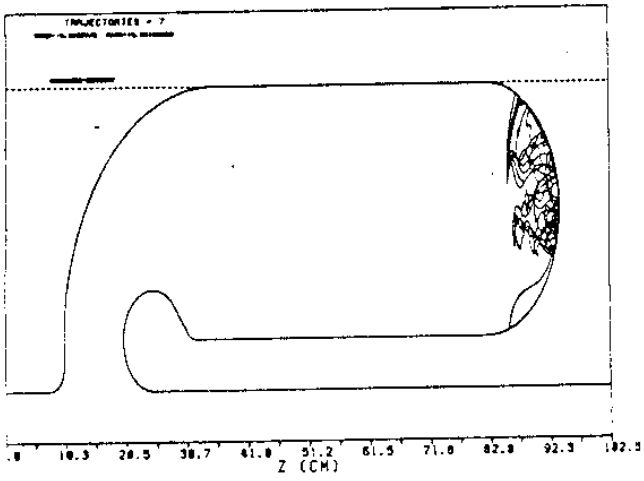

Figure 2. Simulation of a mp trajectory at 190 kVp.
(Cavity not to scale)

The cavity will be fabricated with OFHC copper to ease the cooling and reduce the dissipated RF power. Also, the use of copper is well suited for ultra high vacuum.

The cavity will be coupled with a loop to the 6-1/8" RF coaxial line and tuned with a cylindrical plunger both located in the magnetic field region of the accelerating mode. An additional port on the cavity body is foreseen to connect a vacuum pump.

3. PROTOTYPE TESTING

A copper sheet full scale prototype, shown in Fig.3, was tested in laboratory. The capability of a 116 mm diameter plunger of tuning the cavity over a temperature range 20÷40°C has been checked; the maximum tuner penetration is 3 cm.

The needed coupling factor with the RF station is $\beta = 1.26$ and has been set by rotating the RF input loop.

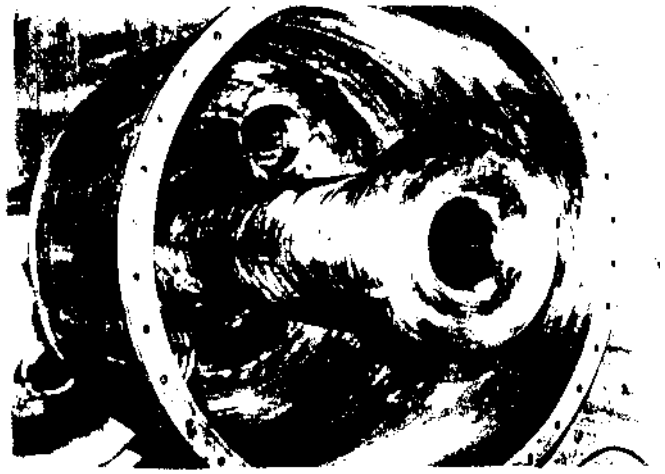

Figure 3. The cavity prototype before testing.

Table 2
Accumultor cavity parameters

	(calculated)	(prototype)
RF Frequency	73.651 MHz	(73.607)
Unloaded Qo	22,000	(19,000)
Shunt Impedance ($V^2/2P$)	1.74 MΩ	(1.50)
Peak Gap Voltage	200 kV	
Cavity wall losses	13.3 kW	
Beam power	3.5 kW	
Coupling factor β	1.26	
Max Surface Electric Field	3.9 MV/m	
Max Axial Electric Field	1.48 MV/m	
Cavity length	900 mm	
Cavity diameter	750 mm	
Gap length	100 mm	

The cavity spectrum has been measured with the network analyzer HP8753C and compared with that calculated with URMEL code. Table 3 reports a list of high order modes (HOM) monopoles and dipoles till 1 GHz which lay very close to a beam spectrum line (that are 9 MHz spaced). In fourth column we list the Q values of these HOM obtained connecting three damping loops to the cavity (two loops are at 90° with respect to each other for coupling the two polarizations of the dipole modes). The (R/Q)'s were measured with the perturbation method [4]. Since the particular cavity shape, the modes may not be classified as usual in technical literature.

Table 3

Monopoles	*Freq.(MHz]*	*Qo·*	Q_L·	*R/Q (Ω)*
TM0-5	607.94	11000	50	0.6
TM0-8	783.36	7000	1500	0.82
TM0-9	884.51	5500	750	0.70
Dipoles	*Freq.(MHz]*	*Qo*	Q_L	*R/Q (Ω)*
1MM-6	709.43	7000	1000	0.31
1MM-7	722.66	3000	500	0.17
1MM-9a	801.15	17400	5300	1.86
1MM-9b	801.64	18000	4200	1.86
1MM-10	828.78	6300	70	0.2

4. COOLING CRITERIA

The heat load due to the RF wall losses (about 13.3 KW) can be removed by means of copper cooling pipes simply brazed on the external surface of the cavity; then the wall temperatures are kept constant as the influence of the surrounding environment (i.e. air temperature) is practically negligible.

A temperature field evaluation can be carried out by means of a finite element analysis [5] and it may be useful to check, during the mechanical design, the behaviour of the cooling system; in other words the design parameters (as pipes number, position and diameter, mass flow rates) can be varied to achieve an optimal arrangement between the cavity permissible deformations and the cooling system requirements; this kind of approach can be useful also from a cost reduction point of view.

In this thermal analysis the quality of brazings plays an important role from the heat exchange point of view; as the effective contact area depends on both the brazing process and the geometry of the surfaces, care must be given during the computation of the real heat exchange coefficient; theoretically the worse obtainable coefficient depends roughly on the ratio between the water convective coefficient and the pipe thermal conductivity, the pipe equivalent diameter and the thickness of the pipe.

Fig. 4 shows the temperature solution of one of the configurations taken into account.

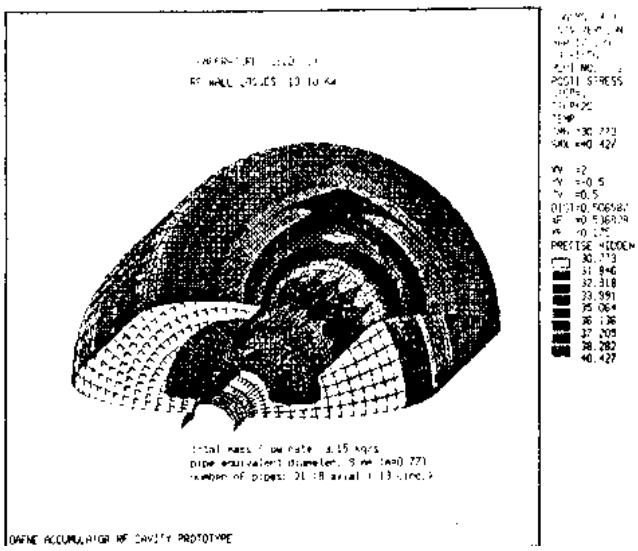

Figure 4. Cavity temperature field.

A structural analysis has also been perfomed in order to evaluate the deformations induced by the temperature gradients (see fig. 5); the total variation of the cavity resonant frequency can also be easily computed by means of the displacements solution and the Slater Theorem.

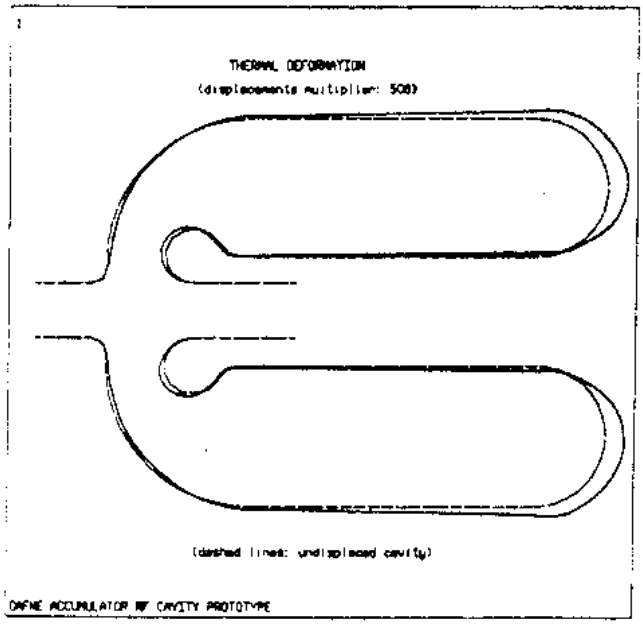

Figure 5. Thermal deformation (greatly amplified).

The dependence of the cavity volume due to the inlet water temperature changes and the mass flow rate changes is shown in fig. 6, where the variations of the cavity resonant frequency are plotted versus the difference between the inlet water temperature Tiw and an "operating temperature" To.

Of course these results depend on the structural boundary conditions of the cavity; in this case the cavity gap does not expand freely and the resonant frequency depends on the volume variations of the regions of only magnetic field as fig. 5 shows. Further computations are still in progress.

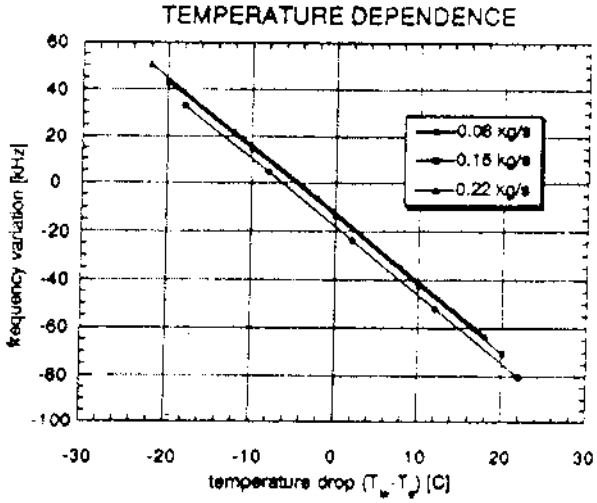

Figure 6. Temperature dependence of the cavity frequency.

5. ACKNOWLEDGEMENTS

The RF tests would have not been possible without the support of the RF technicians P. Baldini, F. Lucibello and S. Quaglia. Also special thanks are due to G. Fontana for the mechanical design of the cavity.

6. REFERENCES

[1] The DAΦNE Project Team, "DAΦNE Status Report", this conference.

[2] R.Boni, S.Kulinski, M.Preger, B.Spataro, M.Vescovi, and G.Vignola, " The Frascati Φ-Factory Injection System", Proc. of the Particle Accelerator Conference, S. Francisco, May 1991 (to be published).

[3] R.Boni, V.Chimenti, P.Fernandes, R.Parodi, B.Spataro and F.Tazzioli, " Design and Operation of a Multipacting Free 51.4 MHz RF Accelerating Cavity ", Nuclear Instruments and Methods in Physic Research, A274, pp. 49-55, 1989.

[4] L.C.Maier and J.C.Slater, " Field Strength Measurements in Resonant Cavities ", Journal of Applied Physics, Vol.23, n. 1, January 1952.

[5] ANSYS, Swanson Analysis System Inc., Houston, Pennsylvania, 15342 (USA).

Magnetic Components for DAΦNE

H. Hsieh, M. Modena, C. Sanelli, S. Vescovi
INFN Laboratori Nazionali di Frascati
C.P. 13 - 00044 Frascati (Roma) - Italy

Abstract

An overview of the magnetic components needed for DAΦNE project is given. The design parameters, engineering realization philosophy, construction approaches and the magnetic measurement methods will be described.

1. INTRODUCTION

INFN-Frascati National Laboratory is currently designing and constructing A 510 MEV electron positron colliding facilities. Figure 1 shows the birds-eye view of the facilities. It is a fully funded project with anticipated construction period of five years. The new facilities will be installed in the existing buildings and tunnels, there are some modifications have to be carried out prior to installation. The removal and storage of old radioactive equipment are very difficult tasks in this space limited campus. The project consists of two storage rings, accumulator, electron positron linac and approximately 200 meters of transfer lines. There are vast numbers of magnets of various types are required for this facilities. Due to lack of in-house manpower, it is anticipated that industrial collaboration will be heavily sought during the course of construction. This paper merely deals with magnetic components in general terms, many special magnets are presented elsewhere in this conference.

2. GENERAL CONSIDERATION

The DAΦNE has an on energy injection system, therefore, ramping of the magnetic components is not the machine function requirement. However, the stringent requirement of field strength uniformity of the storage ring components in the same circuit and reasonably large quantity of identical components warrant the laminated type construction.

The storage ring lattice requires both sector like and parallel end dipole magnets distributed in the machine. The magnet cross sections are distinctively difference between these two type of construction, a pseudo sector like magnet is being contemplated by the project staff. it is essentially a parallel end magnet with pole region machined orthogonal to the beam trajectory. It is obvious that this type of construction enables us to have only one kind of dipole lamination, the fabrication will also be simplified.

The width of the storage ring chamber is in the order of half meter, DAΦNE is a low energy high beam current storage ring, the vacuum quality is one of the important considerations to the performance of the machine. Synchrotron radiation will be absorbed at few discreet locations downstream of either bend magnets or wigglers where appropriate copper absorbers and large pumps can be installed. The chamber will only functioned as a vacuum enclosure capable of resisting atmospheric pressure. The multipoles in the arc sections of the storage ring will have sufficient horizontal aperture to accommodate this wide chamber. We have chosen conventional multipole configuration, with return yokes passing through the midplane of the magnet, for our multipoles in this region. It is our belief that a better quality with comparable component cost can be realized by adopting this option.

The requirements of orbit correctors are very weak, they are in the order of 1-2 mrad. There are horizontal correctors incorporated into storage ring benders, those at other locations are of lump type. There will be no correctors incorporated into either quadrupoles or sextupoles, the undesirable effects due to this type corrector scheme will become bothersome to the machine, one should result to this type approach when the longitudinal space is at premium. All the corrector yoke will be made of 0.3 mm transformer grade steel to achieve faster response.

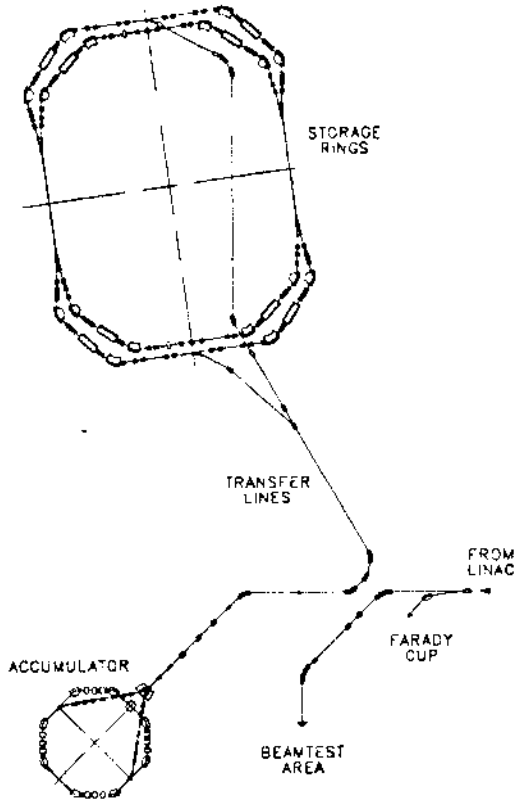

Figure 1. DAΦNE Birds-eye View

The dipoles will be supported on the reinforced concrete pillars to gain better stability and to isolate usual low frequency mechanical vibration transmitted through the ground floor. Multipoles and other components in the same straight

section will be supported on a common rigid girder, either made of meehanite casting or a properly stress relieved welded steel structure. The alignment of these components on the girder will be carried out in the assembly shop so that the placements in the machine will be greatly simplified. The multipoles will have the provision for adjustments individually in the ring should it be found desirable during the course of commissioning.

The alignment of the machine components is relatively simpler to compare with that of large machines. Both accumulator and storage rings are housed in separate open hall, lines of sight will not be obscured. The alignment accuracies are 0.2 mm transverse and vertical; 0.25 mrad. rotational. The alignment instruments for angles and levels will be conventional optical devices and the distance measurements will be done by utilizing Distinvar and invar wires. The survey network, which determines the correct positional relationship between injector system and the storage rings, will be more complicated to establish due to the existing building walls and tunnels.

There are approximately 400 total magnetic components of various type needed for the project. We have made large effort to minimize the number of different variety of the same type magnets so that the construction cost and schedule can be reduced. Most of the magnets are of conventional type. This paper will only describe few of those more interesting components.

3. PSEUDO SECTOR LIKE DIPOLE

3.1 Configuration

Figure 2. shows the preliminary design of pseudo sector like dipole for the storage rings, it is essentially a parallel end magnet with the end of pole area machined orthogonal to the trajectory. The yoke is made of extra low carbon steel sheet of 1.5 mm thick, with the requirement of machining, the end portion has to be glued. The whole assembly will have appropriate solid steel straps and stainless steel end plates welded together to form a self supporting rigid body. The coils are made of copper hollow conductors with low current density of 2.2 A/mm^2.

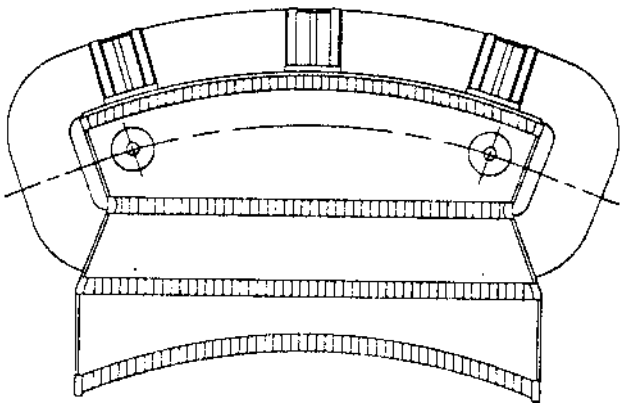

Figure 2. Pseudo Sector Like Dipole

Trim coil packages are part of the magnet to provide horizontal orbit correction and field integral adjustments. There will be three fiducial marks on top of the magnet for alignment purposes. The total assembly weighs six tons, it is supported on kinematic mounts which will be mounted on reinforced concrete pillar to achieve the proper beam height of 1,200 mm.

3.2 Magnetic calculation

A preliminary three dimensional magnetic calculation has been carried out to asses the validity of the engineering approach. Figure 3 shows the field plots at center and end of the magnet. The results of this preliminary investigation indicate that it is possible to have this type of design. We will proceed with more detailed studies in regarding to the higher harmonic contents and ampereturn differential between this magnet and true parallel end dipole which is part of the same circuit. Pole profile optimization will also be carried out to enhance the field quality or to reduce the physical size of the magnet.

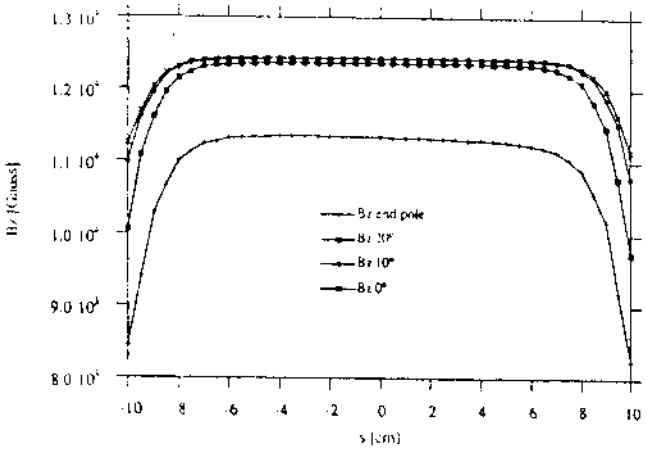

Figure 3. Pseudo Sector Like Dipole Field

4. ACCUMULATOR DIPOLE

4.1 Configuration

The dipole for the accumulator ring is of solid steel, combined function "H" type magnet. Nominal field is 1.55 Tesla with field index of 0.5. The magnet gap along the isomagnetic line is 42 mm. There are total of eight such magnets required for the machine. The total length of dipole is therefore only in the order of seven meters, with such a small quantity, we have decided to make the yoke out of solid steel. A careful quality assurance program will be instituted to guarantee the uniform magnetic performance of all the magnets. There is no corrector windings incorporated into this dipole, the compensation of the field integral will be accomplished by shunting resistors. Figure 4.1 shows the cross section of this magnet. The yoke is made up with six pieces machined steel, the coils are conventional copper hollow conductors with current density of 4.5 A/mm^2.

The higher current density is the result of limited circumference of this machine. The alignment fiducials and supporting approach are similar to that of storage dipoles.

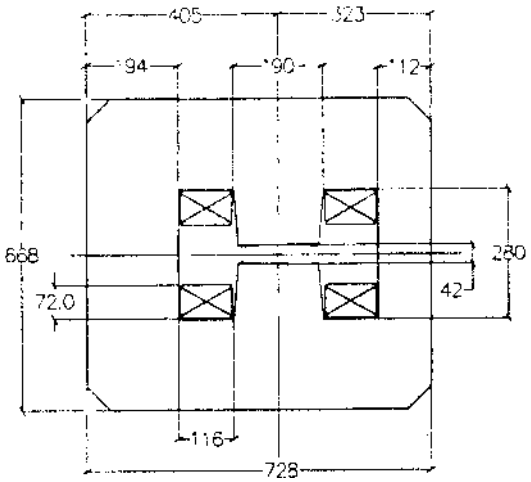

Figure 4. Accumulator Dipole

4.2 Magnetic Calculation

Magnetic calculation has been carried out with POISSON code using circular coordinates. Figure 2 shows the field plot radially. The three dimensional calculation will be done in the near future.

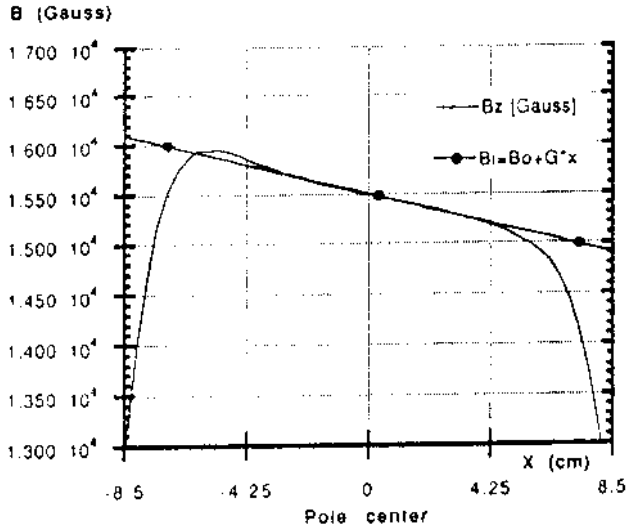

Figure 5. Accumulator Dipole Field

5. MAGNETIC MEASUREMENT

An old experimental hall, $24.5 * 12$ m^2 in area has been completely refurbished to provide a clean and air-conditioned environment for magnetic measurement purposes. The magnetic measurements of prototype magnets for splitter and septum will take place before this summer. Due to very small scanning area inside the gaps of these magnets, a Hall probe (Group 3 Digital Hall Effect Teslameter by Danfysik) will be used. The Hall probe will be placed on the 'nose' of the x-y-z translator which has a 20 micron positional reproducibility. Different Hall probes with the same instrument will be used for different type of magnets. The reading precision is guaranteed to be $\pm 1 * 10^{-4}$.

Quadrupoles and sextupoles magnetic measurement and field characterization will be carried out by means of the Multipole Magnet Measurement System model. 692 of Danfysik. With this system we shall measure all the quadrupoles and sextupoles of DAΦNE facilities. The system is based on well experienced rotating coil technology which will give directly the higher harmonic contents of the multipole under examination. In addition, the alignment of the magnet prior to measurement is automatically performed by the system. The fiducialization of the magnet will be performed after the completion of the measurement by the same system. We expect to be able to characterized two-four magnets a day. Different rotating coils will be used due to both the different bore apertures and multipole strengths. The system meets the following specifications:

- Relative accuracy of integrated main harmonic $\pm 3 * 10^{-4}$
- Accuracy of ratio between integrated field of a multipole component and the main component $\pm 3 * 10^{-4}$
- Fiducialization with respect to magnetic central axis to within $\pm$ 30 μm.

We are currently considering different options for our dipole measurements, no final decision has been made yet. The approaches under consideration are Hall probe scanning; movable integral coil; or fixed coil with field ramped. The measurements will be carried out with respect to a reference magnet. For the wigglers, we shall proceed with integral measurements on a full scale prototype, to determine the correct end poles and clamps shape to vanish the field integral. This will be accomplished by using an existing device based on 3 m long rotating coil that can be radially translated.

Splitter Magnets for DAΦNE Project

C. Sanelli, H. Hsieh
INFN-Laboratori Nazionali di Frascati
C.P. 13, 00044 FRASCATI (Roma) ITALY

Abstract

This paper describes the design of the splitter magnets which separate the circulating beams immediately after passing through the DAΦNE interaction point. The results of both 2-D and 3-D magnetic calculations will be presented, the electrical and mechanical design will be described. A 1/3 length prototype of this magnet is under construction.

1. INTRODUCTION

A 510 MeV electron positron colliding beam facility, known as DAFNE, is currently under design and construction at Laboratori Nazionali di Frascati dell'INFN. The project consists of two storage rings, accumulator, electron/positron linac and transfer lines. There are two splitter magnets, located on the either side of the interaction point, they deflect the circulating beams into IP with appropriate crossing angle and guide them into the appropriate storage ring afterward. The magnets are of iron core electromagnetic type, the design field is 0.17 Tesla at a magnetic gap of 50 mm. A full scale prototype of reduced length is presently under construction. A very careful magnetic calculations, both in two and three dimensions, have been carried out to assure that both the dipole field uniformity and the other harmonic contents of this magnet are within the limits required by machine lattice.

2. MAGNETIC CALCULATIONS

The design parameters of the Splitter Magnet for DAΦNE are:

Energy	510	MeV	
Bending angle	0.15		rad
Bending radius	10		m
Magnetic field	0.17		Tesla
Full gap	50	mm	
Magnetic length	1.5		m
Entrance beam-beam separation	10		cm
Exit beam-beam separation	32.46		cm
Field quality ($\Delta B/B$ at ±25 mm)	$< \pm 5 * 10^{-4}$		

A simple minded way to generate an alternate and compact magnetic field is to place, side by side, two H-type magnets with opposite polarity (shown in Fig. 1a). This arrangement can be further simplified by observing the magnetic flux path (Fig. 1b) in the central return leg, the fluxes from the two magnets cancel each other, and so no iron is necessary (Fig. 1c).

Figure 1c shows the configuration which has been studied carefully in two dimension by means of POISSON computer code [1]. We have focussed our attention to the beam entrance end,where due to the small trajectory separation, is a more critical area.

Many different magnet geometries have been studied:

- Magnet with iron poles and correction shims
- Magnet with iron poles without correction shims but with pole face windings
- Window-frame type magnet with different type coil geometry.

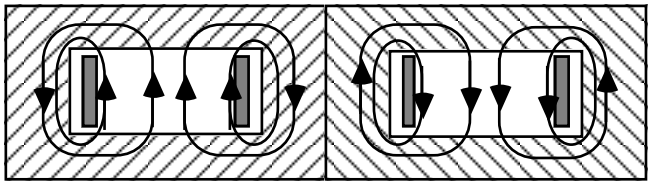

Fig. 1 a

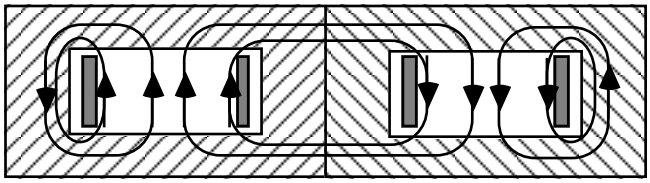

Fig. 1 b

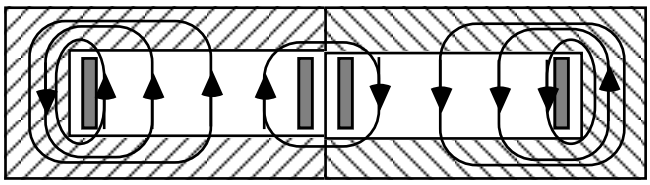

Fig. 1 c

Figure 1a,b,c - Split field magnets

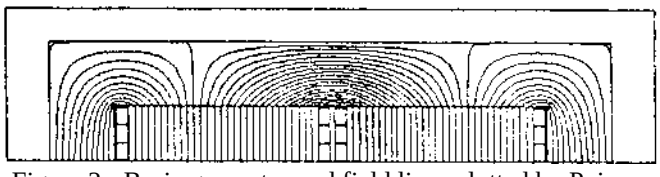

Figure 2 - Basic geometry and field lines plotted by Poisson

This paper will only discuss the configuration shown in Fig. 1c, since it is the more favourable one from the field quality point of view.

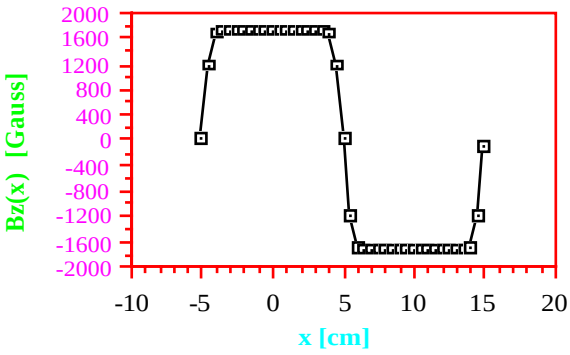

Figure 3 - Bz(x) Poisson code

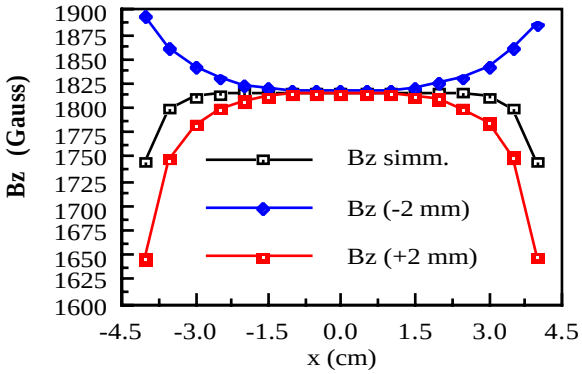

Figure 4 -Bz(x) as function of the coil position

A 2-D Poisson analysis was carried out on the magnet geometry shown in Fig. 2 which also shows the flux lines within the magnet boundary. The mesh size of this particular run is of 1 mm in order to obtain more precise results.

The horizontal coil size has been chosen as small as possible, in order to improve the magnetic field homogeneity. The copper conductor size used in these calculations are: 7.5 ∗ 5.5 mm^2.

Fig. 3 shows the magnetic field, as calculated by Poisson, in the section under examination.

The maximum deviation with respect to the median plane central magnetic field is in the order of $-7*10^{-4}$ at x=-25 mm, where "x" axis represents the radial coordinate, perpendicular to the beam direction. The "beam centers" are located at x=0.0 cm and x=10.0 cm respectively.

Being a picture frame window magnet, It is therefore very important to understand the influence of the coil location accuracy to the field quality. Two cases, where the coil has been considered as a single turn having the same external dimensions as that of the three turns, have been investigated due to the effect of a 2 mm upward and downward shift on the field homogeneity. The figure 4 depicts this effect. It is clear that during the magnet engineering design and manufacturing, a great care must be excised to assure that the proper coil location accuracy can be achieved.

A 3-dimensional calculation of a 40 cm long magnet has been performed with the Magnus code [2]. The coil ends have been assumed to be saddle-type to provide more space for the machine vacuum chamber and to improve the fringing field quality.

At the present time, a pseudo elliptical shape vacuum chambers, one for each beam, have been considered. Fig. 5 shows the upper half of the iron with the four coils.

The resolution of the results was not satisfactory, even if we had used nearly the maximum number of mesh points (≈14,000) of the present version of Magnus, because the variations of the magnetic field take place within the distance comparable to that of mesh dimension, about 1 cm in the input section. Consequently, the magnetic potential best fit done by the code cannot be very accurate giving an overshoot phenomenon with damped oscillations that can be clearly observed in the table of the magnetic field values.

Point by point results must be analyzed very carefully, although the general field slopes confirm qualitatively the Poisson results, taking into account the coil end fringe field effects that Poisson cannot evaluate.

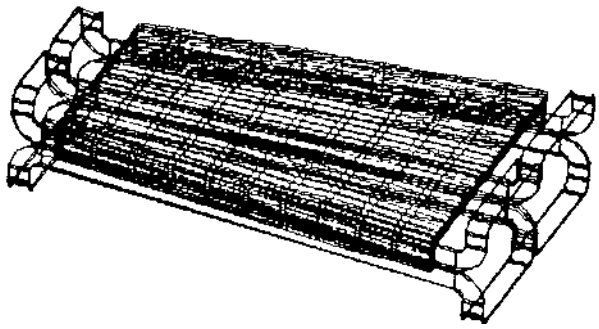

Figure 5 - Upper half magnet with the coils

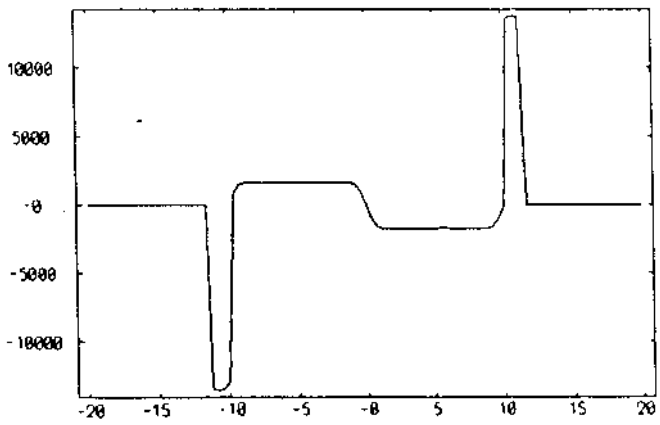

Figure 6 - Bz(x) at the center of the magnet (Magnus code)

The figure 6 shows the magnetic field as a function of the radial coordinate, Bz(x), on the median plane of the magnet. The high and narrow peaks correspond to the magnetic induction inside the iron return legs (≈ 1.3 Tesla). The flat-tops are the good field regions. The useful zone, going from the entrance to the end of the magnet increases moving away from the interaction point.

Fig. 7 shows the results of Poisson and Magnus (200 against 20 mesh points are compared) at the end section. It is evident that the field decreases due to the fringe field induced by the coil saddle ends..

One can notice that the field predictions between Magnus and Poisson are inconsistent, with finer mesh, Poisson seems to do better than that of Magnus. One can also notice that the field directives appears to compare well between these two codes.

Fig. 8 shows the vertical component of the magnetic field Bz(x) along the beam trajectory, 5 cm apart, starting from the I.P.end, moving towards the magnet center.

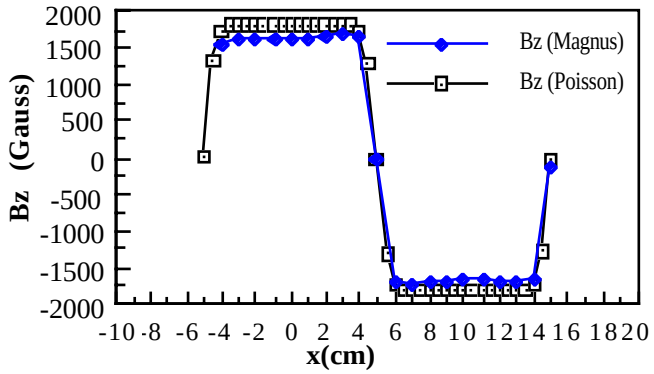

Figure 7 - Magnetic field at the magnet entrance as evaluated by POISSON and MAGNUS

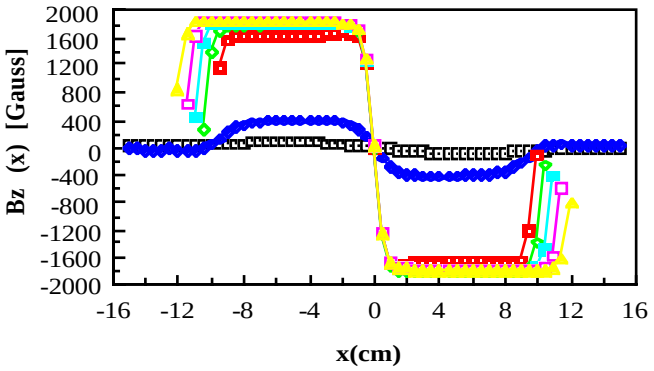

Figure 8 - 3-D magnetic field vs. radial coordinate at different longitudinal position.

A 40 cm long, full cross section prototype magnet is presently being built. Detailed magnetic measurements will be carried out to verify the validity of the field calculation and proper shaping of the magnet ends

3. Electrical and Hydraulic Parameters

Each coil has 3 turns that are in series for electrical connections and in parallel for hydraulic connections. The two right side coils, as the two on the left, will be electrically in series. It is not sure, at the moment if it will be used only one or two power supplies to compensate minor differences of the magnetic field flat-tops.

The following list shows some of the more important parameters of the splitter magnet:

		Prototype	Final
Mag.length	(m)	0.4	1.5
Cu. conductor	(mm)	7.5 * 5.5	Ditto
Conductor hole	(mm)	5.5 * 3.5	Ditto
Ave. turn length	(m)	1.8	4.1
Cond. length/coil	(m)	5.4	12.3
R/ Coil (60 ° C)	(mΩ)	5	11.2
Total resistance	(mΩ)	20	44.8
Nom. current	(A)	1128	1128
Max.current	(A)	1660	1660
Nom. Amp/mm^2	51.3	51.3	
Max Amp/mm^2		75.5	75.5
Nom Voltage	(V)	22.6	50.5
Max Voltage	(V)	33.2	74.4
Total power	(kW)	25.5	57
Max power	(kW)	55.1	23.5
Water flow m^3/secx10^{-4}		4.4	9.8
Water ΔT	°C	30	30
Water ΔP	ATM	0.35	3.3

4. Mechanical Design

The splitter magnet is a picture frame window solid iron yoke type. It essentially is made of two conventional septa. The location of the multi-turn coils have to be located and aligned properly in order to achieve good field quality. The electrical insulation will be accomplished by applying multi-layer of Kapton tapes with pressure sensitive backing, the insulated coils will be confined in a well made mechanical mold and cured at temperature consistent with the adhesive of the Kapton tape. The coil packs will be located and confined accurately at appropriate locations inside the magnet yoke by mechanical means. Two fiducial marks capable of accepting Taylor Hobson spherical targets will be provided for alignment purpose. The roll and pitch will be determined by placing an electronic inclinator on the surfaces precisely machined on the magnet top with respect to the median plane of the magnet.

5. References

[1] Poisson/Superfish Reference Manual - Los Alamos Accelerator Code Group MS H829, Los Alamos National Laboratory, Los Alamos, NM 87545 USA.

[2] The MAGNUS Package - Ferrari Associates, Inc. - P.O. Box 1866, Orange Park, FL 32067 USA.

A New Hybrid Tunable Quadrupole Proposal for the DAΦNE Main Ring Low Beta Insertions

C. Sanelli, A. Cattoni
INFN-Laboratori Nazionali di Frascati
C.P. 13, 00044 Frascati (Roma) Italy
L. Barbagelata, F. Crenna, M. Grattarola, G.C. Gualco and F. Rosatelli
ANSALDO RICERCHE, Divisione Nuove Tecnologie
Corso Perrone 25, 16161 Genova, Italy

Abstract

A hybrid, tunable, p.m. quadrupole prototype, 5.3 T/m, 45 mm bore radius, 280 mm in length, for Daϕne has been designed and built in a collaboration between Ansaldo Ricerche - Genova and the Frascati National Laboratory Magnet Group. Magnetic calculation, constructive design and the first acceptance test results are briefly reported in this paper.

1. INTRODUCTION

In the Daϕne Φ Factory, electrons and positrons circulate in two separate storage rings, whose top view is about elliptical, intersecting in the horizontal plane, giving rise to two interaction points (I.P.), each one placed at the centre of a long straight section. On both side of each I.P. a triplet of quadrupoles is needed, to focalize the beams and to obtain a minimum value of the β_y function, which is a design parameter of paramount importance to achieve a high luminosity (1, 2, 3). Likely every I.P. will be surrounded by a large detector incorporating the most of the straight section, vacuum chamber and the triplets of the low-beta insertion included. In addition the first detector will be equipped with a big solenoid, may be superconducting, about 6 m in diameter and 5 m in length, whose magnetic field should not be seen by the machine beams. Shielding solenoids, coaxial with the beams are needed (4), limiting even more the allowance for the low-beta insertion quads.

2. BOUNDARY CONDITIONS FOR THE LOW BETA INSERTION QUADRUPOLES

The detector requests, aimed to maximize the solid angle, impose to confine the machine components, shielding solenoids included, in a conical zone with the vertex centred in the I.P. and a half aperture angle of 8.5 degrees. Taking into account the machine optics lay-out, this comes out in the following constraints for the overall radial extension of the quads:

- First quadrupole, the closest to the I.P., outer radius $\leq$0.067m
- Third quadrupole, the farthest from the I.P., outer radius $\leq$0.156 m.

Having available in our storage a stock of about 500 prismatic Recoma Magnets, 9x9 mm^2 in cross section, 70 mm in length, we came to the decision of trying a hybrid permanent magnet quadrupole, equipped with two tuning studs per pole, wedge shaped, just to learn what were the possibilities of solving our problems.

3. MAGNETIC CALCULATIONS

The hybrid quadrupole geometry has been analyzed with PANDIRA (2D-code) at LNF and with PE2D and TOSCA at Ansaldo (2D and 3D codes respectively). Pandira and PE2D gave nearly the same results but the 3D analysis gave quite different results. The basic geometry has been carefully studied and modified to obtain the maximum gradient. At the beginning we set the radial length of the iron wedge the same of that of the p.m blocks. The calculations showed that there is (like on the p.m. undulators (5)) a gradient increase of the order of 3 % when the p.m. block is overhanging the wedge. Consequently we decided to shorten the wedge length, decreasing at the same time the fringing field outside the quadrupole. Even the position of the permanent magnets was optimized to get a higher gradient, moving the p.m. block toward the quadrupole centre. Note that when this distance is too much reduced, the flux going out from the p.m. block closes on itself and it does not penetrate into the iron, so that one loses the 'iron dominated' condition.

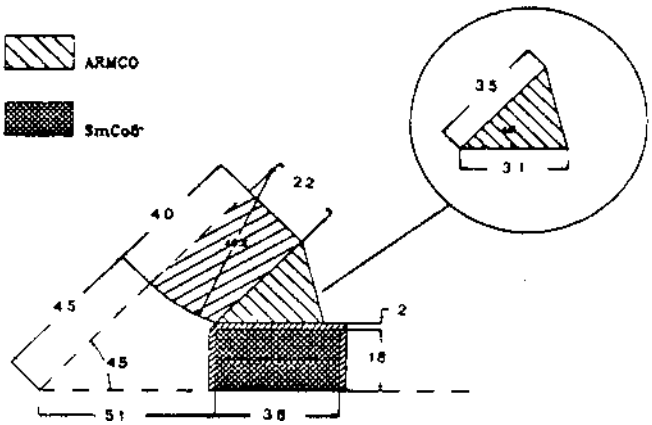

Fig. 3.1 - Basic geometry, 1/8th of the quadrupole

Taking into account all these considerations the Pandira run predicted a gradient of 5.74 [T/m]. The pole profile was approximated with an arc of circle. The calculations made at Ansaldo by means of PE2D showed nearly the same results, 5.84 [T/m] with circular pole profile and 5.67 [T/m] with hyperbolic pole profile. The last profile had the advantage to reduce the gradient variation from 8 to 3 * 10^{-3} at 12 mm far from the quadrupole centre.

Fig. 3.1 shows the basic geometry. Fig. 3.2 shows the gradient variation as calculated by Pandira with the wedges closed and opened respectively.

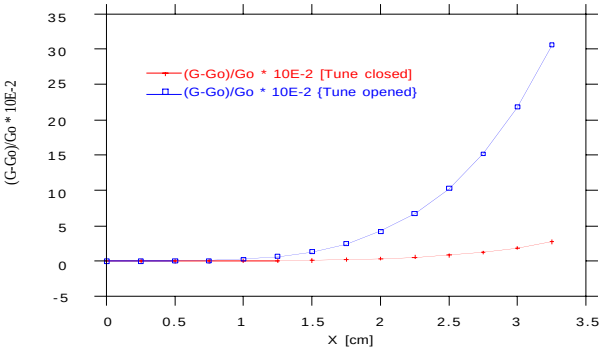

Figure 3.2 - Gradient uniformity from Pandira

The Tosca calculations, made at Ansaldo, gave results strongly different from the 2D codes. The predicted value at the centre of the quadrupole was 4.87 [T/m].

4. PERMANENT MAGNET MEASUREMENTS AND SORTING

The characterization of the permanent magnets for the quadrupole has been carried out in three steps :

1) Preliminary characterization by a Hall effect gauss-meter
2) Dimensional measurements
3) Measurements of the angular deviation and of the relative strength of magnetization.

A total of 568 permanent magnets have been measured. The average measured magnetic field has been: $B_{average}$ = 0.281 Tesla with standard deviation 0.008 Tesla. Only 426 magnets were chosen and dimensionally measured. The magnets whose transverse dimensions differed from the nominal value (9 mm) by more than 0.05 mm have been discarded. 397 magnets have been accepted.

These magnets have then been magnetically characterized. The equipment set up at Ansaldo Ricerche, allows to measure the relative strength of magnetization (with respect to a reference magnet) and the angular deviation of magnetization from the nominal direction. The nominal direction is defined as the vertical axis perpendicular to the reference magnet face. The magnet to be measured ($|M|$) and the reference magnet ($|M_r|$), both with parallel and anti-parallel magnetic moments, are kept in rotation inside the bore of a coil at a frequency of 1200 turns/minute. An harmonic analysis (FFT) of the induced voltage allows to obtain the amplitude and the phase of the fundamental and then the ε and θ values (where ε is defined as $(|M| - |M_r|)/ |M_r|$ and θ is the angular deviation of the magnetization with respect to the reference one). The experimental errors are : $\pm 10^{-4}$ for ε and $\pm$ 1 mrad for θ.

After the preliminary magnetic characterization, 13 magnets, whose $|M|$ and θ were as close as possible around the distribution centre, have been chosen and 12 of them have been measured with respect to an arbitrary magnet, then, among these, the magnet number 186 was picked out for final reference. 396 magnets have been measured with respect to that magnet and the following results were obtained:

- standard deviation of ε = 0.014
- standard deviation of θ = 0.010 rad.

The hybrid quadrupole needs four flux generators, four layers of 16 magnets each, for a total of 256 permanent magnets. Sorting has been carried out forming 8 groups of magnets, 32 magnets for each group. The magnets of the same group are as similar as possible among them, both in regard to ε and to θ. Each 32 magnet group has at its time been divided in 8 groups, 4 magnets each, as similar as possible. The 4 magnets have been mounted one behind the other to obtain the best longitudinal homogeneity.

One time the four flux generators have been assembled, they have been magnetically tested using a Hall effect Gaussmeter. The Hall Probe was put at 29 mm from the permanent magnets surface and it was moved longitudinally along four lines parallel to the quadrupole axis, two above and two below the flux generator surfaces, and the magnetic field was recorded. In addition a map along a transverse axis, at the same distance from the magnets surface, in correspondence of the flux generator mid-plane, has been carried out. The maximum deviation among the four flux generators is about 4%.

5. MECHANICAL DESIGN AND CONSTRUCTION

5.1 Mechanical design

The quadrupole prototype is essentially composed by four iron poles, four magnet assemblies, above defined as flux generators, and eight tuning studs (wedges), all supported by an outer cylindrical structure. Each pole is fixed to the structure. Calibrated spacers of different thickness can be placed on the pole back in order to be able to change the bore radius. Each magnet assembly is made up by magnet blocks not glued but mechanically clamped by an external aluminum structure. The four magnet assemblies are mounted in calibrated slots in the outer cylindrical structure. The movable tuning wedges slide on the lateral sides of the magnet assembly boxes. The gap between the tuning wedges and the poles can be set from 0 to 4.5 mm. The outer cylindrical structure was designed to allow the splitting of the quadrupole in two parts for mounting operations around the vacuum chamber.

5.2 Materials and machining

The following materials have been used for the different quadrupole parts :

- Magnet assemblies: SmCo5 magnet blocks with nominal residual field Br=8.5 kGauss and coercive force Hc=8300 Oe.
- Poles and tuning wedges: ARMCO pure iron (99.7 %)
- Outer cylindrical structure: ERGAL aluminum alloy.
- Screws and bolts: AISI 304 stainless steel and brass.
- Pins: AISI 304 stainless steel.

The two parts of the cylindrical structure were obtained from a massive extruded bar. After a pre-machining they were heat treated for stabilization and then finished on the contact surfaces, pinned and bolted each other. The whole assembly was then finished machining to obtain the final structure. The pole profile was realized by means of a numerical control machine.

The calculations were performed in 2D geometry by means of the PE2D code (Vector Field).An hyperbolic profile was chosen. The optimization was performed to minimize the relative gradient variation $\Delta G = (G-Go)/Go$ at 20 mm from the quadrupole centre (G=local gradient; Go = gradient in the centre). The optimization started with the theoretical pole profile: $y(x) = Ro^2 / 2 x$; where Ro=45 mm is the bore radius and

only those profiles compatible with the geometrical and the assembling constraints were taken into consideration. The ΔG value was decreased from $8.13*10^{-3}$ to $2.92*10^{-3}$ with the profile:

$$y(x) = \frac{h*x+a-h^2}{x-h}$$

where : a = 700 mm^2, h=5.362 mm $(20 \leq x \leq 50$ mm)

6. MAGNETIC MEASUREMENTS

A first set of magnetic measurements has been performed by means of a Hall effect Gauss-meter at Ansaldo Ricerche.Field maps on the horizontal and vertical axes laying on the medium transverse plane and on the planes in front and on the back of the quadrupole, for different wedge positions, have been carried out. In addition, field integral maps along lines parallel to the longitudinal axis at ±16, ±18, ±20, ±22 and ±24 mm from the quadrupole centre on the horizontal and vertical axes have been recorded. Finally, the fringing field outside the magnet has been measured and the relative curves plotted. For obvious reasons only a few curves are reported here. The average measured gradient with the wedges closed is 5.268 T/m. The gradient with the wedges completely opened is 4.574 T/m. This allows a tune range of 13.2%. The maximum measured gradient value is -8.2 % lower than the Pandira calculation and +8.1 % greater than the Tosca evaluation.

Fig. 6.1 shows how the gradient decreases opening the wedges.

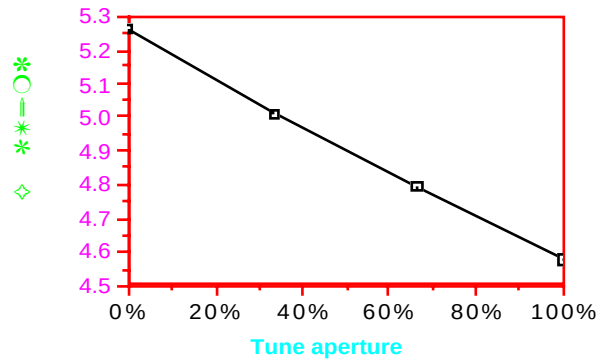

Fig. 6.1 - Absolute gradient variation vs tune aperture

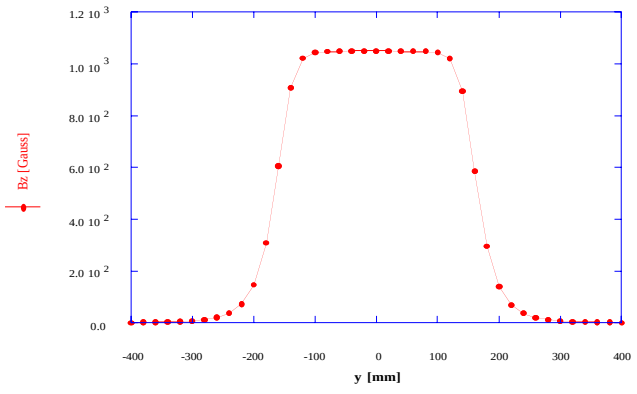

Fig. 6.2 - Longitudinal field profile

The magnetic length of the quadrupole has been calculated using the field integral maps. The average value, on a total of 20 curves, is 338.74 mm ±0.4 mm. Fig. 6.2 shows the field variation along an axis parallel to the quadrupole axis but horizontally shifted 20 mm from the quadrupole centre.In fig. 6.3 the gradient variation in terms of ΔG/Go, where Go is the gradient at the quadrupole centre (Go=5.268 T/m) , is reported.

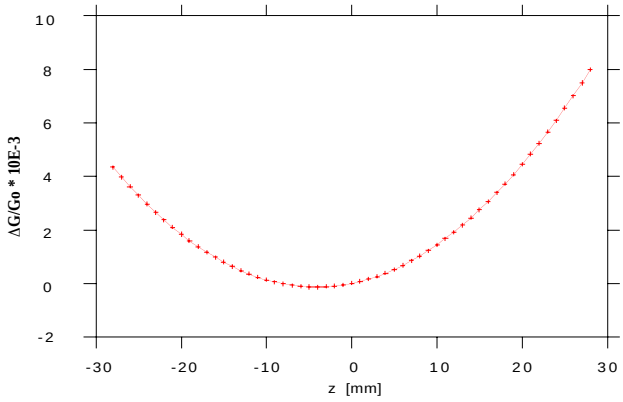

Fig. 6.3 - Gradient uniformity at the quad midplane

7. CONCLUSIONS

The magnetic measurement program is not yet completed and a deeper investigation is still needed. The major items that must be analyzed are:

- determine the displacement of the magnetic axis with respect to the mechanical one;
- made the harmonic content analysis by means of rotating coil;
- balance the quad, using the tune wedges, at a fixed gradient value;
- modify the pole profile to increase the gradient homogeneity and consequently decrease the multi-pole terms;
- superimpose a solenoidal field and measure the total effect;
- study the better way to shield the external fringing field.

We hope to complete the work before the end of this year, using the automatic multi-pole magnet measurement system, model 692, based on rotating coil technology, that has been ordered to Danfysik and whose delivery term is October 1992.

This type of hybrid, tunable quadrupole is Patent pending.

8. REFERENCES

[1] The DAΦNE Project Team: "DAΦNE Design Criteria and Project Overview", Proc. of the Workshop on Physics and Detectors for DAΦNE, Frascati, April 9-12, 1991.

[2] The DAΦNE Project Team: "DAΦNE: The Frascati Φ-Factory " Proc. of P.A.C.1991, S. Francisco, May 6-9, 1991.

[3] M.E. Biagini et Al.: DAΦNE Lattice Update, Technical Note L-4, INFN LNF,Accelerator Division, Dec.2, 1991.

[4] "Proposal for a Φ–Factory" LNF-90/031(R) 30/Apr./1990

[5] K.Halbach et Al. "CSEM-Steel Hybrid Wiggler/Undulator Magnetic Field Studies- IEEE Trans. Nuclear Science NS-32-5 (1985).

Review of Studies of Electron-Positron Factories

Miro Andrea Preger
INFN Laboratori Nazionali di Frascati
C.P. 13 - 00044 Frascati (Roma) - Italy

Abstract

Research in elementary particle physics based on accelerators exhibits nowadays two complementary trends: the first points towards unexplored high energy regions, the second searches the answers to fundamental theoretical questions through high resolution experiments, based on the detection of a very large number of events in the energy range already covered by existing accelerators. Following the latter direction, high luminosity electron-positron colliders optimized at the center of mass energies of the quark-antiquark resonances Φ (1 Gev), J/ψ (4 GeV) and ° ("upsilon", 11 GeV), where the cross section for particle production is high, are being proposed by several laboratories in the world. The luminosity requirements of such "factories" exceed by two orders of magnitude the results obtained by operational accelerators, mainly limited by beam-beam interaction. To achieve this goal, substantial changes to the classical scheme of single ring colliders with few crossings are under study, spanning from compact structures with extremely high current density, to double intersecting rings with a large number of bunches interacting only one or two times per turn with the other beam. Experimental requirements on the geometry of the crossing region, such as center-of-mass momentum and magnetic fields for produced particles detection, set additional challenges to the design. The main accelerator physics and technology issues of electron-positron factories are discussed, advantages and drawbacks of possible collider schemes are compared, and the status of the existing proposals is reviewed.

1. INTRODUCTION

Strong interest has been demonstrated by the high energy physics community towards the realization of high luminosity electron-positron colliders optimized around the center of mass energy of the hadronic resonances Φ (1 GeV), J/ψ ("τ/charm", 4 GeV) and ° ("beauty", 11 GeV). The large cross section at the peak of the resonances enables the production of high hadron fluxes, and this is the reason for the name of "factories" assigned to these projects. Due to the relatively low energy required, the typical size of such colliders is often compatible with the possibilities of small, national, laboratories, in contrast with the huge financial and technical effort required for the realization of colliders beyond the energy range already covered by existing machines. On the other hand, the experiments proposed in this "low" energy range are always very high precision measurements of physical quantities, the most important being the study of CP violation, or search for rare decay modes of the resonant state, and a common feature to such proposals is the requirement for very high luminosity, typically two orders of magnitude above the performance of existing storage rings ($4x10^{30}cm^{-2}s^{-1}$@1.02GeV at VEPP2M [1], $7x10^{30}cm^{-2}s$-1@4.4GeV at BEPC[2], $1.8x10^{32}cm^{-2}s^{-1}$ @10.6GeV at CESR [3]). The experiments are in most cases extremely sensitive to the backgrounds created by the machine, such as synchrotron radiation and lost particles, and even radiation damage of experimental setups my become one of the constraints to be respected in the collider project. The high luminosity is a common requirement for the three kinds of factories: a peculiarity for the ° decay physics is the requirement for different energies in the two beams (asymmetric B-factories), while τ/charm factories are characterized by the need of very good energy resolution, to match the tiny width of the J/ψ resonance.

To achieve the strong improvement required for the luminosity, new structures are proposed for the factories, as alternatives to the standard layout of a single storage ring with counterrotating electron and positron beams: the preferred one is based on the use of two separate rings with one or two interaction regions, but also small superconducting single rings or superconducting electron linacs against positron storage rings have been considered.

2. MACHINE PHYSICS OVERVIEW

2.1. Luminosity

The luminosity of an electron-positron collider is

$$L = f \frac{N^+ N^-}{A} \qquad (1)$$

where N^+ and N^- are the numbers of electrons and positrons in a single bunch of the machine, f the collision frequency and A an "effective" interaction cross section, which, in the simple case of equal beam sizes of the two beams and gaussian horizontal and vertical distributions, takes the simple form

$$A = 4\pi\sigma_x\sigma_y \qquad (2)$$

Beam-beam interaction limits the maximum number of particles stored in a single bunch. A good probe for the intensity of the perturbation is the linear tune shift

$$\xi_{x,y} = \frac{r_o N \beta_{x,y}}{2\pi\gamma \sigma_{x,y} (\sigma_x+\sigma_y)} \qquad (3)$$

where r_o is the classical electron radius, γ the energy of the beam in units of the electron rest mass and $\beta_{x,y}$ the betatron functions at the interaction point (IP).

From the experience on existing storage rings and from the results of beam-beam numerical simulations, it can be stated that the tune shift cannot exceed a maximum value ξ_o, whose value, averaged over the experimental results from operating machines does not depend on energy and is

$$\xi_o = 0.038 \pm 0.013 \qquad (4)$$

The tune shift can reach its maximum value in both planes if

$$\frac{\beta_y}{\beta_x} = \frac{\varepsilon_y}{\varepsilon_x} = \frac{\sigma_y}{\sigma_x} = k \qquad (5)$$

where ε_x and ε_y are the horizontal and vertical emittances and k is the coupling factor in storage rings without vertical bendings. In this configuration the luminosity is optimized: combining (1) and (3) under the assumption (5) one finds for the luminosity and the number of stored particles the following expressions

$$L = f\,\pi\,\gamma^2\,\xi_o^2\,\varepsilon_o\,\frac{1+k}{r_o^2\,\beta_y} \qquad N = 2\,\pi\,\gamma\,\varepsilon_o\,\frac{\xi_o}{r_o} \qquad (6)$$

where ε_o is the sum of the horizontal and vertical emittances of the beam. Formula (6) shows that, keeping the other parameters constant, the achievable luminosity scales with the square of the beam energy. This behaviour is almost compensated by the decrease of the hadron production cross section: the typical luminosity requirements for the factories are $>10^{32}$ for the Φ, $\approx 10^{33}$ for the τ-charm and $\approx 10^{34}$ for the beauty.

The limit imposed by beam-beam interaction can be overcome in colliders where one or both beams are lost after crossing at the IP, thus allowing strong beam-beam interaction, which largely exceeds the above mentioned limits for conventional storage rings. In these colliders, the beams sizes at the IP are pushed to the minimum value allowed by the achievable emittance. The beams are strongly focused by the interaction itself, and numerical simulations predict a "pinch effect" that increases the luminosity beyond the value foreseen in (1). Proposals have been put forward both for linac on linac and for superconducting electron linac on positron storage ring schemes. These solutions are limited by beam power considerations, and, of course, superconducting structures have been proposed [4]. In the first case the main difficulties come from the beam emittance and from the positron production: a damping ring is inserted in the structure to improve positron emittance, while the electron beam is used both to produce luminosity at the IP and for positron conversion. The hybrid solution [5] is based on the strong disruption of a weak electron beam on an intense stored positron beam with very small emittance. This scheme exploits the experience based on small emittance storage rings for synchrotron radiation, and, although no experimental data are available on such kind of interaction, it seems the most promising.

As already mentioned, an improvement of about two orders of magnitude in luminosity, with respect to existing machines, is required for the factories. In the absence of new basic ideas to improve the luminosity, the proposals for new machines push the parameters appearing in (6) towards their technically achievable limits. Table 1 shows typical values of these parameters for double ring projects in the three energy ranges.

Table 1
Design parameters for e^+e^- factories

	Φ [6]	τ/Charm [7]	e^+ Beauty [8] e^-
Energy (GeV)	0.5	2.5	3.1 9.0
Luminosity ($cm^{-2}\,s^{-1}$)	5.0×10^{32}	6.10^{32}	3.10^{33}
Collision frequency (MHz)	368.2	30.0	238.2
Horizontal linear tune shift	0.04	0.05	0.03
Vertical linear tune shift	0.04	0.007	0.03
Number of particles per bunch	8.9×10^{10}	1.2×10^{11}	5.9×10^{10} 4.1×10^{10}
Number of filled bunches	120	30	1658
β_x at IP (cm)	450.0	1.0	37.5 75.0
β_y at IP (cm)	4.5	15.0	1.5 3.0
Vertical dispersion at IP (m)	0	±0.4	0
Crossing angle (mrad)	20	0	0
Horizontal emittance (m)	1.0×10^{-6}	3.6×10^{-9}	9.7×10^{-8} 4.8×10^{-8}
Vertical emittance (m)	1.0×10^{-8}	0.2×10^{-9}	3.9×10^{-9} 1.9×10^{-9}
σ_x at IP (mm)	2.12	6.0×10^{-3}	0.19
σ_y at IP (mm)	2.12×10^{-2}	0.4	7.6×10^{-3}
Coupling factor	0.01	0.06	0.04

2.2 Betatron Function at the Interaction Point

The luminosity is inversely proportional to one of the two betatron functions at the interaction point ($k\beta_x$ can be put in formula (6) instead of β_y): the vertical one is usually preferred, according to (5), for small values of the coupling factor k. The slope of the betatron function in the interaction straight section grows linearly from the crossing point to the first magnetic element and is inversely proportional to its value at the IP, so that a strong focusing quadrupole triplet is necessary on each side to maintain it within reasonable limits. These quadrupoles limit the solid angle covered by the experimental setup, and are a source of chromatic effects, which must be corrected by means of sextupoles in the arcs where the dispersion does not vanish. The sextupoles make the lattice strongly nonlinear, with a consequent restriction of the stable area for betatron oscillations (dynamic aperture).

The most important limitation to the value of β at the IP is the condition that it must not be smaller than the bunch length, since otherwise the particles would cross at positions where, due to the increase of the betatron function, the beam-beam limit would be exceeded. Small bunch lengths call for very high voltage in the R.F. system, and, anyway, there will be a limit coming from the microwave instability [9], which mainly depends on the peak current and the longitudinal broad-band impedance in the ring. The vacuum chamber must be carefully designed, in order to avoid contributions to such impedance coming from any parasitic cavity, such as bellows, pumping ports, injection elements and so on. The R.F. cavity itself is in principle an important source of longitudinal impedance, and special designs are being carried on to overcome this difficulty. Two harmful implications of a small bunch length are, on the other hand, the larger sensitivity to single bunch longitudinal instabilities and the reduction of single beam lifetime due to the Touschek effect (intrabeam scattering), which is inversely proportional to the bunch volume. For conventional structures the achievable bunch length (and the β function at the IP) is few centimeters.

A solution to the small bunch length problem is suggested by the idea of the "quasi-isochronous storage ring" scheme [10], where the linear part of the momentum compaction is made as small as to maintain the stability of synchrotron oscillations. In this way the betatron function can be decreased to few millimeters.

2.3. Collision Frequency

Operating colliders in the energy range of the factories are all single rings, where electrons and positrons are stored in opposite directions, and an obvious way to improve the luminosity is to store many bunches in the ring. The first difficulty of having many bunches in a single ring collider is that the lattice should provide many interaction points with small β's, and, as explained before, this would lead to unacceptable chromatic limitations. Moreover, it has been observed that the maximum tune shift per crossing depends on the number of crossings per revolution, and scales roughly with the inverse square root of this number. In order to optimize the luminosity at a single interaction point (IP), it is therefore necessary to separate the beams at the unwanted "parasitic" crossings, and the number of possible separations is typically twice the number of betatron oscillations per turn. Since the wavelength of these oscillations is much longer than the R.F. buckets (which set the maximum number of bunches in the ring), this becomes a practical limit to the collision frequency for single rings.

Most of the proposals are therefore based on machine designs where the beams travel in two independent rings, with one or two crossings where the experimental setups are located. For such machines the collision rate is limited, in principle, by the R.F. frequency, typically in the range of $3 \div 5 \times 10^8$ Hz, the maximum number of storable bunches being equal to the R.F. harmonic of the revolution period. In the double ring scheme the beam-beam interaction limits the maximum current stored in single bunches, and the luminosity is proportional to the number of circulating bunches. The total stored current and the synchrotron radiation power are therefore very large, setting challenging requirements on the vacuum system design and making damping of longitudinal instabilities a crucial point for reliable machine operation. Sophisticated bunch-to-bunch digital feedback systems are under study to match these needs [11].

Multibunch beams travelling in opposite directions near the IP cross each other at multiples of half the distance between bunches, where the β functions are much larger and the beam-beam limit would be exceeded. It is therefore necessary to separate the beams at these "parasitic" crossings, and this can be more easily accomplished in the beauty factories, where the two beams have different energies, so that a couple of bending magnets around the IP can give the two beams different deflections. These magnets must, however, be located very near the IP, at a distance smaller than half the distance between bunches, and they become a dangerous source of synchrotron radiation backgrounds.

Parasitic crossings contribute to beam-beam interaction: the additional incoherent tune shifts are given by

$$\xi_x = - \frac{r_o N \beta_x}{2\pi\gamma d^2} \qquad \xi_y = \frac{r_o N \beta_y}{2\pi\gamma d^2} \qquad (7)$$

where d is the distance between the centers of mass of the two bunches at the parasitic crossing point, and they must be kept much smaller than the tune shifts from the IP crossing. Beam-beam simulations including parasitic crossings [8] should be performed to assess the minimum required separation.

Electrostatic separation or crossing at an angle must be provided in the case of equal energy beams (Φ and τ/charm factories). The first solution is rather difficult from the technical point of view, because the required deflection is large, and therefore, due to the limitations on the maximum attainable voltage, the plates must be long; the spacing between bunches must be increased and the contribution of the plates to the broadband longitudinal impedance is strong.

Crossing at an angle is, in principle, prone to synchrotron-betatron coupling which may strongly reduce the

luminosity [12]. This drawback can be overcome by the Crab-crossing scheme [13], where the trajectories cross at an angle, but the bunches are tilted by transverse R.F. fields by the same angle so that they "see" each other head-on. However, it has been shown that harmful effects of the crossing angle θ can be neglected, if the following condition is satisfied (σ_l is the longitudinal r.m.s. bunch length)

$$\theta_{x,y}\,\sigma_l < \sigma_{x,y} \qquad (8)$$

and this may be a good approach for flat beams crossing at an angle in the horizontal plane, the tolerable angle being in the order of 10^{-2} rads [6]. On the other hand, condition (8) is also a strict tolerance on the maximum angle between the two beams in the vertical plane, due to their tiny vertical size.

High collision frequency can be obtained also with small, superconducting, single storage rings with one or two bunches. The proposals based on this concepts are however limited to the Φ-factories, because of the small energy of the ring: in this case collision frequencies around 20 MHz can be realized [14,15] . To compensate for the smaller collision rate, these proposals are based on very small betatron functions at the IP, with a large number of particles per bunch. The major drawbacks of this approach are the very short beam-beam decay rate (proportional to the luminosity divided by the total number of particles in the ring), the small space available for the experimental setup and the complexity of chromatic correction.

2.4. Beam emittance

Formula (6) shows that large emittance is beneficial to luminosity in the case of tune shift limited colliders: this is the case for the Φ-factories, where wigglers are proposed both to increase the emittance and to contribute additional damping, since beam-beam interaction observations suggest that the tune shift limit increases with the amount of radiated power [16]. The price to pay comes however from the increase in stored current, with strong implications on beam stability and vacuum requirements.

A large emittance lattice is less favourable in the high energy region (B-factories), where the radiation problem is much more troubling and the ratio of luminosity to stored particles per bunch is better by an order of magnitude.

Small emittance is also required in τ/charm factory projects where "beam monochromatization" is proposed [7] to enhance hadron production at the resonance. In this scheme the idea is to have very small betatron contribution to the beam size at the interaction point together with a strong energy/position correlation, in such a way that the sum of the energies of the interacting particles is much less spread out than the particle energies themselves. This approach leads to a peculiar set of machine parameters, as it can be observed in Table 1.

Small beam emittance is also foreseen in linac-linac [4] and electron linac against positron storage ring, where the electron beam is lost after interaction and the positron beam is brought near the maximum tune shift calculated for conventional two rings structures [5].

2.5. Coupling

A factor two in luminosity could be gained, as shown in (6), by working with the stored beams in full coupling. The question if the maximum tune shift can be influenced by the shape of the interacting beams is still open, since some numerical simulations predict that round beams can help in reaching larger tune shifts. No experimental evidence is however available to support this prediction.

Full coupling requires the two β functions at the IP to be of the same in order to obtain the maximum luminosity: this is an additional difficulty to the design of the low-β section, strong focusing in both planes being required. As a consequence, the chromaticity is increased and the chromatic correction more complicated. A solution to this problem is suggested by the Novosibirsk Φ-factory proposal [14], where round beams are foreseen and a solenoidal field around the IP is used both to focus the beams and as energy analyzer for the experimental setup.

3. INTERACTION REGION GEOMETRY AND BACKGROUNDS

A crucial point in the design of the factories is the interaction region geometry and its protection from machine backgrounds, such as synchrotron radiation photons or lost particles from beam-gas or intrabeam scattering. A fundamental requirement to the layout of the machine around the crossing point is the availability of free space for the experimental setup, which should subtend a solid angle as close as possible to 4π to avoid loosing substantial sensitivity in the observation of CP-violating processes. Low-β focusing at the IP is realized with quadrupole triplets and these quadrupoles limit the solid angle available for the detector. Compact structures, realized with permanent magnets, are a common feature to many projects, because they are able to provide the best compromise between internal aperture and external dimensions. In the case of beam crossing at an angle, the maximum angular separation is constrained by condition (8), and the two beams are not far enough at the end of the drift space around the IP to allow the realization of independent focusing triplets. The two beams travel therefore together in a common vacuum chamber and off-axis in the focusing triplets. The lattice is designed in such a way as to improve the separation and help the final splitting of the two rings [6]. For the asymmetric schemes, the design of the IP lattice is more complicate, since the first quadrupoles are common to both beams, and they are more efficient on the low energy one: the high energy beam must therefore be focused mainly by upstream quadrupoles where the two rings are completely independent.

Longitudinal magnetic field in the detector is also required, so that complicate correction schemes must be designed, especially in the case of the low-energy Φ-factories when small coupling is foreseen. Longitudinal field compensators and tilted quadrupoles are necessary to ensure the correct shape and position for the beams at the IP.

Protection against backgrounds in the detector vacuum chamber is one of the main items in B-factory designs. Strict tolerances are set on the number of background particles hitting the detector [8], both for dead-time and radiation damage reasons. Typical limits are in the order of 0.1 particles/cm^{2}μs. To achieve this goal, despite the large number of circulating particles, the interaction region must be protected by masking targets that are the result of thorough investigation and tracing from any possible source of direct or reflected photons and lost particles. The design of the masking system is strongly advantaged in the case of small emittance beams, and this is the main reason for the usual choice, in the majority of B-factory projects in the direction of a large number of bunches with relatively small emittance and number of particles per bunch.

4. CONCLUSIONS

As a consequence of the strong interest demonstrated by the high energy physics community towards the above described research field, several proposals have been forwarded by many laboratories in the world: particular emphasis is put on beauty-factories, also because they can be realized as upgrades of operating machines. Linac on Linac [4], Linac on ring [5,17,18] and double storage rings [8,19,20,21,22,23] have been studied and proposed.

Two projects based on the double ring scheme are being studied in the τ/charm energy range [7,24,27], and five in the Φ region, two of them proposed as compact single rings [14,15]. The other three are double ring systems [6,25,26]: one of them, the Frascati Φ-factory DAΦNE [6], has been funded and is under construction.

5. REFERENCES

[1] P.M. Ivanov et.al, "Luminosity and beam-beam effects on the electron-positron storage ring VEPP-2M" in Proceedings of the 3rd Advanced ICFA beam dynamics Workshop, Novosibirsk, URSS, 1989.

[2] Y. Wu et.al., "The BEPC Storage Ring - Status and prospects" in 1991 Particle Accelerator Conference, S. Francisco, USA, May 1991.

[3] D.L. Rubin and L.A. Schick, "Single Interaction Point Operation of CESR" in 1991 Particle Accelerator Conference, S. Francisco, USA, May 1991.

[4] U. Amaldi and G. Coignet, "Conceptual design of a multipurpose beauty factory based on superconducting cavities", Nuclear Instruments and Methods, A260, p.7, 1987.

[5] P. Grosse-Wiesmann, et. al. "Linac-Ring-Collider B factory", in EPAC90 Proceedings, Nice, France, June 90, pp.383-385.

[6] The DAΦNE project team, "DAΦNE status report", this Conference.

[7] Y.I. Alexahin, A.N. Dubrovin, A.A. Zholents, "Proposal on a tau/charm factory with monochromatization", in EPAC90 Proceedings, Nice, France, June 90, pp. 398-400.

(8] "An asymmetric B factory based on PEP", Conceptual Design Report, LBL PUB 5303, SLAC-372,February 1991.

[9] P.B. Wilson et.al., "Bunch lengthening and related effects in SPEAR II" in 1977 Particle Accelerator Conference, Chicago, USA, March 1977, pp. 1211-1214.

[10] C. Pellegrini and D. Robin, "Quasi-isochronous storage rings: a possible low current, high luminosity meson flavor factory" in 1991 Particle Accelerator Conference, S. Francisco, USA, May 1991.

[11] D. Briggs et.al., "Prompt bunch by bunch synchrotron oscillation detection via a fast phase measurement", SLAC-PUB-5525, LBL-30604, May 1991.

[12] A. Piwinski, "Synchro-betatron resonances" in Nonlinear dynamics Aspects of Particle Accelerators, S. Margherita di Pula, Italy, February 1985, Lecture Notes in Physics 247, pp.104-120.

[13] K. Oide and K. Yokoya, "The Crab-crossing scheme for storage ring colliders", SLAC-PUB-4832, January 1989.

[14] L.M. Barkov et.al., "Phi-factory project in Novosibirsk" in 14th Int. Conf. on high Energy Accelerators, Tsukuba, Japan, August 1989, pp.1385-1390.

[15] C. Pellegrini et. al. "A high luminosity superconducting mini-collider for phi meson production", in 1991 Particle Accelerator Conference, S. Francisco, USA, May 1991.

[16] J.T. Seeman, "Observations of the beam-beam interaction" in Nonlinear dynamics Aspects of Particle Accelerators, S. Margherita di Pula, Italy, February 1985, Lecture Notes in Physics 247, pp.121-153.

[17] C. Johnson, "The incoherent beam-beam effect in Linear-on-Ring collider" in 1991 Particle Accelerator Conference, S.Francisco, USA, May 1991.

[18] J.J. Bisognano et.al., "A beauty factory using an SRF linac and a storage ring" in Linear Accelerator Conference Proceedings, CEBAF, Newport News, USA, October 1988, pp.586-588.

[19] F. Willeke et.al., "A B-factory in the PETRA tunnel" in 1991 Particle Accelerator Conference, S.Francisco, USA, May 1991.

[20] A.N. Dubrovin, A.A. Zholents, "A combined Symmetric and Asymmetric B-factory with monochromatization"in 1991 Particle Accelerator Conference, S.Francisco, USA, May 1991.

[21] B. Autin et.al.,"Preliminary study of a beauty factory in the ISR tunnel" in EPAC90 Proceedings, Nice, France, June 90, pp.392-394.

[22] K. Satoh, Y. Funakoshi, H. Koiso, E. Kikutani, A. Sato, "An asymmetric collider with the Tristan main ring" in 14th Int. Conf. on High Energy Accelerators, Tsukuba, Japan, August 1989, pp.1349-1354.

[23] "CESR-B, Conceptual Design for a B-factory based on CESR", Cornell Note CLNS 91-1050.

[24] J. Jowett, "The τ-charm factory storage ring" in EPAC88 Proceedings, Rome, Italy, June 1988, pp.368-370.

[25] K. Hirata, K. Ohmi, "Feasibility of a Φ-factory in KEK" in 1991 Particle Accelerator Conference, S.Francisco, USA, May 1991.

[26] A. Streun, "Φ-factory design studies at Mainz" in Workshop on Physics and detectors for DAFNE, Frascati, April 1991, p. 99-105.

[27] J. Gonichon et al., “Preliminary study of a high luminosity e+ e- storage ring at a CM energy of 5 GeV”, LAL/RT 90-02 January 1990.